Physical scale model experiments into local sediment displacement around hydraulic structures of Xstream

J. Frunt

MSc thesis

Faculty of Civil Engineering and Geoscience
Departments of Hydraulic Engineering and Water Management

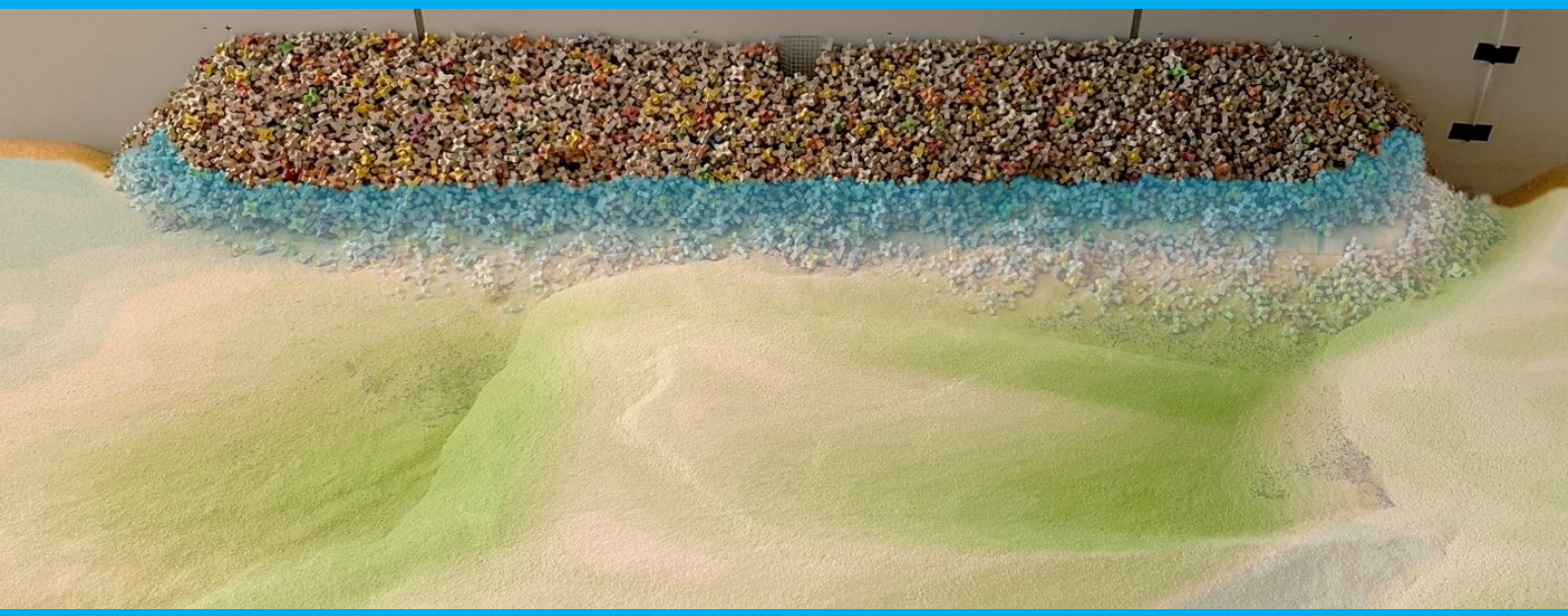

TU Delft

Physical scale model experiments into local sediment displacement around hydraulic structures of Xstream

by

J. Frunt

to obtain the degree of Master of Science
at the Delft University of Technology,
to be defended publicly on Monday December 4, 2023 at 16:00.

Student number:	5178908	
Project duration:	November 7, 2022 – October 26, 2023	
Thesis committee:	Dr. ir. B. Hofland,	TU Delft
	Ir. B. Reedijk,	Royal BAM Group
	Dr. ir. C.J. Sloff,	TU Delft, Deltares
	Dr. ir. R. Hut,	TU Delft
External supervisor:	Dr. ir. B. Vermeulen,	Wageningen University & Research

TU Delft

Preface

This thesis marks the end of my six-year academic journey. At the age of 18, I started studying the Bachelor program International Land and Water Management at the Wageningen University. In three years, I learned a lot about the sustainable and efficient use of natural resources all over the world. I was able to put my knowledge into practice during an internship in Costa Rica. Unfortunately, this adventure came to an abrupt end and further travel plans were cancelled.

In the middle of a pandemic, I moved to a new city starting with my Master program Water Management at the TU Delft. Adapting to a new environment was sometimes hard, but my housemates at Het Scheve Huisje became my best friends! Starting in 2020 within the old Civil Engineering master setup, I had the advantage of being able to freely create my own curriculum. I selected most of my courses from the Hydraulic Engineering track, focusing on the complexity of river systems.

With the topic of my graduation thesis, I specialised on river engineering. I didn't choose the easy path, lacking fundamental civil expertise, but I pushed through. I learned myself programming in Matlab, approaching problems from a practical perspective and applying a physical scale model in academic research. For this, a total of approximately 50 m^3 of plastic granules, 1200 kg of stone and 75000 Xbloc model units were manually moved throughout the experimental phase of this study. At times, I had to be flexible and react fast to achieve what I had envisioned.

Bringing together four organisations from the triangle of education, business and government posed another challenge. Nevertheless, collaborating we have accomplished great results. I would like to thank Bas Hofland from the TU Delft in particular for his guidance during my thesis process and his expert opinion on my work. Of course Bas Reedijk from the BAM, thank you for your inspiring drive to keep innovating. Working in the laboratory of the WUR would not have been possible without the endless dedication and commitment by Nick Wallerstein. Lastly, from Rijkswaterstaat, I thank Yuri Wolf for his enthusiasm from the first moment and for arranging the financial resources from their side.

Finally, I would like to express my gratitude to my parents, brother and close friends for their unconditional support. It's now time for me to explore the world and go backpacking in South America. After that, I'm looking forward for the challenges ahead!

J. Frunt
Delft, November 2023

Abstract

Over the past centuries, the Dutch rivers have been extensively engineered with the construction of hydraulic training works. A changing climate and increasing demands of river functionalities require innovations to the system to ensure its resilience. Exploring potential applications of Xstream elements might contribute to the development of sustainable river management strategies. The 33 cm high concrete three-dimensional cross is the little version of the Xbloc, a widely used breakwater element for coastal protection. Random arrangement of Xstream elements creates 60% porous spaces and the ability to build slopes at a 45° angle. Alterations to the riverbed morphology induced in the near-field of homogeneous Xstream hydraulic structures are assessed in the present study. A physical scale model featuring a movable bed of lightweight sediment was employed to simulate a river section. Minimising any compromises on Froude scaling, this material was used to properly scale the Shields parameter, striving dynamic similarity between the model and reality. Bed load transport processes are reasonably well represented by this material, providing well matched equilibrium scour depths and good qualitative comparisons of the influence of structural variations on these processes. Multiple setups differing in material and geometry were tested in a 12 m long and 2.6 m wide sediment recirculating flume. The primary comparisons of this study include:

- the flexible groyne head in the model against field data;
- two abutments with a 1:2.5 slope, varying in material between stone and Xstream elements;
- two abutments made of Xstream elements, differing in slope between 1:1 and 1:2.5.

Water levels were gauged and flow velocities were measured with acoustic Doppler velocimeters during the experiments. High-resolution bed elevation data was collected by means of a laser scanner. Generally, results of the model show an overestimation of bedform dimensions. This is attributed to the concessions necessitated by the limitations of the test facilities due to the low length scale factor. The effect of contraction was exaggerated in the model as the structure width to flow width ratio was 3 times greater and the influence of any upstream river training works was neglected. The flexible groyne head blocked 43% of the cross sectional flow area in the model. Furthermore, due to the laminar flow behaviour, the water encountered increased resistance within the structure. The deepest scour is found along the leading edge of the structures. This can be explained by the intricate flow patterns created by the primary vortex entering the flow acceleration. Inspired by the longitudinal training wall as built in the river Waal, a less porous stone abutment was constructed to compare the effect of porosity and roughness of Xstream elements on local sediment displacement under high water conditions. The increase in water level in front of the Xstream abutment was half that of the stone abutment and streamwise velocities in the main flow were 5% lower. These findings indicate better dissipation of energy by the Xstream abutment. Nevertheless, the relative turbulence level was 17% higher close to the Xstream abutment due to the higher roughness, resulting in equivalent peak velocities in both experiments. Along the Xstream abutment, however, the scour depth was twice as large. Taking into account the live-bed conditions, where sediment is supplied from upstream causing the scour depth to fluctuate around its equilibrium, a significant difference of at least 20% remained. The principle of a falling apron, a mechanism where individual units at the toe of a structure tumble down, covering one slope of the scour hole and thereby increasing the roughness, could be the reason for this. The erratic shaped Xstream elements enhance complex turbulence patterns very locally. Due to the absence of a supporting filter construction or a bed protection layer, the Xstream abutment was undermined, leading to individual elements decaying at the base of the structure. The interlocking ability of Xstream seems to be stronger when the structure is built with a steeper slope. This insight can be taken into account in the design of Xstream hydraulic structures. The substantial discrepancy in density between the Xstream model units and the angular polystyrene particles must be considered as the geotechnical properties may differ from the real world. The present study has shown the kinetic energy absorbing capacity of Xstream. Turbulence levels increase due to higher roughness. Exposing a uniform structure of Xstream elements to high water conditions might lead to instability which alters both positive and negative effects. Future research must give valuable insight into how the design of Xstream structures could look like for a durable implementation in the Dutch river system.

Contents

List of symbols

Symbol	Definition	Unit
C	Chézy coefficient	$m^{1/2}/s$
d	Water depth	m
d_{15F}	15th percentile filter material size	m
d_{50B}	50th percentile base material size	m
d_{90B}	90th percentile base material size	m
D	Width of obstruction	m
D_*	Dimensionless particle number	-
D_{50}	Median particle size	m
D_{50*}	Dimensionless median particle size	-
D_{90}	90th percentile particle size	m
f_D	Darcy-Weisbach friction factor	-
Fr	Froude number	-
g	Gravitational acceleration	m/s^2
h_s	Scour depth	m
h_0	Initial water depth	m
H	Energy head	m
i_c	Critical gradient	-
k_B	Permeability base material	m/s
k_G	Permeability geotextile	m/s
K_S	Shape factor	-
K_u	Velocity factor	-
K_α	Angle of attack factor	-
L	Length	m
L_*	Dimensionless length	-
n_F	Filter porosity	-
p	Pressure	N/m^2
P	Porosity	-
O_{90}	90th percentile textile openings	m
Q	Discharge	m^3/s
r	Relative turbulence	-
Re	Reynolds number	-
S_0	Water surface slope	m/m
t	Time	h
u	Flow velocity	m/s
u_c	Critical velocity	m/s
$\overline{u_x}$	Mean velocity in x direction	m/s
u_{*c}	Critical shear velocity	m/s
v	Kinematic viscosity	m^2/s
V	Volume	m^3
W	Width	m
W_{wet}	Wet weight	kg
W_{dry}	Dry weight	kg
W_*	Dimensionless width	-
z	Potential head	m

Symbol	Definition	Unit
α	Amplification factor	-
Δ	Relative density	-
θ	Shields parameter	-
ρ_s	Sediment density	kg/m^3
ρ_w	Water density	kg/m^3
Ψ_c	Critical shear stress	-

1 Introduction

1.1. Context

In the 19th and 20th centuries, the Dutch Rhine branches were extensively narrowed and shortened by cutting of river bends (Blom, 2016). This was done to improve navigation, avoid bank erosion, and to allow for a safe transport of ice. For centuries, the Rhine branches have been engineered by constructing levees and groynes (Lely, 1890). Water depth increase and bed slope reduction are responses to these river training works. Yalla Arbós et al. (2019) states that the anthropogenic interference on the river system has been so consistent and strong that the morphological developments in the Rhine are likely mostly related to human interventions.

According to Liefveld et al. (2011), due to incision of the summer bed, an increasing number of groynes are above water for an increasingly longer period of time. Partly because of this, the groynes are now higher than strictly necessary for their functionality. Lowering the groynes increases the flow profile and thus leads to a decrease in the normative high water levels. In the context of the Room for the River measures, floodplains were excavated, dikes were relocated and secondary channels were dug. Furthermore, groynes were lowered and three longitudinal training walls were constructed as a pilot study.

Implementing innovations in the Dutch river system is a response from the Ministry of Infrastructure and Water Management to the increasing pressure from more frequent and intense weather extremes, which have been linked to climate change, and the expansion of both population and economic activities. Higher discharges are becoming more frequent, resulting in the need for rapid discharge to the sea to mitigate flood risks. Conversely, periods of drought lead to low discharge levels, with consequences such as navigation challenges for transport ships and freshwater shortages for water companies. Moreover, these challenges negatively affect the ecological health of the river system.

Rijkswaterstaat, which is responsible for the design, construction, management, and maintenance of the infrastructure and water systems in The Netherlands, explores innovative alternatives for self sustaining river management. In this context, sustainable management strategies that balance competing water usage demands and promote biodiversity are being implemented, along with investments in innovative technologies and infrastructure.

The construction company of Royal BAM Group strives to contribute to the sustainable transformation of the Dutch river system. With its concrete Xstream element, the little version of the widely used Xbloc as a breakwater element for coastal protection and dams, the BAM is exploring new application possibilities in hydraulic structures. This study examines the applicability potential of Xstream in the Dutch river system.

1.2. Literature review

1.2.1. River training works

Rivers and their infrastructure are essential for various purposes, such as inland navigation, preservation of natural habitats and freshwater supply for human consumption and agriculture (Havinga, 2020). To fulfill these functions effectively, river training works are constructed. Each of them is built with specific objectives as reproduced by Blazejewski et al. (1995) and Mosselman (2020): (i) providing flood protection by facilitating discharge during high-water events through the provision of an adequate cross-sectional area; (ii) maintaining navigable waterways; (iii) managing sediment deposition and excavation; (iv) preventing bank erosion; and (v) directing flow along a pre-defined alignment. In the Dutch part of the Rhine, the first groynes were built to prevent the formation of ice, a major cause of dike breaches and flooding. Later river narrowing by extending groyne lengths geared towards improving navigation (Havinga, 2020; Mosselman, 2020).

In addition to transverse structures like groynes and spur dikes, there are also longitudinal structures such as bank revetments and guide bunds, and riverbed structures like solid layers, bendway weirs, and check dams (Mosselman, 2020). Hydraulic structures cause substantial changes to water and sediment flow patterns. Reducing the flow width increases the shear stress on the riverbed. In the search for a new equilibrium, the river cuts in. This causes erosion of the riverbed upstream, which temporarily increases the bed-material load and induces the tilting mechanism of the bed slope (Frings, 2015). This is clearly visible in figure 1.1 by Yalla Arbós et al. (2019). Erosion rates up to 2 cm/year are observed in the river Waal.

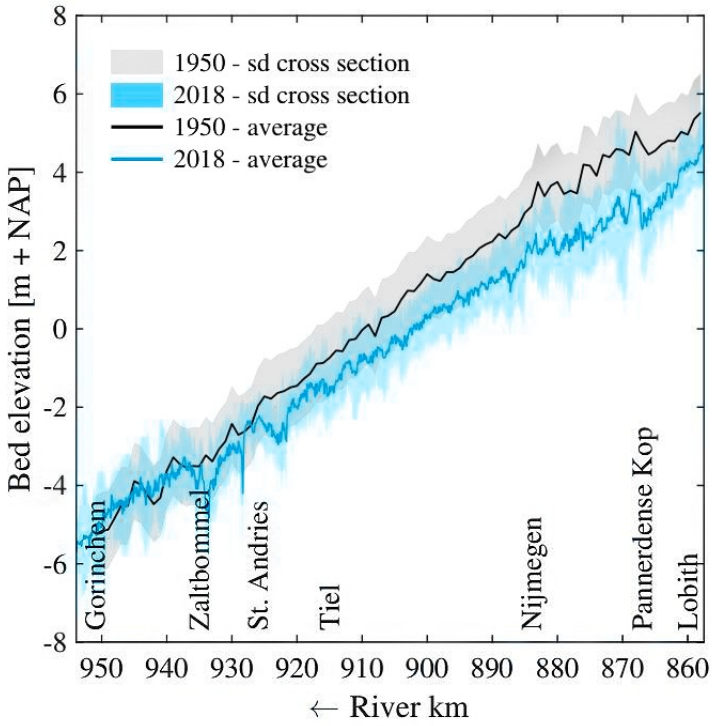

Figure 1.1: Mean bed levels in the Bovenrijn and Waal in 1950 and 2018, with cross-sectional standard deviations (Yalla Arbós et al., 2019).

As a consequence of this river incision, the crest level of the groynes in the river Waal was, relative to the water level, greater than initially designed for. This resulted in an increased flow velocity during high discharges, thereby exacerbating the process of riverbed erosion. Lowering of groynes in the Room for the River projects resulted in an alternating effect of erosion and sedimentation over the entire width of the river. As the cross-sectional area increased during high but relatively low water levels compared to

the situation before lowering of the groynes, the average flow velocity decreased, resulting in net siltation in the summer bed (De Vriend, 2010; Sloff et al., 2014; Van Broekhoven, 2007; Verheij et al., 1997).

Groynes in the Dutch river system traditionally have a layered built-up. They consist of a core of sand or clay, covered with a geotextile which functions as a filter layer, and protected with pitched blocks or large rocks. An immersed, often fascine, mattress is placed on the riverbed to protect the bottom (Buschman & Kosters, 2021; Schiereck, 2019; Verheij et al., 1997). These structures are impermeable. Zooming in on local morphodynamics around a groyne, an erosion pit and a ridge are present just downstream of the head of the groyne as can be seen in figure 1.2.

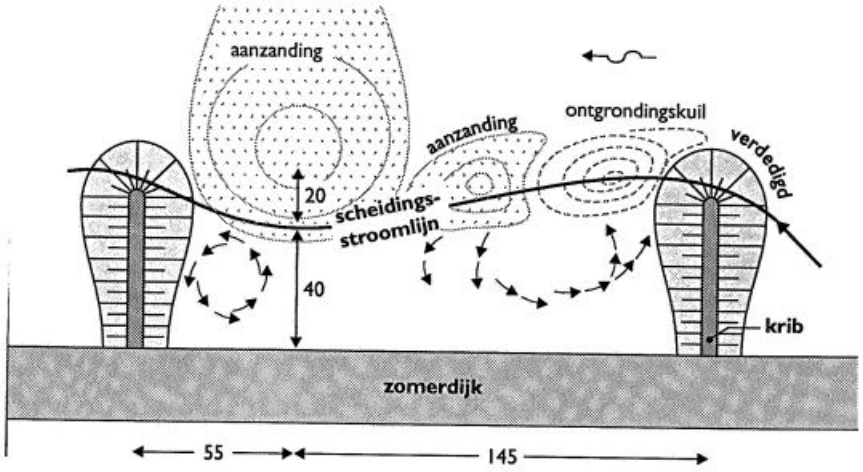

Figure 1.2: Schematic morphological development of the riverbed around groynes (Verheij et al., 1997).

Following Sieben (2007), the average maximum local scour depth around groynes in the river Waal is 2.7 m. While Verheij et al. (1997) states, based on ”highly schematised analytical calculations”, that both local scour depths and siltation reduce due to groyne lowering, the study by Busnelli et al. (2011), which involved field measurements, argues that local erosion is enhanced by the increased frequency of submergence of the lowered groynes. Nevertheless, designing groynes and other river training works comes with great precision. Downstream pointing groynes, for example, attract water and sediment flows towards the river bank, instead of diverting them away. This is the case with groynes that have an upstream inclination and thus function deflectively or repellently (Mosselman, 2020).

In the decades following the first river normalisation operations in the Netherlands, the efforts to enhance individual functions of the Rhine branches have led to conflicting interests. An integrated approach involving regular sediment management and significant structural modifications has emerged according to Mosselman (2020). To deal with these complexities and to increase the delta’s resilience and vitality, alternative approaches to river management are being sought that go beyond conventional ideas. In this context, a pilot project has been initiated, which involves the construction of three longitudinal training walls (LTWs). The project aims to establish a proof of concept for an integrated operation that supports such system-level transformations (Le et al., 2020).

Over a length of 10 km in the river Waal, the traditional groynes have been completely removed from the inner bend and replaced by three LTWs. LTWs are hydraulic structures positioned along the longitudinal axis of the river. They are designed to induce specific flow patterns such as an increase in flow velocity and controlled sediment transport. Additionally, they direct the flow towards the main channel with the intention of enhancing river navigation and stability. The massive structure of these LTWs is similar to that of traditionally layered groynes along almost their entire length. Appendix A provides the technical drawing of the LTW located near Ophemert. During low discharges, the main channel was narrowed by 30 meters (Eerden, 2022).

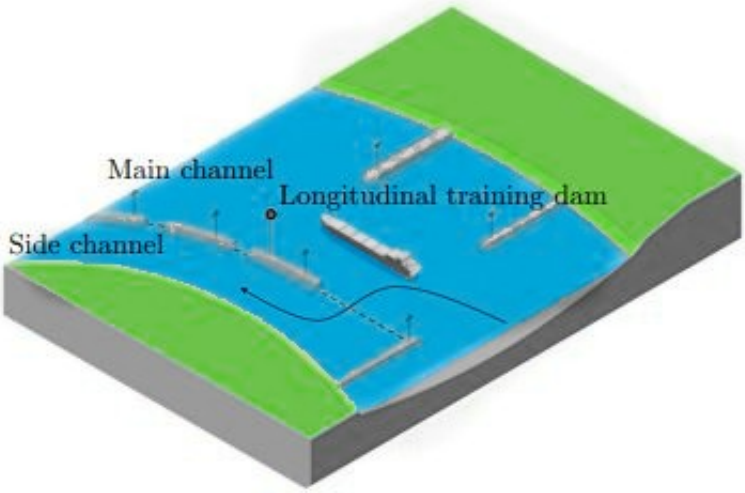

Figure 1.3: Sketch of an LTW (Jammers, 2017).

In the particular section of the Waal, extensive research has been done concerning the impact of the LTWs on the riverbed. Based on field data analysis by Van Weerdenburg (2018), it was observed that the bed elevation decreased during the construction works. This was possibly due to dredging of the river bed material which was used as building material for the LTW cores. Besides, as an initial morphodynamic response to the implementation of LTWs, degradation of the riverbed was observed in the first years after construction. Yalla Arbós et al. (2019) found that the reach where the LTWs were constructed had significant temporal variability in bed level change. However, the final evaluation preformed by Mosselman et al. (2021) from Deltares concluded that, overall, sedimentation had caused the bed level to increase. This aligns with their ADCP measurements. These had shown a decrease in sediment transport capacity. The combination of reduced water depth and lower flow velocity can be explained by the expansion of the total width through bank erosion along the side channel. Field measurements by Czapiga et al. (2022) revealed that, as the river discharge increases, a higher proportion of the flow gets diverted towards the side channel. This leads to the deposition of sediment in the main channel near the upstream end of the LTW. During low water levels, the accumulated sediment tends to redistribute and scour holes fill up.

This temporal evolution in local riverbed morphology raises the concerns about the durability and stability of man-made systems with two parallel channels. Le et al. (2018) carried out 2D numerical tests that replicated an idealized low-land river. They concluded that the location of the upstream starting point of the LTW is of great importance for sediment management in bifurcations, which are inherently unstable. A 3D physical scale model with movable bed by PhD researcher De Ruijsscher et al. (2020) mimicked the upstream end of the LTW near Ophemert. He studied the morphological patterns and discharge division in the entrance region of the LTW by adjusting the sill geometry. His conclusions were that the emergence and decay of bars in especially the side channel can be regulated by the geometry of the sill.

1.2.2. Physical scale models

In hydraulic research, development, and design, laboratory experiments are crucial as many hydraulic processes elude analytical formulation or are not easily or accurately reproduced by numerical simulation (Muste et al., 2017). The application of physical scale models can therefore lead to valuable insights, if scaled correctly. Scaling laws as defined by De Vries (1975) and laboratory techniques written down by Hughes (1993) guarantee a reliable approximation of reality through geometric, kinematic and dynamic similarity.

Experiments with mobile beds where bed load is the dominant sediment transport mode primarily rely on scaling of the Shields parameter. This generally results in a larger Froude number in the model than in the field situation (Ettema & Muste, 2004). To compensate for this scale effect, a lightweight

material can be used as sediment (Frostick et al., 2011). Research by, amongst others, De Ruijsscher (2020), Gorrick and Rodríguez (2014), Kleinhans et al. (2012), and Vermeulen et al. (2014) adopted this method, thereby keeping the Reynolds number high enough to represent fully turbulent conditions. In general, these studies suggest that lightweight granules are appropriate in physical modelling of sediment transport processes (Kocyigit et al., 2005). Being validated on field measurements, numerical model predictions and calculations with founded sediment transport formulae, only slight distortions of bedform dimensions were observed in physical scale models.

1.2.3. Flexible groynes

To effectively assess whether a particular new technology does what it is supposed to do, the next step is to actually put it into practice. As part of Rijkswaterstaat's Self Supporting River Systems (SSRS) program, BAM was granted the opportunity to develop innovations for sustainable river management. In close cooperation with involved stakeholders, BAM designed a groyne made entirely of Xstream elements. In various aspects, this groyne differs from conventional groynes. There is no need to apply a filter or bottom protection layer, a steep slope of 1:1 can be build, and a porosity of 60% is achieved.

Following a thorough period of development, testing and validating, the first flexible groynes were constructed as a pilot project. They were located near the city of Kampen in the summer bed of the river IJssel: two in the inner bend and one in the outer bend of the river. After three years of monitoring, the two groynes in the inner bend were removed in November 2022. The released Xstream elements were used to extend the groyne in the outer bend to the beacon line of the existing groynes. Intensive monitoring on the stability of the groyne, sediment relocation and ecological status in the near-field is done using motion sensors, ADCP and radar measurements and cameras. Figure 1.4 shows a picture of this flexible groyne.

Figure 1.4: Extended flexible groyne in the river IJssel where the dark coloured Xstream elements on the left used to be the groyne before extension.

Scientific publications about the flexible groyne are not available. However, a number of students dedicated their graduation project to this pilot. Jongschaap (2022) used a physical scale model to understand the impact of groyne slope and permeability on the river discharge coefficient. In his master's thesis, Van Alderwegen (2021) employed a numerical model to study the difference in local flow characteristics for the features of a flexible groyne compared to conventional groynes.

1.3. Knowledge gap

The literature review preceding the current research reveals a gap in understanding of the local morphological variations induced by Xstream structures. The properties of Xstream elements can reasonably expected to alter the flow patterns of water and sediment in the river. It is, however, unclear yet to what

extend contraction scour and local scour are affected. Furthermore, placing Xstream elements directly on the river bed creates an open filter-like construction. If the occurring gradient is above the critical value for sediment transport, the material under the construction may erode leading to the subsidence of individual elements and possibly instability of the structure.

The higher porosity inherent to the random arrangement of Xstream elements may lead to a reduced diversion of water towards the main channel compared to traditionally constructed river training works. The application of Xstream elements is likely to effectively absorb motion forces of flowing water. A potential positive implication could be the mitigation of local scouring effects, resulting in shallower and/or shorter erosion pits in comparison to those encountered with conventional structures. Conversely, a decreased average flow velocity over the entire width and along the engineered reach of the river might enhance sedimentation and therefore the need for regular maintenance and dredging works.

On the contrary, structures composed of Xstream units exhibit an increased hydraulic roughness due to the erratic shaped elements protruding compared to precisely pitched blocks. Furthermore, the achievable steeper slope when building with Xstream might result in more severe turbulence, amplifying local scour effects in the adjacent vicinity.

1.4. Research questions

The primary objective of this research is to determine the feasibility of applying Xstream elements in the construction of river training works. Sediment displacement in the near-field around different structures will be analysed and predicted by means of a physical scale model. By accomplishing the objective, this study aims to assess the alterations in riverbed morphology in response to steep and porous hydraulic structures of Xstream, thereby contributing to the fundamental knowledge on riverbed formation. Appendix B briefly elaborates on the iterative process of formulating the exact research questions throughout this thesis. The following ones will be answered in this report:

What flow patterns influence the morphodynamics around Xstream river training works?

How well does the used physical scale model perform in mimicking reality?

To what extent plays a higher porosity and wall roughness part in local sediment displacement?

How does the slope of an embankment affect erosion and sedimentation?

1.5. Scope

Water entering The Netherlands through the Rhine is distributed into three main tributaries. Via the Pannerdensch Kanaal, water enters the IJssel and the Lower Rhine. Most of it, however, finds its way towards the North Sea through the river Waal (Hooijer et al., 2007). With 80%, the share of water received by the Waal from the Upper Rhine is highest at lower discharges. The weir at Driel regulates this share as water in the Pannerdensch Kanaal is impounded as long as this weir is in operation. As the Upper Rhine discharge increases, this effect decreases the Waal's share in percentage terms to 64% at extreme discharges (Rijkswaterstaat, 2012).

Promising outcomes from the pilot with LTWs in the Waal have stimulated Rijkswaterstaat's keen interest in implementation on a broader scale, where practically feasible (Mosselman et al., 2021). Looking at the design of the LTW near Ophemert, which is included in Appendix A, in detail, it can be seen that two sections do not have a typical layered structure but are built completely from large rock. These sections are located at the entrance of the side channel and approximately 2 km downstream at the sill, both of which are only submerged during high water. The rock used in these lower sections has a

coarse grading of 40 - 200 kg and a porosity of around 30%. This application of hydraulically permeable structures in the Dutch river system is only one example, yet it is the starting point for this study into the possible expansion of Xstream usage.

The present study focuses on the hydraulic conditions in the river Waal during high water. In this case, hydraulic loads can exceed soil resistivity levels, initiating erosion and sedimentation processes. The riverbed predominantly consists of sand with a median particle size (D_{50}) of 1.2 mm, and a 90th percentile particle size (D_{90}) of 2.0 mm, which results in mainly bed load sediment transport (Duró & Gradussen, 2022; Ten Brinke, 1997; Vermeulen et al., 2014). In a high water situation, the water depth reaches 8 m, which corresponds to a total discharge of 4600 m³/s, while the flow velocity typically averages around 1 m/s (Reeze et al., 2017; Van de Mortel, 2005; Visser & Klopstra, 2002).

Due to limitations, about which more later, the employed physical scale model mimics only a small width of a river's cross section. The focus is therefore on the near-field (an area with a radius of ca. 15 m on field scale) morphodynamic changes to the riverbed induced by Xstream hydraulic structures. These structures will have a shape similar to spill-through abutments. Influenced by the quantity and size of the available Xstream model units, this design was devised to examine the interaction between the river bed and the water and sediment flows that frontally strike and parallelly flow along the Xstream embankments, as in the case of the LTWs.

1.6. Thesis outline

Chapter 1 provided some background information about river training structures and the engineered Dutch river system. Following this, a knowledge gap was revealed and research questions were defined and confined to a specific scope. The methodology to answer these research questions is explained in Chapter 2. This chapter describes the materials, facilities and measuring equipment used in the physical scale model and summarizes on the different setups whereas Appendix C gives detailed information on the parameters set in the model. Next, Chapter 3 presents the results of the model. These are analysed in Chapter 4. A selection of pictures taken during the experimental phase of present research is included in Appendix D. In Chapter 5, results of the physical scale model are questioned and discussed. A critical note is made and a some practical applications are listed. Finally, the conclusions and recommendations are given in Chapter 6.

2

Methodology

2.1. Approach

2.1.1. Flow patterns

The first research question to be answered, *What flow patterns influence the morphodynamics around Xstream river training works?*, is approached by extensively analysing literature. With this question, I want to sketch an image of the existing knowledge on water and sediment flow patterns around hydraulic structures. In particular, I aim for permeable groynes and abutments. What vortexes exist at groyne heads? What are the flow characteristics along longitudinal structures? What is the effect of flow depth, velocity and uniformity on the local morphology?

2.1.2. Model accuracy

How well does the used physical scale model perform in mimicking reality? is the second research question to be addressed. The head of the flexible groyne will be mimicked and exposed to high water conditions in the river IJssel in an experimental setup. Bed scans and flow velocity data of the model will be compared to field measurements and observations. The location and dimensions (length, width and depth) of the resulting erosion pit close to the groyne head will be evaluated in particular. Additionally, the average measured flow velocity in the downstream direction through the structure in the model will be verified on dye tests and Acoustic Doppler Current Profiler (ADCP) measurements conducted in the field. This way, I will be able to relate the likelihood of occurrence of certain results from the physical scale model to the real world.

2.1.3. Porosity and roughness

The answer to the next research question: *To what extent plays a higher porosity and wall roughness part in local sediment displacement?* is three-fold and required data will be gathered by means of two scale model setups. One will be made out of Xstream and one out of stone. One of the unique specifications of Xstream elements is their high porosity when randomly placed. Furthermore, the surface roughness of Xstream structures is considerably high as a result of the shape of each individual element. First, I will quantify the difference in porosity and wall roughness between the two setups. By saturating a known volume of each of the two materials, the pore volume can be determined. The difference in permeability between Xstream and stone will be measured by comparing the mean flow velocity in downstream direction through the model structures. High-resolution elevation data allows the comparison of the mean standard deviation over the average cross-sectional height of each structure. This value will serve as a measure of the roughness of a structure.

As a second step, I want to show that a higher porosity and wall roughness induce a lower average streamwise flow velocity but a higher relative turbulence. The latter is defined as:

$$r = \frac{\sqrt{\overline{u_x}^2}}{\overline{u_x}} \quad [2.1]$$

where $\overline{u_x}$ is the mean flow velocity in the downstream direction (m s^{-1}) to the formulation by Schiereck (2019). Throughout the experiments, flow velocities in the x, y and z direction will be measured.

The last thing to do is compare morphological data by analysing erosion and sedimentation patterns. Especially the scour development at the leading edge and along the longitudinal direction of a structure is of interest for this study. The degree of morphological development over the experiment will be linked to other observations and measurement results.

2.1.4. Slope

The data that is needed to give answer to the next research question: *How does the slope of an embankment affect erosion and sedimentation?* will be acquired by building a setup with an increased slope. The structure will consist of the same Xstream elements as used to answer the previous research question. Therefore, porosity and roughness of both structures will be the same. A notable feature of Xstream is the strong interlocking capability between individual elements, enabling the construction of steep slopes.

By continuously measuring flow velocities in the main channel in three dimensions, I aim to prove that the relative turbulence is higher at steeper slopes. The effect of this on the elevation of the river bed will be analysed using the same statistical method as before.

2.2. Dimensional analysis

A physical scale model aims for an idealised representation of reality. To achieve geometric similarity between the model and existing river training works and bank protections, the dimensional variables for a characteristic length (L), width (W), depth (d) and median particle diameter (D_{50}) in metres must be set. Through dimensional analysis, the non-dimensional variables for length, width and median particle diameter respectively become L_*, W_* and D_{50*} according to:

$$L_* = L/d \quad [2.2]$$

$$W_* = W/d \quad [2.3]$$

$$D_{50*} = D_{50}/d \quad [2.4]$$

To ensure dynamic similarity between the model and reality, the dimensionless variables that characterize flow, sediment transport, and morphology must be equal. The submerged density of sediment, Δ, which represents the ratio of gravity and buoyancy, can be calculated according to equation 2.5 where ρ_s is the sediment particle density (kg^{-1} m^3) and ρ_w the density of water (kg^{-1} m^3).

$$\Delta = (\rho_s - \rho_w)/\rho_w \quad [2.5]$$

The Reynolds number describes the ratio of inertial forces to viscous forces in a moving fluid. Open channel flow is turbulent for Re > 2000 - 3000. Its value can be determined by equation 2.6 in which u is the flow velocity (m s^{-1}) and v is the kinematic viscosity (m^2 s^{-1}).

$$Re = ud/v \quad [2.6]$$

A non-dimensional number to describe the ratio between inertia and gravity is the Froude number. The value is typically less than 1 for flows where gravity is the dominant force. It is often used in conjunction

with the Reynolds number. Quantifying the Froude number can be done according to equation 2.7. The gravitational acceleration (m s^{-2}) is expressed by g.

$$Fr = u/(gd)^{0.5} \quad [2.7]$$

The equilibrium slope is the balance between gravity and drag and is described by equation 2.8 The Chézy friction coefficient in this formula, C ($m^{0.5}$ s^{-1}), can be determined by measuring the water surface slope during the experiments.

$$S_0 = u^2/C^2 d \quad [2.8]$$

From the set of previously defined parameters, the dimensionless particle number can be obtained (Van Rijn, 1984a). The bed-form regime is based on this D_* (Van Rijn, 1984b), which represents the relation between the combined effect of gravity and buoyancy.

$$D_* = \Delta^{1/3} Re^{2/3} Fr^{-2/3} D_{50*} = D_{50} \left(\frac{\Delta g}{v^2} \right)^{1/3} \quad [2.9]$$

The stability of loose grains is approached by Shields, who considered the friction force caused by flowing water on an area significantly larger than one individual grain (ie. the river bed). Instead of using the critical flow velocity, the actual velocity was used to define the Shields parameter in his study. This caused the Shields parameter to describe the mobility rather than the stability of the bed. The ratio between drag, buoyancy and gravity acting on one single particle is therefore expressed by the Shields parameter, θ, which can be approached by equation 2.10 (Engelund & Hansen, 1967).

$$\theta = \frac{u^2}{C^2 \Delta D_{50}} \quad [2.10]$$

2.3. Facilities and materials

2.3.1. Straight flume

The experiments were carried out in the Kraijenhoff van de Leur Laboratory for Water and Sediment Dynamics at the Wageningen University & Research. The straight horizontal flume of 0.7 m x 2.6 m x 12.6 m (internal height x width x length) is equipped with water and sediment recirculation pumps. The pumps are connected to electromagnetic flow meters to monitor discharge. To reduce inlet induced turbulence at the upstream end of the flume, a stacked pile of PVC tubes is used as a laminator. A weir at the end of the flume can be moved up and down to adjust the water level as required.

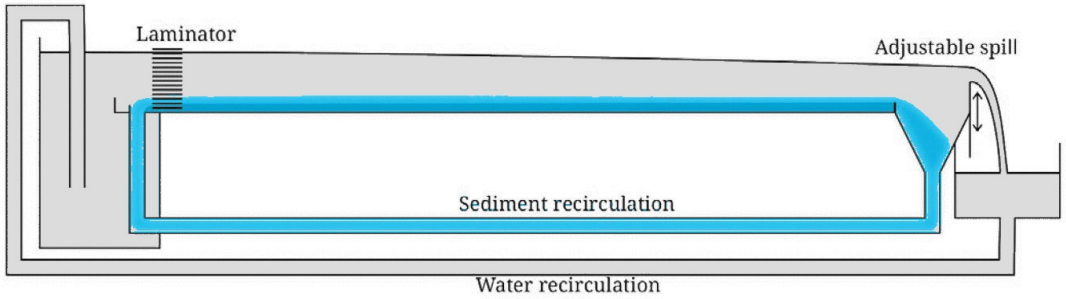

Figure 2.1: Schematic drawing of the straight flume with a separated water and sediment recirculation system (Vermeulen et al., 2014).

2.3.2. Lightweight polystyrene

In this study, lightweight sediments were employed to study the local morphological response to variations in porosity, roughness and geometry of river training works. The lightweight polystyrene granules imitated a sandy river bed. The material has a density of 1055 kg/m^3 and consists of angular and of cylindrical-shaped particles with a D_{50} of 2.1 mm and a D_{90} of 2.9 mm. These granules are originally used as raw material in the plastic molding industry but have been employed in physical model research before. Since the last experiments a few years ago, the material has been in outside storage in large big bags. This left it exposed to weather fluctuations and biotic and abiotic influences for quite some time.

2.3.3. Xbloc model units

As part of the Royal BAM Group, Delta Marine Consultants carries out 2D physical model tests for breakwaters and shore protections in their hydraulic laboratory in Gouda. Xbloc model armour units, which are in shape the same as the Xstream blocks, are available in many different sizes. The model units used for this study are 4 cm in height (D in figure 2.2) and each weigh close to 49 grams. This makes that they have a density of 2367 kg/m^3, which is about the same as the density of concrete.

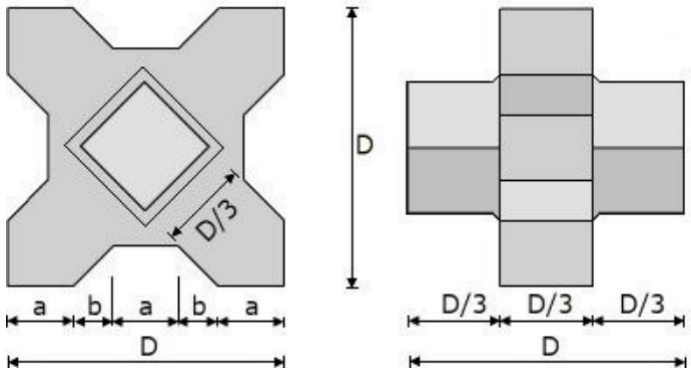

Figure 2.2: Shape and proportions of an Xstream element.

2.3.4. Quarry stone

Scaled down quarry stone was used to imitate materials commonly used in the field of hydraulic engineering. The circled sections of the LTW in Appendix A consist mainly of rocks in the 40-200 kg range, with average diameters of 37-42 cm. For this study, stones ranging in size from 5 to 7 cm were used. These are typically used in gabions or as decorative elements in gardens. Similar to the Xbloc model units, the quarry stone retains the same density as in reality.

(a) Xstream model units

(b) Scaled quarry stone

Figure 2.3: The two materials to be compared.

2.3.5. Geotextile

A fly screen with a very fine mesh was applied in some of the model setups to allow for more support of the structure on the much lighter plastic granules. The plastic mesh fabric imitated a geotextile, which is commonly used in layered structures as filter and protection layer to enhance the soil's mechanical properties. The criteria for geometrically closed filters defined by Schiereck (2019) were met by the mesh fabric. Equation 2.11 presents the retention criteria which means that the openings of the geotextile should be small enough to prevent excessive migration of soil particles. Equation 2.12 describes the permeability criteria for a geotextile as it must be permeable enough to allow water to pass through it without significant impedance.

$$O_{90} < 2d_{90B} \quad [2.11]$$

$$k_G > 10k_B \quad [2.12]$$

2.4. Data collection and processing

The laboratory is equipped with high-end instrumentation and measuring equipment. This section explains the most relevant methods of data acquisition and handling throughout and after the experiments.

2.4.1. Line laser scanner

To measure bed forms before and after each experiment, a line laser scanner will be used. This system allows for the collection of high-resolution bed elevation data with an accuracy of up to 1 mm^2. The measurement method features a line laser and a SICK Ranger 3D camera, both mounted on a carriage that can move on a fixed rails along the length of the flume. Via a remote desktop with a self-developed software program by the WUR, the carriage is controlled and the data is directly stored in a data file. The laser projection is oriented perpendicular to the flow direction and the camera is positioned at an angle as illustrated in figure 2.4. The camera's alignment with the laser line, together with the positioning of the instrument in the spatial, is accurately calibrated. The bed elevation of each point on the laser line, consisting of 154 individual points, is interpreted by means of triangulation.

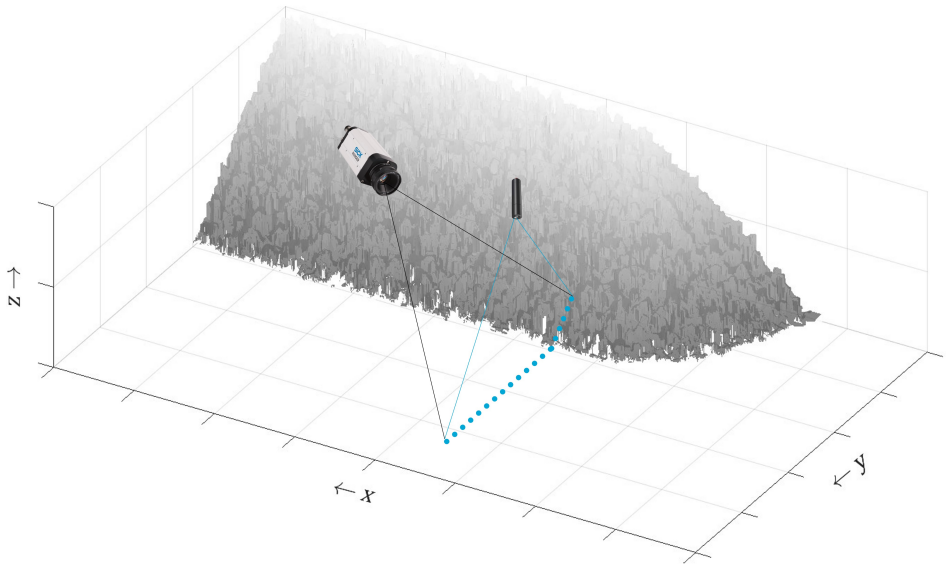

Figure 2.4: A 3D camera measuring the elevation of the projected laser line made up of 154 individual points.

The bed elevation is measured with a 2 mm resolution in the x direction along the length of the flume. The present study allows a lower resolution than what is possible for the purpose of speeding up each

scan. Multiple parallel and partly overlapping strokes were necessary to measure the full width of the flume, as the width of the laser beam swath is limited by its 50° angle. The camera was positioned at a constant height, the z plane, of approximately 400 mm above the initial bed level. Starting at 120 mm from the left side of the flume, looking in downstream direction, and with y-steps of 360 mm, the entire width of the flume was covered with seven strokes of the laser scanner.

To make the raw data workable, the programming and numeric computing platform Matlab is used. The irregularly dispersed elevation data points in the y direction are arranged in a 1 cm x 1 cm regular grid. Each cell value is determined by interpolating the average from the data points that fall within the corresponding grid cell. Any outliers and measurement errors are removed.

2.4.2. Acoustic Doppler velocimeters

For the purpose of this study, it is interesting to measure the exact flow velocity through both the main channel and the porous structures. Therefore, two acoustic Doppler velocimeters (ADVs) are installed in the flume: one inside each structure, surrounded by a bird wire cage, and one roughly 30 cm out of the base of the structure. Both ADVs are submerged at a depth equal to 0.6 times the initial water depth, taken from the water surface.

An ADV operates by the principle of Doppler shift which is used to measure the velocity of water in three dimensions. An acoustic transmitter sends out sound pulses with a fixed frequency. The sound waves bounce off of moving suspended particles and are detected by three or four probes as backscatter reflections. The change in frequency of the received sound wave is then used to compute the velocity of the water in the x, y and z direction.

Two different types of velocimeters are employed in this study: one vertical Vectrino Profiler and one with side-looking probes. In essence, both instruments function in the same way. However, where the one has a better response in the vertical z velocity component, the other has lower noise in the vertical y direction. Both instruments run with their own software program. The analysis of the data is performed using both of these software programs as well as Matlab.

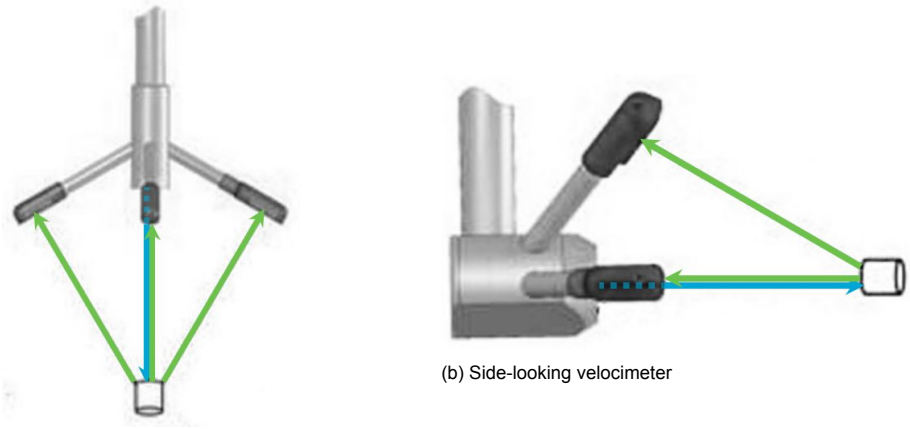

(a) Vertical Profiler

(b) Side-looking velocimeter

Figure 2.5: Two velocimeter probes where the blue arrows indicate the emitted signal and the green arrows the reflected signal.

2.4.3. Linear position sensors

Along the length of the flume, strategically positioned tubes gauge water into four stilling wells. Gauging the water effectively mitigates sudden fluctuations in water levels, minimising the disturbance of water level readings. In each stilling well floats a magnetic sphere. The linear position sensors, relying on the principle of magnetostrictive ultrasonic time measurements, continuously measure the distance to each sphere. The measurement results of these transducers are up to 0.1 mm accurate. Post-processing of the data is done in Matlab.

2.5. Model setups

The hydraulic conditions in the rivers Waal and IJssel during high flow are the basis for all experimental setups in this study. In theory, only adjusting one parameter each experiment would be most beneficial for measuring the effect that one parameter has on the sediment displacement around hydraulic structures. This, however, is practically impossible for the scale of these experiments. The focus is therefore to keep at least the most important parameters constant for all experiments, about which in paragraph 2.5.1 more. The set of variables that remains the same in all experiments is listed in table 2.1.

Table 2.1: Set of unchanging parameters.

Symbol	Variable	Unit	Prototype	Model	Ratio
D_{50}	Median particle diameter	mm	1.20	2.10	0.57
ρ_w	Density of water	kg m^{-3}	1000	1000	1
ρ_s	Sediment density	kg m^{-3}	2650	1055	2.51
Δ	Difference in density	-	1.65	0.055	30
v	Kinematic viscosity	m^2/s	1.33e^{-6}	1.08e^{-6}	1.23
g	Gravitational acceleration	m/s^2	9.81	9.81	1

Extensive descriptions of each experimental setup, including tables with particular parameter values, can be found in Appendix C. Table 2.2 lists the different experiments and table 2.3 gives an schematised overview of the experimental setups built for this study. The code names will be used later in this thesis to refer to the relevant configuration. In table 2.3, ”Blockage” refers to the cross sectional flow area of the flume that is obstructed by each structure.

Table 2.2: List of experiments.

Code	Configuration	Slope	Date	Remarks
FG1	Flexible groyne	1:1	June 29th 2023	High water conditions
FG2	Flexible groyne	1:1	June 30th 2023	Extreme high water conditions
XG1	Xstream abutment	1:2.5	May 25th 2023	No Vectrino Profiler
XG2	Xstream abutment	1:2.5	June 9th 2023	-
SG1	Stone abutment	1:2.5	June 1st and 2nd 2023	Spread over two days
XS1	Xstream abutment	1:1	June 15th 2023	Collapsed structure
XS2	Xstream abutment	1:1	June 22nd 2023	-
T1	Structure-less	-	April 21st 2023	One hour duration
T2	Structure-less	-	April 26th 2023	Complications during draining
T3	Structure-less	-	May 3rd 2023	Discharge of 165 l/s
T4	Structure-less	-	May 15th 2023	Two hour duration
E1	Empty flume	-	April 13th 2023	-
E2	Empty flume	-	April 13th 2023	-

In the weeks before to the actual experiments, multiple test runs were carried out in the flume. T1 - T4 featured only a horizontal bed of polystyrene material without a structure being built on it. The length of the test section was shortened to 10 m by means of a movable wall of 20 cm high, which was put 2 m downstream for the actual experiments. Appendix D includes a collection of photos taken from the preparation to the execution of the experiments.

At the beginning of each experiment, the polystyrene bed was levelled and compacted by gradually filling the flume with water. Once the bed was settled, the flume was slowly drained after which the setup could be built. At the end of each experiment, all materials, except for the polystyrene, were taken out from the flume, allowing the bed to be prepared for the next run.

Table 2.3: Graphical overview of experimental setups.

Code	Top view	Cross sectional drawing	Blockage
FG1 FG2	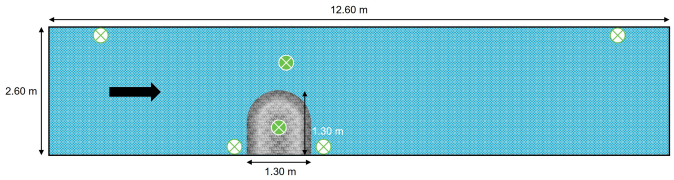	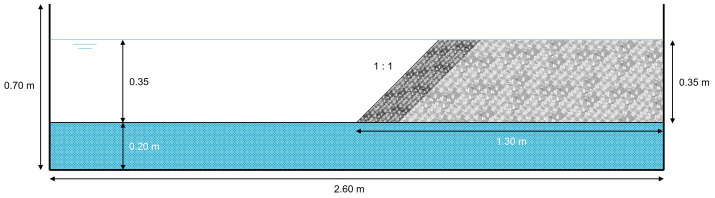	43%
XG1 XG2	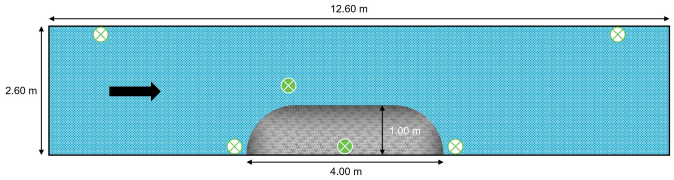	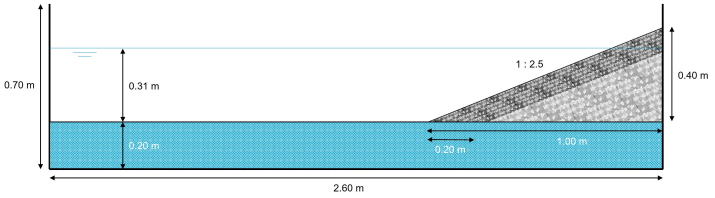	23%
SG1	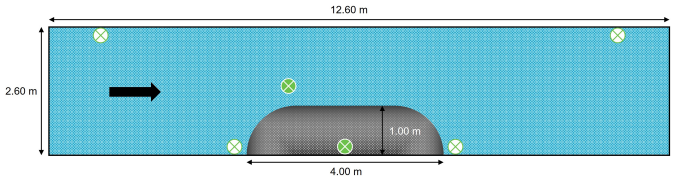	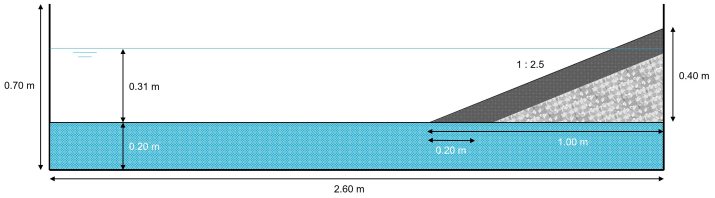	23%
XS1 XS2	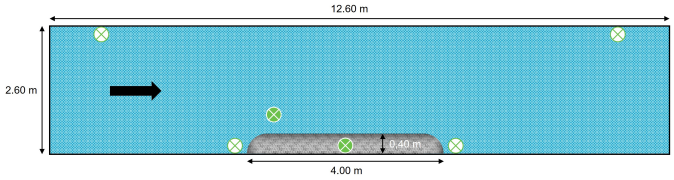	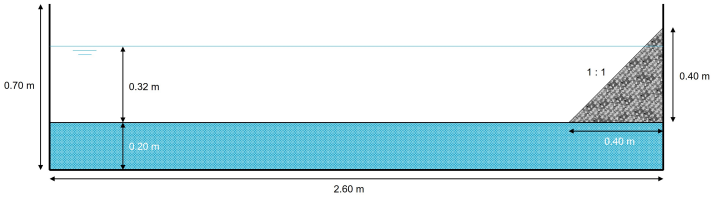	9%

Xstream model units
(D = 4 cm)

Xstream model units
(6.7 < D < 7.2 cm)

Quarry stone

Polystyrene

Stilling well

Vectrino meter

2.5.1. Scaling laws

According to Vermeulen et al. (2014), physical scale models with movable beds primarily rely on scaling of the Shields parameter. Scaling based on the shear stress leads to a much higher Froude number, which significantly influences the resulting morphology (Ettema & Muste, 2004). However, to scale water movement properly, the Froude number and hydraulic roughness must be in the same range. Using lightweight sediments that magnify the mobility is one way to achieve dynamical similarity of both sediment transport and the basic characteristics of the mean flow in a physical scale model. Although Frostick et al. (2011) argues potential drawbacks related to buoyancy, the angle of response, skin friction and bed-form shapes when working with lightweight sediments, its use in physical scale models may be considered one of the few options to achieve dynamical similarity of both sediment transport and the basic characteristics of the mean flow (Vermeulen et al., 2014).

Scaling laws 2.13 - 2.15, where n is the scale ratio, applied for these experiments.

$$\theta_p = \theta_m \implies n_\theta = \frac{n_u^2}{n_C^2 n_\Delta n_{D_{50}}} = 1 \quad [2.13]$$

$$D_{*p} \approx D_{*m} \quad [2.14]$$

$$D_* = D_{50} \sqrt[3]{\frac{\Delta g}{\nu^2}} \quad [2.15]$$

2.5.2. Constrictions and concessions

Due to limitations of the test facilities, the theoretically most optimal conditions could not be reached during the experiments. Prioritizing reliable scaling of key parameters, therefore, was inevitable when confronted with these constraints. The Shields parameter, which represents the sediment transport capacity in relation to the shear stress induced by the flow, and the Froude number, which describes the ratio between inertia and gravitational forces, emerged as the key parameters for this study. To replicate the real-world situation, the high water characteristics of the Waal river were scaled down while maintaining these two parameter values unchanged. This approach, however, required trade-offs concerning other parameters.

1. **Xstream scale model units**
   In reality, Xstream elements are 33.2 cm high. This means that the geometric scaling factor of the physical scale model n_L = 8.3 when using the 4 cm high model units. As a result, the flume could mimic a river section of about 20 metres wide and 100 metres long at most. The primary purpose of river training works is to concentrate water in the main channel. However, contraction in the laboratory setups was greater than in reality due to the high structure-to-channel width ratio.

2. **Flume specifications**
   The internal flume height and maximum pump discharge capacity were two facility limitations that necessitated iterations of the intended flow depth and velocity to correctly scale the Shields and Froude parameters. Whereas in reality, water levels at high water can reach up to 8 m, the model can only mimic a maximum of around 3 m. This is due to its effective maximum flow depth of 45 cm, allowing for a margin to the edge of the flume. By compromising on the flow depth, the flow velocity should be reduced for proper scaling of the Froude number. The maximum pumping rate of 185 l/s, led to another decrease of both flow depth and velocity. When looking at the Shields parameter, the most significant concession was made to the Chézy coefficient. The lower this coefficient is, the lower the average flow velocity or the steeper the hydraulic gradient will be.

3. **Setting parameter values**
   Vermeulen et al. (2014) argued that the Chézy coefficient could not be determined a priori to the experiments and therefore adjusted the discharge based on the measured water surface slope to obtain the correct Shields parameter value. Unlike their study, the present study relies

entirely on the assumption that the theoretically calculated parameter values will be met during the experiments. However, as the low geometric scaling factor is expected to result in a minimal difference in water level over the reach of the experiments, the water surface slope can not be determined with absolute certainty during the experiments. As a consequence, the intended parameter values will not exactly correspond with the measured values.

4. **Cross-sectional area**
   To compensate for the reduction in cross-sectional area caused by the size of the model setups, the discharge was adjusted for each experiment with a unique geometry. This adjustment was necessary to ensure that the Shields and Froude parameter values at the location of the structure corresponded to the actual conditions in the river.

5. **Structure length**
   River training structures are often longer than 100 metres. The LTW in Appendix A, for example, is almost 3 km in length. With the geometrical scale factor used in these experiments, it is physically not possible to reproduce the full length of such structures in the experimental flume. As the aim of this study is to obtain the most accurate representation of the local morphology over the length of the abutment, the model setups should be as long as possible. Nevertheless, the availability of Xstream scale model units is limited. A combination of larger size units will therefore be used to construct the core of the structures.

6. **Run time**
   Since presence will be required at all times during each experiment, proper scaling of the run time based on Froude scaling will not be possible.

3

Results

3.1. Flow patterns and sediment transport

In a natural river system, the processes of erosion and sedimentation are inevitably present. Human interventions alter hydraulic flow patterns and sediment movement. Scour is affected by flow rates, channel and sediment characteristics, and the location and type of hydraulic structures. The total scour depth is the sum of any applicable natural scour, contraction scour and local scour. The effect of river training works on the former scour type is beyond the scope of present study and will therefore be disregarded.

3.1.1. Contraction scour

Lateral river constriction resulting from man-made structures induces an increase in flow velocity. This aligns with the principle of continuity, which states that a reduced flow area corresponds to an increased flow velocity in a fluid like water. As the Bernoulli principle implies (equation 3.1), an increase in flow velocity in the streamwise direction is accompanied by a decrease in pressure:

$$H = z_1 + \frac{p_1}{\rho g} + \frac{{u_1}^2}{2g} = z_2 + \frac{p_2}{\rho g} + \frac{{u_2}^2}{2g} \qquad [3.1]$$

$$\text{Energy head} = \text{location} + \text{pressure head} + \text{velocity head}$$

The pressure decrease over the riverbed at the contraction can cause sediment erosion. The water depth, z, will therefore become larger in the contracted section and a new balance will be established. Contraction scour refers to the difference in bed elevation between the narrowed and wide river cross-sections (Kirby et al., 2015).

Figure 3.1 illustrates how the flow lines are forced around the constriction, resulting in a convergence of these flow lines.

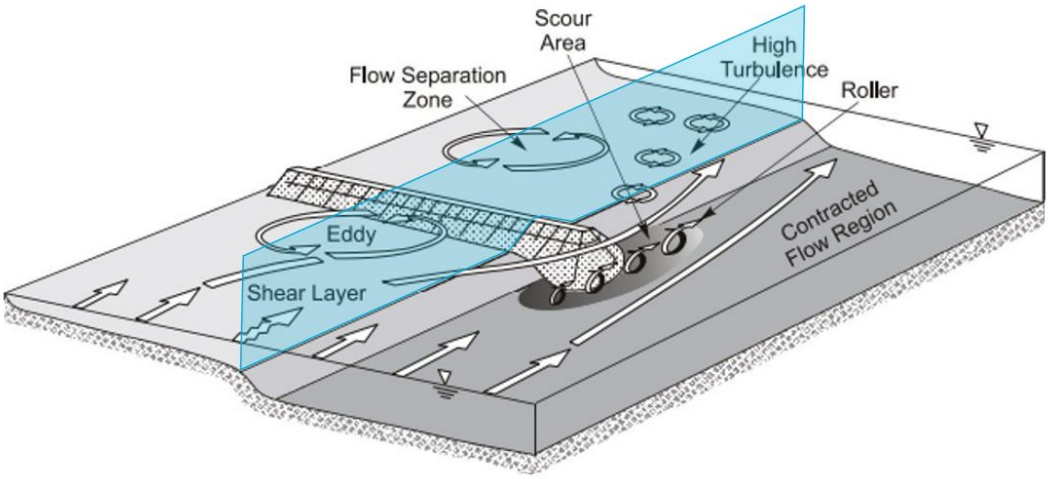

Figure 3.1: Contracted flow pattern (Ettema et al., 2003). The area in front of the blue surface was modelled in this study.

3.1.2. Local scour

Local scour near an obstruction is caused by the vortices and flow acceleration resulting from flow striking the obstruction and moving past it. The increase of turbulence can exert increased erosive forces on the adjacent bed. As a result, the rates of sediment movement and erosion are locally enhanced around these structures.

At the upstream end of an abutment, the water decelerates and the water level rises with the local velocity head ($u^2/2g$). The pressure rises with $\Delta p = 1/2\rho u^2$ as a result of a decreased flow velocity. A downward pressure gradient is the result of higher flow velocities near the water surface than near the bottom, while there is a constant piezometric level over the waterdepth. This causes a vertical flow as can be seen in figure 3.2. A circulating current accelerates along with the flow, leading to a horseshoe-shaped vortex. This vortex enlarges its size with the development of the scour hole (Schiereck, 2019). Based on experiments, Fakhimjoo et al. (2023) found that the downward vertical velocities are highest at the leading edge of an abutment. The primary vortices, which become stronger with depth (Ong et al., 2004), were the main cause of the scour around the abutment.

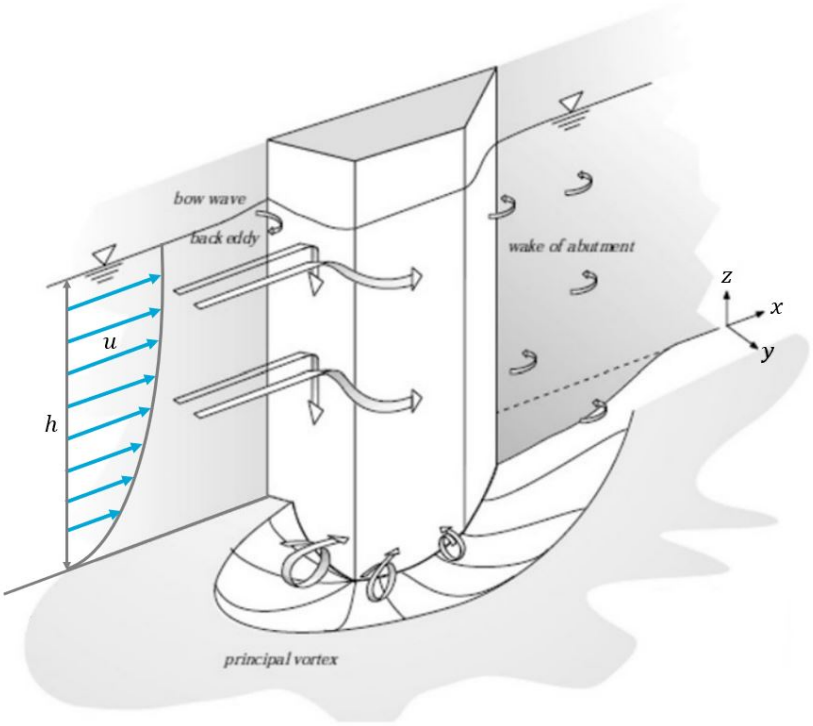

Figure 3.2: Local flow patterns around an abutment (Graf & Altinakar, 2016).

3.1.3. Porous flow

The principle of conservation of energy states that the total energy remains constant along a streamline in a steady flow. The extent to which the kinetic energy of flowing water is transformed into potential energy depends on the absorptive capacity of the obstruction. The porosity created during the construction of these hydraulic structures can increase their ability to absorb water motion forces.

Porosity, together with the shape, size and interconnectivity of the open spaces, are properties of a structure that determine how easily a fluid can flow through it. This is called the permeability. Amplified permeability reduces the resistance to water flow through or around hydraulic structures and improves the efficient dissipation of energy by evenly distributing the water.

The design of river training structures built from Xstream elements is very similar to the open filter principle. The underlying concept of a geometrical open filter is that the grains in the base layer can physically erode through the filter layer, but the resulting gradient remains below a critical value. As

shown in Figure 3.3, the gradient in both layers is more or less identical ($i_F = i_B$), but the flow velocity in the filter layer is significantly higher than in the base layer ($u_F >> u_B$). This difference in flow rate at the interface generates a shear stress on the upper particles within the base layer (Schiereck, 2019).

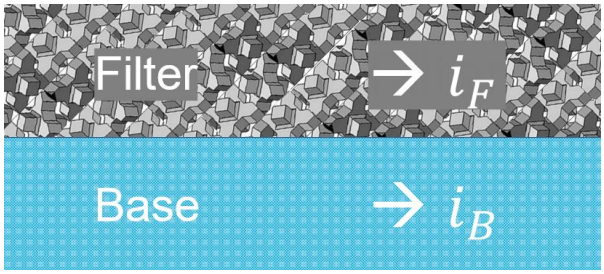

Figure 3.3: Parallel flow in granular open filter. The filter material consists of Xstream elements and the base material is the lightweight polystyrene.

Typically, the Darcy approach is used to calculate flow in porous media. However, this approach is not suitable for describing the non-linear behaviour of turbulent flow in permeable structures. Instead, the Forchheimer equation, which defines turbulent flow as a pressure difference over a length scale, can be employed for these computations. De Graauw et al. (1984) adapted this equation and came up with an empirical relationship to calculate the critical gradient of the base material.

$$i_c = \left[\frac{0.06}{n_F^3 d_{15F}^{4/3}} + \frac{n_F^{5/3} d_{15F}^{1/3}}{1000 d_{50B}^{5/3}} \right] u_{*c}^2 \qquad [3.2]$$

Equation 3.2 includes the porosity (n_F) and the diameter of the filter material, where 15% is smaller (d_{15F}). In addition, the mean diameter of the base material (d_{50B}) and the critical shear velocity according to Shields (u_{*c}) are part of it.

3.1.4. Steepness

In his thesis, Van Alderwegen (2021) concludes that increasing the head steepness of groynes results in an elevated intensity of shear stresses acting on the riverbed. Furthermore, this leads to higher flow velocities in the near-field and increased turbulence. Together, these factors contribute to more severe erosion.

This aligns with the initial theoretical approach to the erosion depth, (h_s), as described by Schiereck (2019):

$$\frac{h_s}{D} = 2 K_S K_a K_u \tanh\left(\frac{h_0}{D}\right) \qquad [3.3]$$

Here, D represents the width of the obstruction, and h_0 is the initial water depth. K_S, K_a, and K_u are factors that account for the shape and orientation of the structure and flow velocity, respectively. For abutments with lower horizontal to vertical ratios, the shape factor increases, resulting in an increase in scour depth (Breusers & Raudkivi, 1991).

3.2. Model accuracy

To gain familiarity with the laboratory facilities and observe the reaction of polystyrene to running water, a series of experiments were conducted without a structure built. A selection of these results can be found in Appendix E. The experiment featuring the flexible groyne head, FG1, was conducted on June 29 2023. In FG2, this setup was exposed to scaled extreme high-water conditions the following day. These findings are not of interest for the purpose of present study but are for internal use of the BAM.

3.2.1. Bed morphology

The morphological changes in the riverbed induced by the construction of the flexible groyne are depicted in figure 3.4. Making use of a multibeam echosounder, the riverbed was surveyed, comparing measurements taken five months after the groyne's construction with the initial riverbed profile. Mapping of the bed was done in November 2022 and March 2023 by autonomously operated sonar equipment, yielding data with a resolution of 50 by 50 cm. The black-outlined rectangular section of the river in figure 3.4 was replicated in a physical scale model.

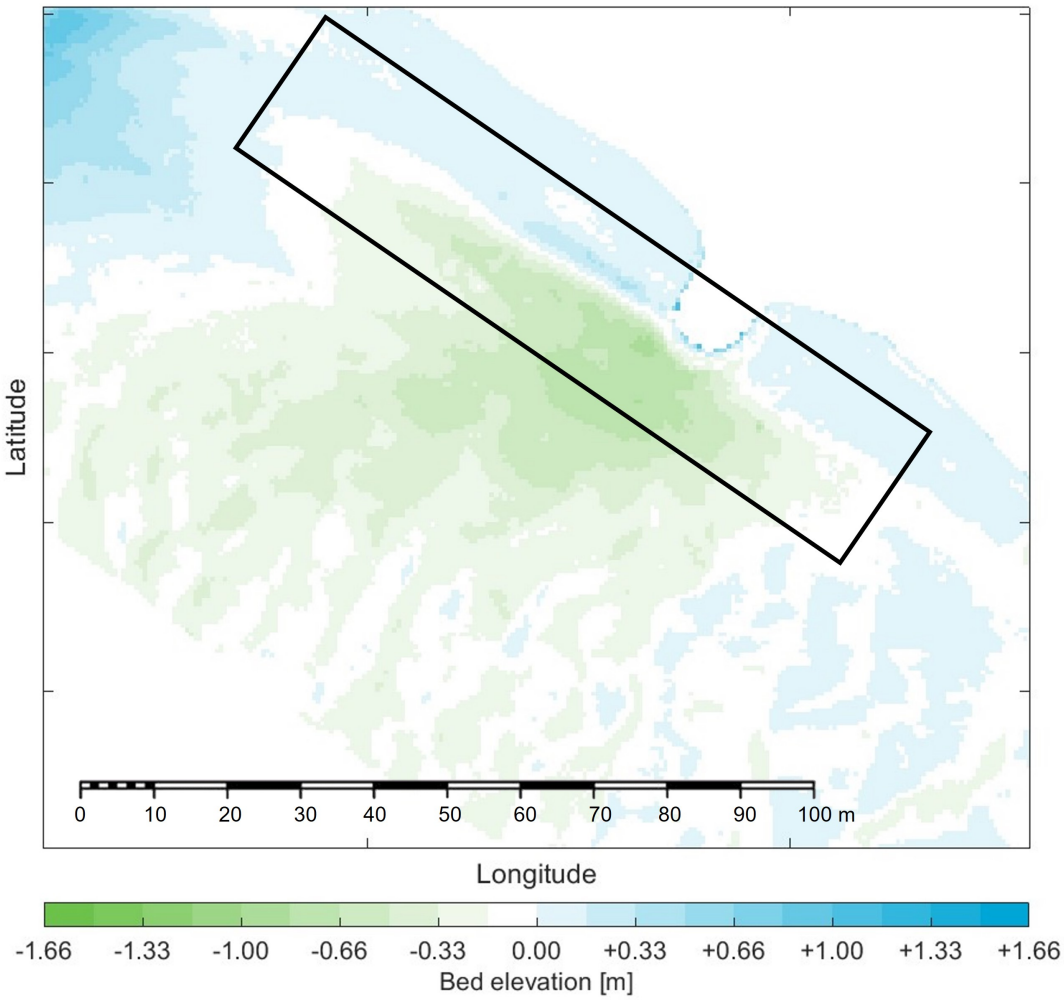

Figure 3.4: Field data difference in bed elevation between pre- and 5 months post-construction of the flexible groyne, spatially depicted in a 50 x 50 cm grid.

The result of the physical scale model is plotted in figure 3.5. Due to the flow contraction, the increased flow velocity has led to erosion in the near-field. It is clearly visible that the deepest scour hole has formed just downstream of the groyne head. In this computation, the pattern of locally scoured sediment follows the curved shape of the groyne head. Where the flow width increased again and the flow velocity decreased, sediment was deposited. A ridge has formed behind the groyne head in the streamwise direction.

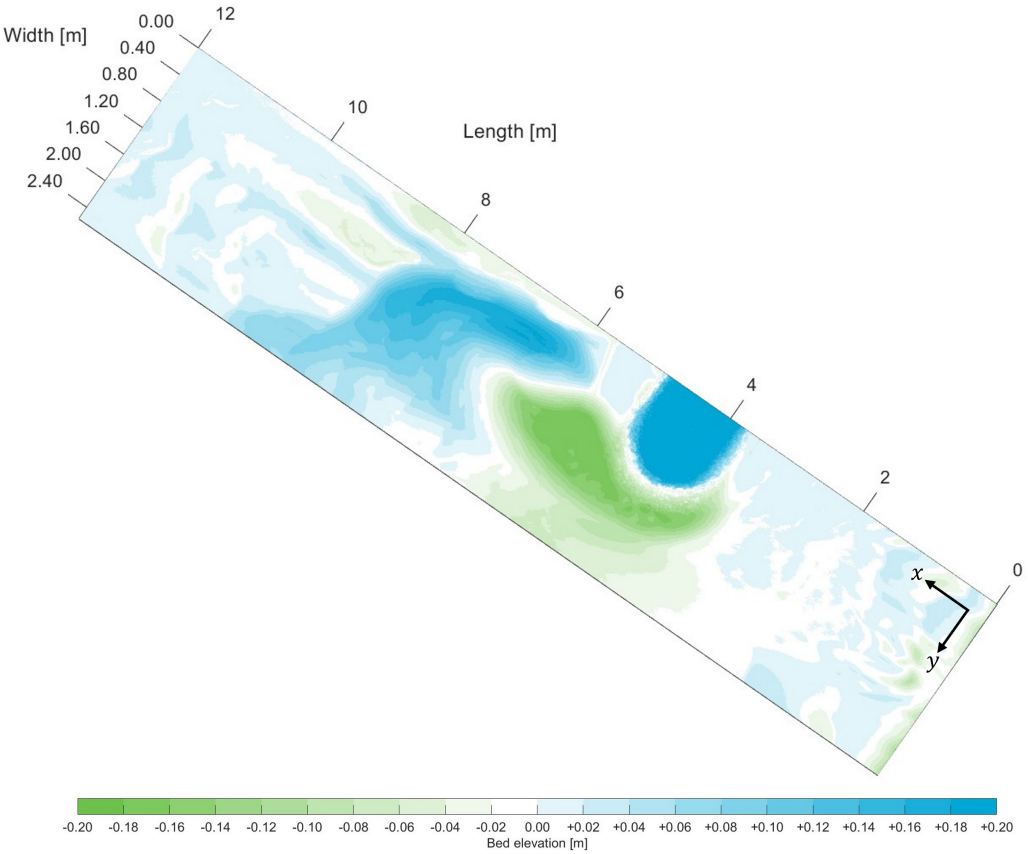

Figure 3.5: Measured difference in bed elevation before and after the experiment with the Xstream groyne head.

3.2.2. Flow velocities

On April 7, 2023, a velocity profile was recorded directly behind the flexible groyne using an ADCP. It registered a flow velocity of 0.06 m/s at one meter below the water surface and reduced to only 0.02 m/s at two metres depth. Additionally, dye tests indicated that water passed through the flexible groyne in less than 10 seconds at the water surface. The discharge that day was 619 m^3/s, so the crest of the flexible groyne just protruded above the water level. Therefore, the flow velocity through the flexible groyne at the water surface was approximately 0.10 m/s (Groenewege & Buschman, 2023). The detailed results of these measurements are included in Appendix F.

During the experiment, the flow velocity inside the flexible groyne was continuously measured at a depth of 0.6 times the initial water level. This gave an average streamwise flow velocity of 0.0003 m/s.

3.3. Porosity and roughness

The experiments that were needed to compare the difference in morphological behaviour induced by a stone abutment and an Xstream abutment were carried out on May 25 (XG1), June 1 (SG1) and June 9 2023 (XG2). On the first experiment date, there was not yet a Vectrino Profiler installed in the structure and complications while draining the flume occurred.

3.3.1. Porosity

The porosity difference between the stones and Xstream model units was determined by measuring the amount of water that was needed to fill up a known volume of construction material. For this purpose, an aquarium that measured 0.26 m x 0.25 m x 0.39 m (internal height x width x length) was used. In equations 3.4 and 3.5, W_{dry} (kg) is the weight of the aquarium filled with stone/Xstream, W_{wet} (kg) is the weight of the aquarium filled with both water and stone/Xstream, $V_{aquarium}$ (m^3) is the volume of the aquarium and ρ_{water} (kg m^{-3}) is the density of water.

$$P_{stone} = \frac{W_{wet} - W_{dry}}{V_{aquarium} \cdot \rho_{water}} \cdot 100\% = \frac{55.0 - 43.4}{0.025 \cdot 1000} \cdot 100\% = 46.2\% \quad [3.4]$$

$$P_{Xstream} = \frac{W_{wet} - W_{dry}}{V_{aquarium} \cdot \rho_{water}} \cdot 100\% = \frac{44.4 - 29.5}{0.025 \cdot 1000} \cdot 100\% = 59.6\% \quad [3.5]$$

From these equations, it appears that the porosity of Xstream elements is with a factor 1.3 significantly higher compared to the quarry stone used in this study. A side note here is that due to the flat sides and bottom of the aquarium, the voids at the edges have not been filled with stones or Xstream elements. Consequently, the pore spaces are bigger on the sides which causes the porosity to be slightly overestimated. In Appendix D, photos of these measurements clarify this observation.

In figures 3.6 and 3.7 the stilling well data is plotted in green for experiment SG1 and in blue for experiment XG2 respectively. For each 30 minutes, starting from the moment when the pumps are at full capacity and the stilling wells are stabilised, the average water level was plotted.

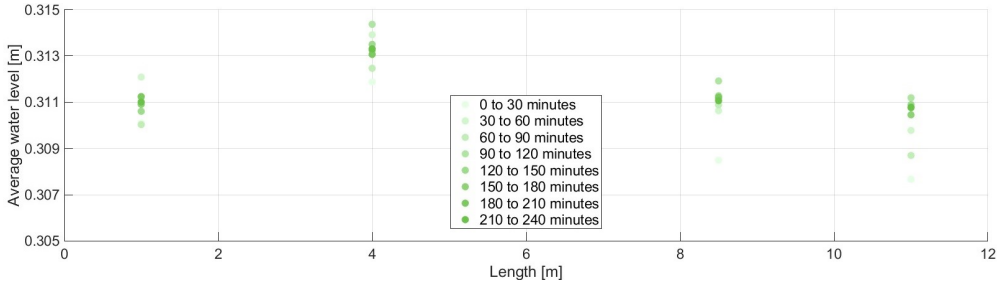

Figure 3.6: Average water level measured every 30 minutes during the stone abutment experiment with linear position sensors.

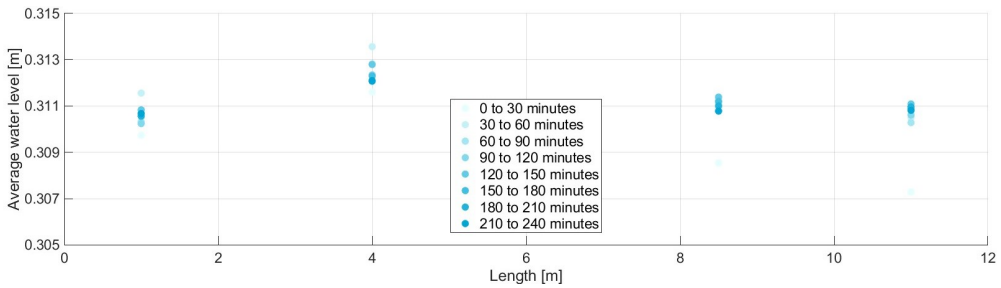

Figure 3.7: Average water level measured every 30 minutes during the Xstream abutment experiment with linear position sensors.

On first sight, the data in both figures appears to be rather similar. This is the result of the same water level eventually being measured for both the rock and Xstream experiments at the most downstream stilling well, at x = 11 m. Furthermore, the water level averages out between the measurement of the first 30 minutes (the lower limit) and the subsequent 30 minutes (the upper limit). There is, however, a difference in the average water surface slope over the whole reach of the flume, from x = 1 m to x = 11 m. The value of S_0 is found to be $9e^{-5}$ m/m for the experiment with the stone structure whereas S_0 = $2e^{-5}$ m/m in the Xstream structure experiment.

Over time, the average measured water levels tend to move closer to each other as can be seen from the figures. The difference in water levels, Δh, between the most upstream stilling well and the subsequent stilling well is the increase in water level at the point where the flow stagnates. During the last 30 minutes of the experiment with the stone abutment, the average water level measured at x = 4 m was 2.3 mm higher than at x = 1 m. With the Xstream abutment, this difference was only 1.4 mm.

The pressure rise due to stagnation of the flow velocity in front of the obstruction can be approached by equation 3.6.

$$\Delta p = 1/2 \rho u^2 \quad [3.6]$$

However, due to the lack of velocity measurements directly upstream of the abutments, the assumption is made that the pressure is hydrostatic. This way, using Δh, the pressure rise can be calculated without knowing the exact velocity with equation 3.7.

$$\Delta p = \rho g \Delta h \quad [3.7]$$

Filling in these equations reveals a pressure rise at the upstream heads of the stone and Xstream structures of 23 and 14 Pa respectively.

3.3.2. Roughness

Figure 3.8 plots the stone (left) and Xstream (right) structures as scanned with the line laser. The structures are divided into 5 sections by the transparent black lines. In the narrow middle, a cage was installed where the Vectrino Profiler could be lowered in during the experiments. This section is therefore ignored when determining the roughness of the structure, as are the curved sections at the upstream and downstream ends of the structures.

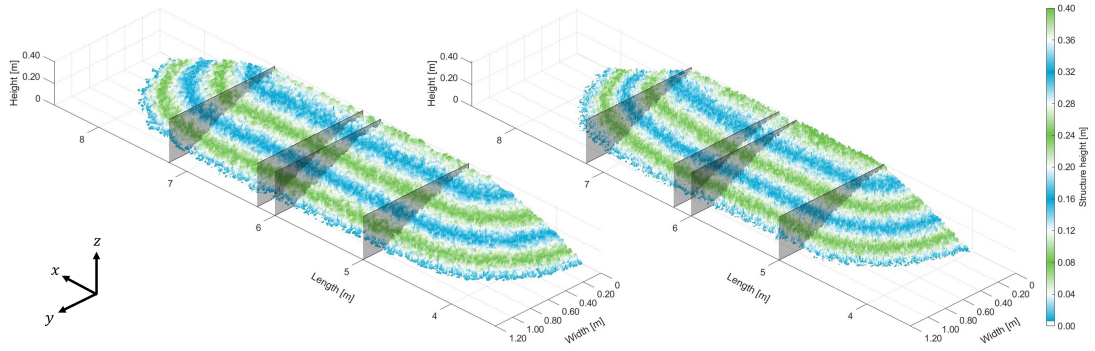

Figure 3.8: Stone structure on the left and Xstream structure on the right.

For both stone and Xstream structure, the average height over its width are plotted in figure 3.9. Between y = 0.10 m and y = 0.90 m, the Xstream structure exhibits a steeper average slope compared to the stone structure due to negligence in building the model setups. The grey bars represent the average height plus and minus the standard deviation over the width of the measurements.

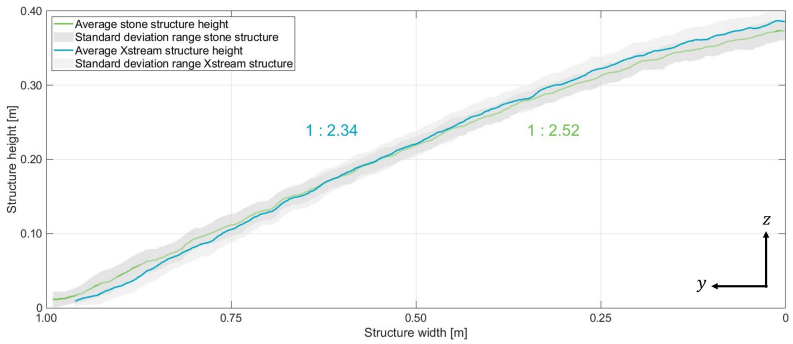

Figure 3.9: Average structure height between the straight sections of figure 3.8.

The average stone structure height has a mean standard deviation of 13.3 mm, while the corresponding value for the Xstream structure is 16.7 mm. Therefore, the roughness of the Xstream structure is larger.

3.3.3. Bed morphology

The data obtained with the line laser scanner is plotted in figure 3.10. In both experiments, local effects are found at the leading edge, along the length and behind the abutments. Sediment is eroded at the head and in the near-field down the structures. This resulted in a net degradation of the river bed in the section where the abutments were built. On the contrary, aggradation occurred in the sheltered area behind the abutments. Here, the accumulation of sediment has led to the formation of a ridge.

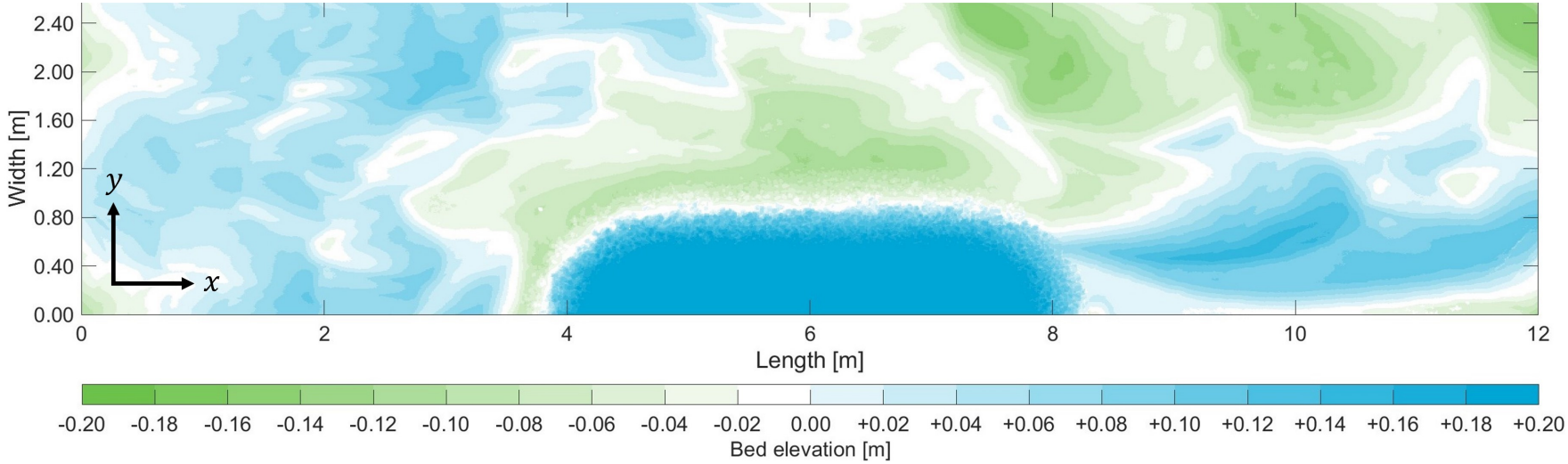

(a) Experiment SG1

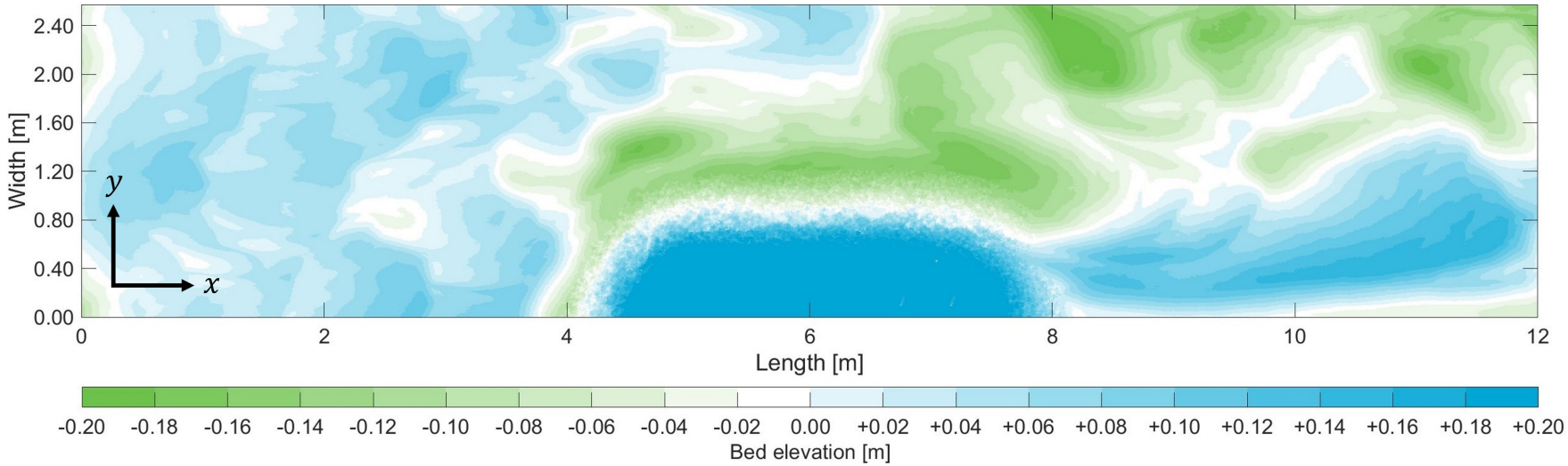

(b) Experiment XG2

Figure 3.10: Measured difference in bed elevation before and after the experiments with the stone (a) and the Xstream (b) abutments.

3.3.4. Flow velocities

The Vectrino Profiler that was installed inside the stone and Xstream structures measured very small average flow velocities in the x, y and z direction with a lot of noise. In the streamwise x direction, the ADV measured a velocity of 0.0004 m/s on average during experiment SG1. During experiment XG2, this value was ten times as small: 0.00004 m/s.

The side-looking velocimeter collected valuable data that provides insight into the relative turbulence difference induced by stone and Xstream. As summarized in table 3.1, the relative turbulence in the mixing zone close to these abutments is amplified by the application of Xstream. Important to mention is that the measured velocity is not depth-averaged as it is measured at one constant depth from the water surface of 0.6 times the initial water depth.

Table 3.1: r-values in the main stream during the stone vs. Xstream abutment experiments.

Symbol	Variable	Unit	1:2.5 stone	1:2.5 Xstream
$\overline{u_x}$	Mean streamwise flow velocity	m/s	0.233	0.222
$RMSE(u_x)$	Root mean square error	m/s	0.027	0.030
r	Relative turbulence	-	0.12	0.14
$(1+3r)\overline{u_x}$	Peak velocity	m/s	0.314	0.312

The side-looking Vectrino took 25 flow velocity measurements per second. For over 90% of these samples, the correlation and its signal-to-noise ratio were sufficiently high to be valid. This was determined by the software accompanying the measuring instrument. With such a large dataset, two normal distributions were plotted in figure 3.11. In these graphs, the mean value, represented by μ, indicates the average streamwise flow velocity. The standard deviation, denoted by σ, represents the average difference of all individual measurements from the mean flow velocity. The squared value of σ is known as the variance, which is a measure of the spread of a set of values. The confidence interval within which 95% of the measured values lie is indicated by the shaded 0.025th and 0.975th percentiles.

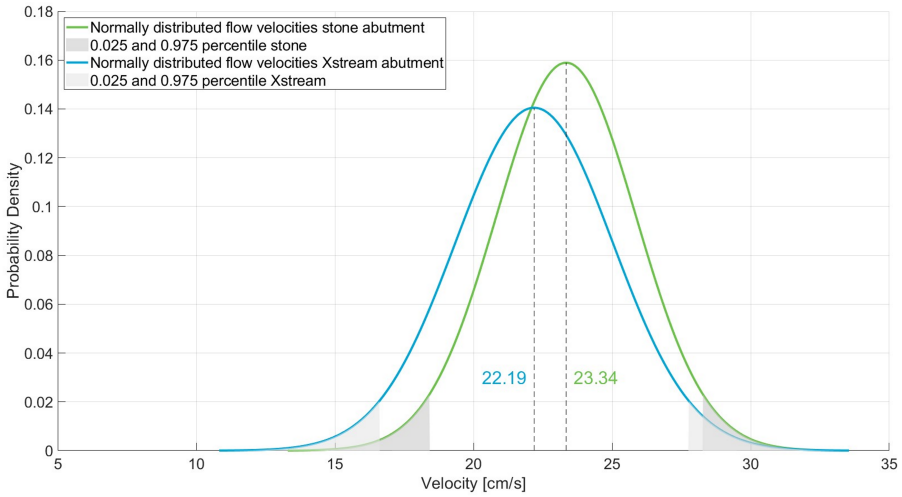

Figure 3.11: Probability density functions of the measured streamwise flow velocities in the stone abutment experiment (green) and the Xstream abutment experiment (blue).

The flow velocities directly upstream of the abutments were derived by using equation 3.6 and taking the assumed hydrostatic pressure rise. This resulted in a flow velocity of 0.212 m/s in front of the stone structure and 0.166 m/s in front of the Xstream structure.

3.3.5. Observations

After running experiment SG1, it appeared that stones had fallen into the scour hole at the leading edge of the structure. From picture 3.12 it can clearly be seen that these stone dragged the filter fabric with them, thereby protecting the bed material under the structure from eroding.

Figure 3.12: Leading edge of the stone abutment after the experiment.

The Xstream abutment that was built for experiment XG2 also became unstable as the erosion of sediments caused individual elements to slide into the scour hole. Picture 3.13 was taken after the experiment revealing the decay of Xstream elements along the toe of the structure.

Figure 3.13: A picture from the downstream end of the Xstream structure after the experiment.

3.4. Slope

On the 15th of June 2023, the Xstream abutment with a 1:1 slope was put to the test (XS1). It soon emerged that the structure was sinking deep into the sediment bed under the weight of the model units. This experiment was therefore repeated on June 22 2023, this time with a filter fabric under the setup to distribute the loads (XS2).

3.4.1. Geometry

As with comparing the stone and Xstream structures, the scans of the steep and gently sloped abutments made of Xstream are presented in figure 3.14. Again, to determine the average cross-sectional height of the structures, the head, middle and tail sections were neglected.

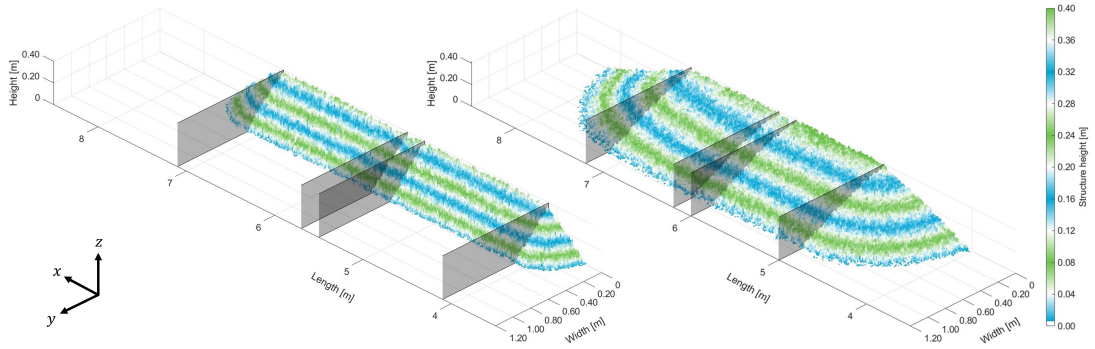

Figure 3.14: Steep Xstream structure on the left and gentle Xstream structure on the right.

As illustrated in figure 3.15, the aimed difference in slope steepness has been achieved. For the abutment with a gentle slope, the identical data of the Xstream abutment in the previous section was used.

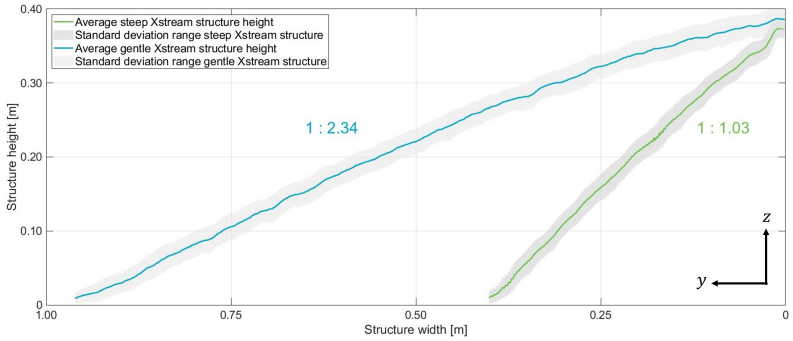

Figure 3.15: Average structure height between the straight sections of figure 3.14.

The mean standard deviation of the steep Xstream structure height is 16.6 mm whereas this is for the gentle Xstream structure 16.7 mm. The roughness of both Xstream structures is therefore the same.

3.4.2. Bed morphology

The difference in bed elevation, as measured with the line laser scanner, is presented in figure 3.16. Comparing both experiments, something that stands out is the resulting dune-like pattern directly at the toe of the steep abutment. Whereas sediment was eroded over the whole longitudinal length of the 1:2.5 structure, this was not the case in the 1:1 structure experiment. In addition, the ridge formation is less extended and high due to a steeper slope.

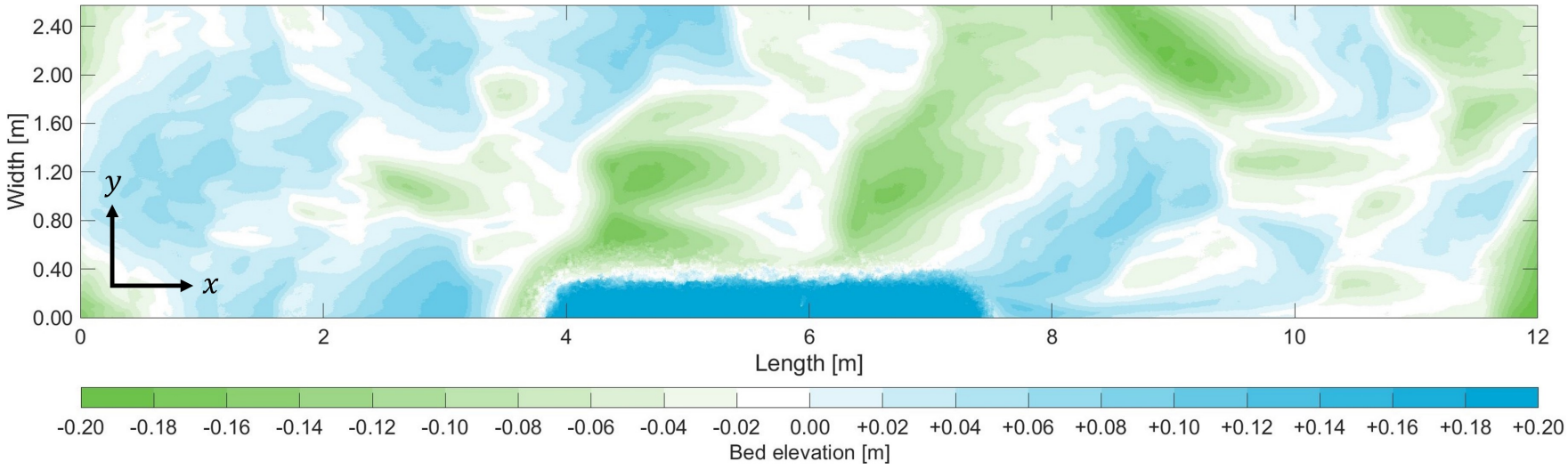

(a) Experiment XS2

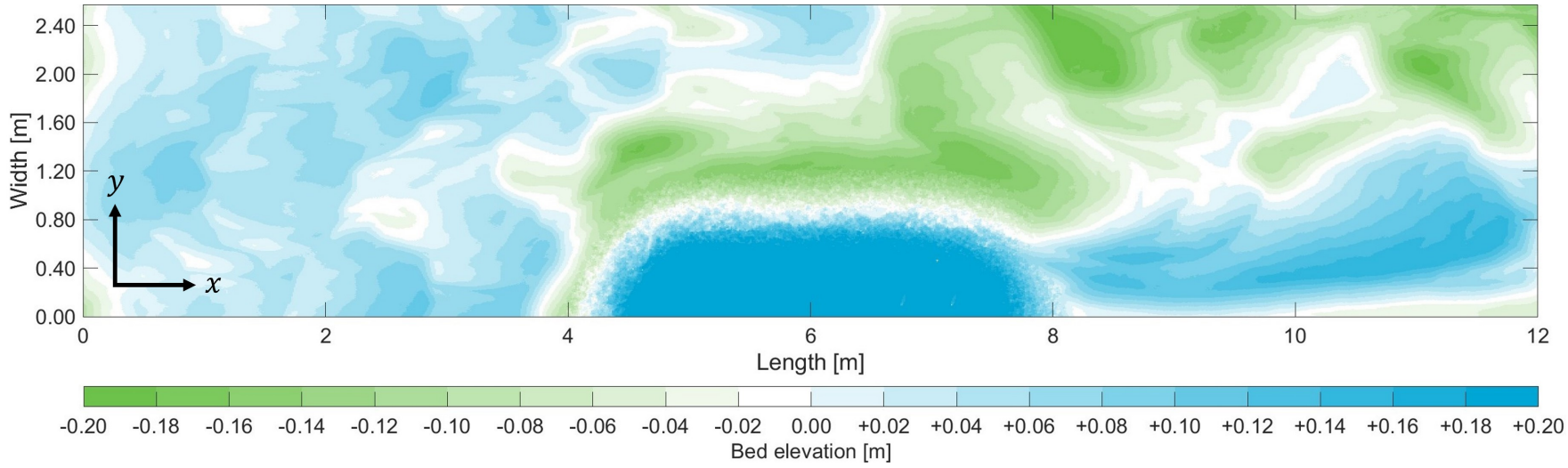

(b) Experiment XG2

Figure 3.16: Measured difference in bed elevation before and after the experiments with the steep (a) and the gently sloped Xstream (b) abutments.

3.4.3. Flow velocities

As of the results of the vertically measuring ADV, flow velocity measurements in the streamwise direction are of no significance with average values of 0.0007 m/s inside the steep abutment and 0.00004 m/s inside the gently sloped abutment.

The side-looking Vectrino measured the flow velocities in the x, y and z direction in both experiments. Table 3.2 presents these measurement results. The relative turbulence in the near-field of a steeper sloped abutment is minimally enhanced and peak velocities are lower.

Table 3.2: r-values in the main stream during the steep vs. gentle Xstream abutment experiments.

Symbol	Variable	Unit	1:1 Xstream	1:2.5 Xstream
$\overline{u_x}$	Mean streamwise flow velocity	m/s	0.208	0.222
$RMSE(u_x)$	Root mean square error	m/s	0.029	0.030
r	Relative turbulence	-	0.139	0.135
$(1+3r)\overline{u_x}$	Peak velocity	m/s	0.295	0.312

The measured valid flow velocity data was used to plot normal distributions (figure 3.17). The smaller the standard deviation of a set of measured data, the steeper this distribution appears, thus the higher the peak reaches on the probability density axis.

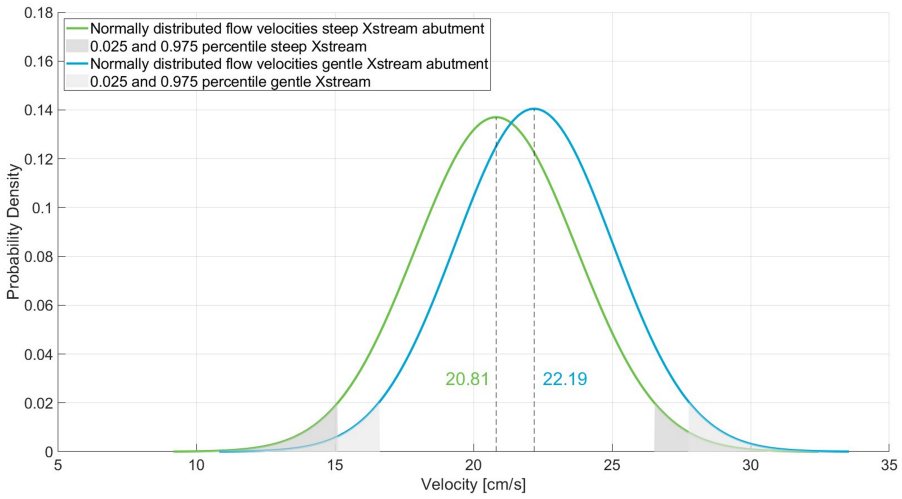

Figure 3.17: Probability density functions of the measured streamwise flow velocities in the steep Xstream abutment experiment (green) and the gentle Xstream abutment experiment (blue).

3.4.4. Observations

The geotechnical constraints of the lightweight polystyrene granulates became evident when the flume was filled with water to run experiment XS1. This structure was built directly on the bed without a filter fabric placed underneath it. The concentrated load was not uniformly distributed, resulting in the structure sinking into the bed as soon as the polystyrene became saturated. One possible explanation why this did not occur to the same extent in the XG2 experiment is that the larger Xstream model units were not employed in the XS1 experiment, which would have contributed to a larger surface area on the bed material.

Figure 3.18: Collapsed steep Xstream abutment after experiment XS1.

In reality, Xstream structures do not settle to this extend on a densely packed sandy river bed. This is known from the experience of the flexible groyne pilot in the river IJssel. Therefore, the experiment with the steep Xstream abutment was repeated in experiment XS2, but this time a supporting filter fabric was placed under it.

Figure 3.19: Steep Xstream abutment after experiment XS2, supported by a filter fabric.

Comparing the pictures in figures 3.18 and 3.19, it is clearly visible that the unsupported abutment has subsided in its entirety.

4

Analysis

This chapter will consider the interpretation of the results and their significance. Measured effects and observed phenomena are put into their theoretical context.

4.1. Flow patterns and sediment transport

4.1.1. Morphodynamic response

Figures 4.1 and 4.2 present the theory regarding the short and long term effects on water levels and bed elevation resulting from river narrowing (Blom, 2021). The illustrations are not drawn to scale but are exaggerated representations of reality. Section 1 is upstream of the constriction, section 2 at the narrowed part, and section 3 downstream of the hydraulic training works. Among other terms, like structure and abutment, these three all mean the same. The blue downward-pointing arrows indicate the positions along the length of the flume where the stilling wells were installed to measure the water levels.

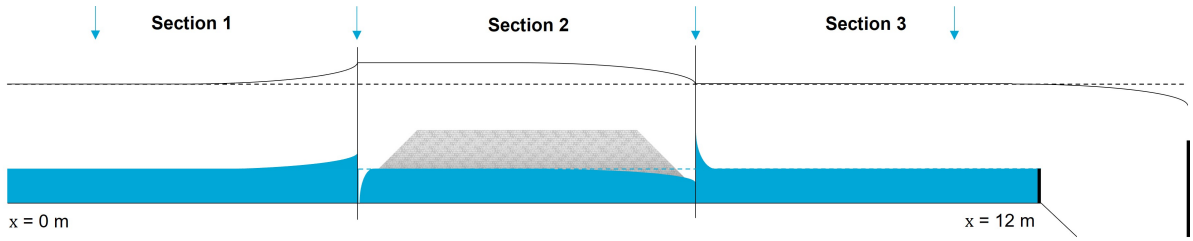

Figure 4.1: Initial response to river narrowing.

Immediately following the construction of a river training structure, the water level rises at the upstream end of this structure. Consequently, the velocity of the flow decreases, which in turn reduces its capacity to carry sediment, resulting in the deposition of sediment. Due to the abrupt reduction in cross-sectional area caused by the constriction, the flow velocity increases. This leads, next to the resulting vortexes, to local erosion. Along the length of the river narrowing, the water level drops, the flow accelerates and the erosion of the river bed is enhanced. Downstream, the water level is regulated by, in this case, the weir at the end of the flume. Where the channel width suddenly widens again, the flow slows down, causing the suspended sediment to settle.

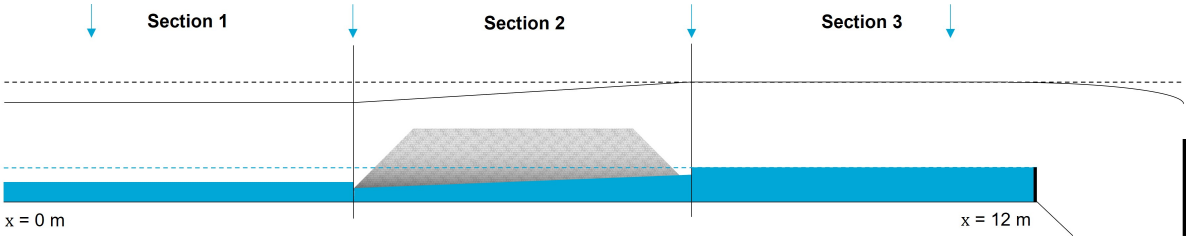

Figure 4.2: New equilibrium after river narrowing on the long term.

Over time, the riverbed cuts into the section where the river is narrowed. As a result, both the equilibrium slope of the riverbed and the water level decrease in this region. The water level upstream is influenced by these changes, resulting in a slight decline of the bed elevation on the long term in section 1. Downstream, in section 3, the initially deposited sediment is gradually transported in the flow direction. This way, both the water level and the bed level downstream remain unchanged compared to the situation prior to the construction of the river training structure.

4.1.2. Live-bed scour

Making use of equation 2.9 and the parameter values listed in table 2.1, the dimensionless particle number, D_* was calculated to be 17. Reading Van Rijn (1984a)'s curve yields a critical shear stress, Ψ_c, of 0.03. If the shear stress exceeds this value, the bed is in continuous movement at all locations. The revised equation 2.10, in which θ is replaced by Ψ_c and $\overline{u}$ by u_c, can be rewritten to determine the critical flow velocity. Depending on the value of the Chézy coefficient, C, which in these experiments is between 30 and 40 $m^{1/2}/s$, $0.06 < u_c < 0.08$ m/s.

In the experiments, general transport of bed material occurred as the value of $\overline{u_x}$ was significantly greater than u_c. Sediments that ended up in the sediment catch at the end of the flume were recirculated back into the flume, creating live-bed scour conditions with the supply of sediment from upstream. If the flow velocity is below the point at which general bed movement occurs, erosion can still happen due to local scour resulting from the aggravation of the load around the obstruction. This type of scour is called clear-water scour.

The time-variation of clear-water and live-bed scour in time are compared in figure 4.3. The equilibrium depth under live-bed scour conditions is reached much faster and is about 10% smaller compared to the equilibrium scour depth in clear-water.

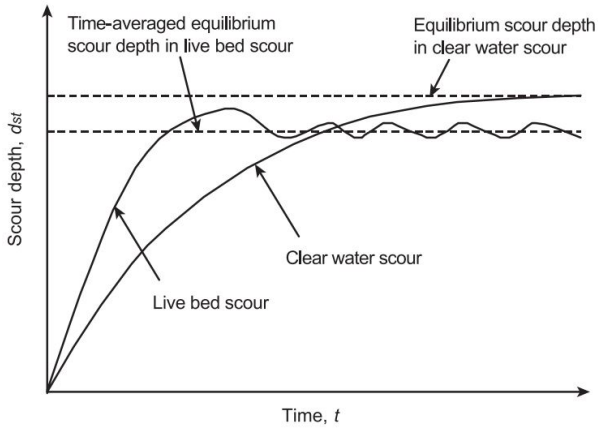

Figure 4.3: Time development of clear-water and live-bed scour (Barbhuiya & Dey, 2004).

Due to the supply of material from upstream, the scour depth tends to fluctuate around the equilibrium. Measuring the scour depth is challenging due to bed forms like dunes and ripples migrating past the

structure. Arneson et al. (2012) imply that the maximum scour depth in live-bed conditions is approximately 10% greater than the equilibrium scour depth.

4.1.3. Mixing layers

Whenever there is a velocity difference between two bodies of water, a mixing layer develops. As previously mentioned, the flow velocity in the near-field increases at and decreases after the narrowed river section. The flow characteristics around an abutment result from a combination of horizontal constriction and expansion. Figure 4.4 schematically presents the place where a mixing layer will have developed.

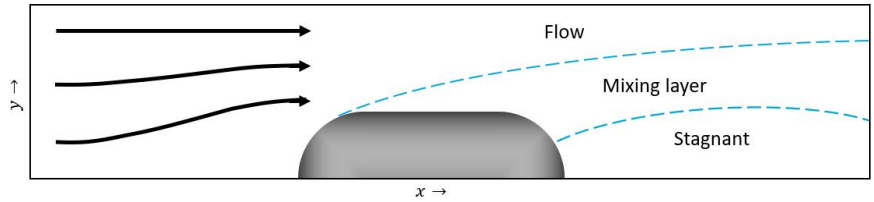

Figure 4.4: Flow details around an horizontal constriction.

At the upstream end of the obstruction, the flowing water is forced from the side of the flume, creating a curved mixing layer. The relative turbulence, r, is at maximum and the pattern of the peak velocities largely coincides with this mixing layer. This is mainly due to the behaviour of the flow velocity which is accelerated around the leading edge of horizontal constrictions (Ariëns, 1993).

As the flow width increases downstream of the obstruction, the flow propagates into the zone with stagnant water leading to recirculation beyond the expansion. Since bed friction dominates at the river bed, the effect of the mixing layer - which creates turbulent fluctuations - is mostly found at the water surface. In contrast to the horizontal constriction, the highest peak velocities near the bottom are measured in the main stream when the flow width horizontally expands by Zuurveld (1998).

The scour depth can be approximated by applying equation 4.1. This relation is established based on experimental data and describes the clear-water scour behind a bed protection.

$$h_s(t) = \frac{(\alpha\overline{u} - \overline{u}_c)^{1.7} h_0^{0.2}}{10\Delta^{0.7}} t^{0.4} \qquad [4.1]$$

$h_s(t)$ is the maximum scour depth in metres as a function of time, which is included as t (h) in this empirical relation. $\overline{u}$ is the depth average streamwise velocity (m s^{-1}), $\overline{u}_c$ the critical velocity (m s^{-1}) and h_0 the original waterdepth (m). The non-dimensional amplification factor for velocity is given by the variable α, which expresses the flow disturbances. The value of this factor is related to the relative turbulence r according to:

$$\alpha = 1.5 + 5r$$

so there is correlation between the relative turbulence and flow velocity for time-dependent scour. During the experiments performed for present study, the flow velocity was continuously locally measured using an ADV. As presented in the Results chapter of this thesis, the mean flow velocity in the x direction were higher than the r values in all experiments. Therefore, in this context, it is expected that the influence of $\overline{u}$ will have a greater impact on the preliminary prediction of the scour depth compared to the influence of r.

Based on this theoretical approach, the maximum scour depth should be between 0.20 and 0.25 m which would mean that the bottom of the flume will be reached in some cases.

4.2. Model accuracy

4.2.1. Bed morphology

When comparing the morphological data from figure 3.4 and figure 3.5 (in which the colour scale is displayed by equivalent means), substantial differences in bed level evolution can be observed. First, the depth of the resulting scour hole in the model compared to reality is remarkable. Converted with the scaling factor n_L of 8.3, the maximum scour depth in the model is between 1.3 and 1.5 m, whereas in reality the deepest pit after construction of the flexible groyne is at maximum 1 m. Moreover, the model exaggerated the height of the ridge that has formed behind the groyne by three times its actual size.

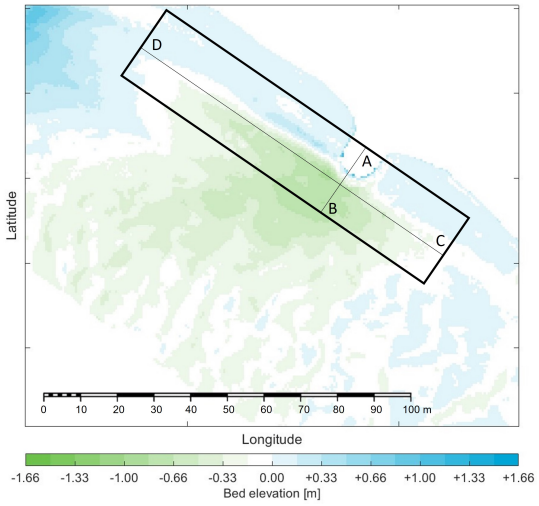

(a) Transects in bed elevation field data

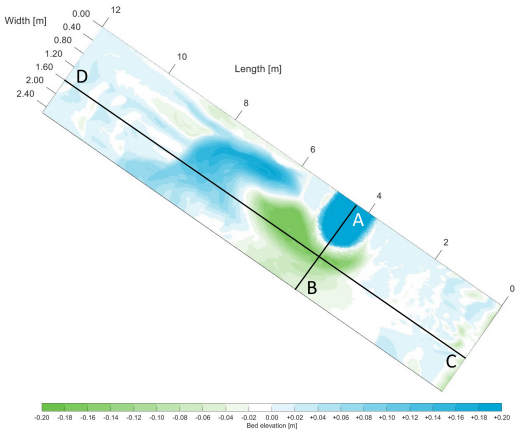

(b) Transects in bed elevation physical model

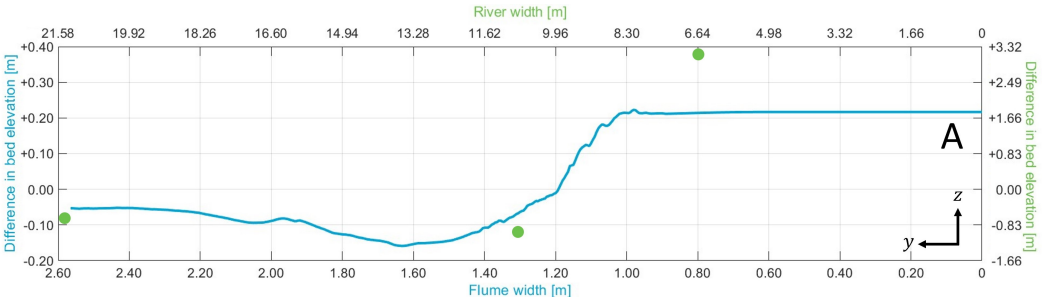

(c) Bed elevation along transect AB

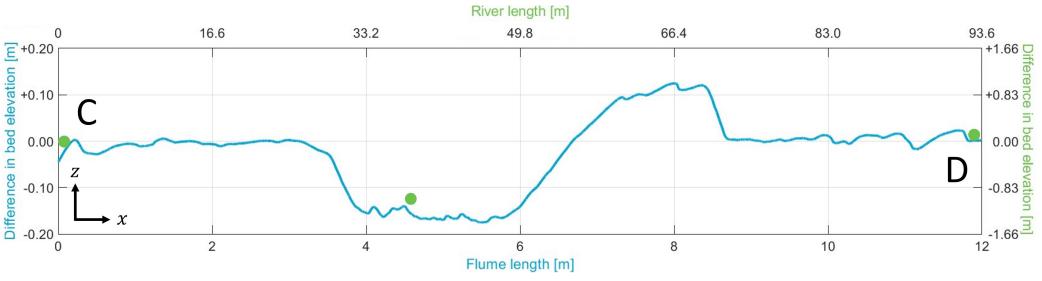

(d) Bed elevation along transect CD

Figure 4.5: Difference in bed elevation between field data (green dots) and the physical model (blue lines) for transversal and longitudinal transects.

The elongation of the erosion and sedimentation profile also deviates in the model from the field measurements in the river IJssel. In the longitudinal direction, the actual scour induced by the flexible groyne extends from the beginning to the end of the modelled river section. In the transverse direction, the effect of the river narrowing stretches far beyond the limits of the flume. The two transects in figure 4.5 illustrate the differences in vertical bed position along the length and across the width between the field measured morphology and 3D modelled river section.

The position of the deepest point of the scour hole in the xy-plane appears to align with the field data. This deepest point is the result of the combined effect of contraction and local scour. Whilst the influence of local water and sediment flows is clearly visible in the morphological changes around the groyne head in the model, it is more complex to observe in the field. In transect AB (see figure 4.5c) of the model, a well-defined transition in the cross-sectional bed slope is present around y = 2 m. This sharp contrast divides the contraction from the local scour that results from the construction of the flexible groyne. In the real world, the total scour depth gradually decreases towards the river's centre axis.

4.2.2. Flow velocities

Due to the negligible mean flow velocities (in the order of tenths to hundreds of millimetres) through the structure, these measurement results are excluded from this analysis. The streamwise velocity inside of the flexible groyne will therefore not be used to verify the extend to which the physical model represents reality.

4.3. Porosity and roughness

4.3.1. Porosity

As the downstream water level impacts the upstream water level, the in-depth analysis of the stilling well data as plotted in figures 3.6 and 3.7 starts with the measurements at x = 11 m. After experiencing fluctuations during the initial response of the river bed, the water levels stabilise as the experiments progress. On average, the downstream water levels in the two experiments, featuring 1:2.5 sloped abutments of stone and Xstream, are exactly equal in the last hour. Despite this consistent downstream water level, a slightly higher water level was measured in the stilling well at x = 8 m with minimal difference in the stone structure experiment. The average water levels in both experiments at x = 8 m, however, were slightly higher than the water level at x = 11 m, possibly due to the influence a back water curve resulting from water flowing over the weir at the end of the flume.

Theoretically, the water level at the beginning of section 1 should be equal to the water level at the end of section 2, which is the beginning of section 3, according to the schematic illustration in figure 4.1. For both experiments, this seems to hold reasonably well. The main difference appears to be the measured water level at x = 4 m, just in front of both structures. The stone-built structure creates a stronger blockage than the structure built with Xstream units. The reason for this is the difference in porosity between the two structures. The lower porosity of the stone structure requires a higher pressure build-up for water to penetrate into the structure compared to the more porous Xstream structure that offers lower resistance. Hence, this leads to a difference in water level increase, with the Xstream structure not backing up as much water towards x = 1 m.

4.3.2. Roughness

Due to the irregular shape of the interlocking individual Xstream units, the roughness of this structure is greater than that of the stone structure. This is shown by a higher value of the average standard deviation, a measure that quantifies the amount of variation in a set of values from their mean.

4.3.3. Bed morphology

In figure 4.6b, the average bed elevation between the two dashed lines in figure 4.6a, showing the river morphology of the stone abutment experiment, is plotted with a blue line. The grey band around it corresponds to the average bed elevation plus and minus the standard deviation over the width between y = 1.20 m and y = 2.40 m.

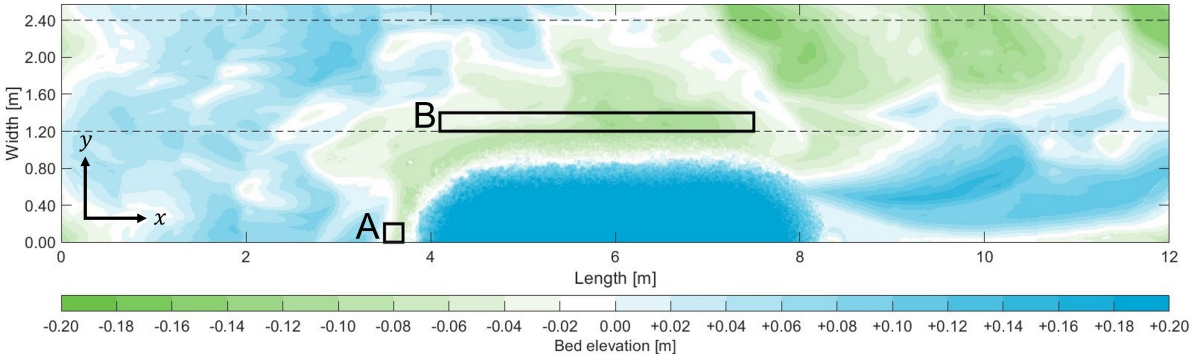

(a) Bed morphology with analysis indicators

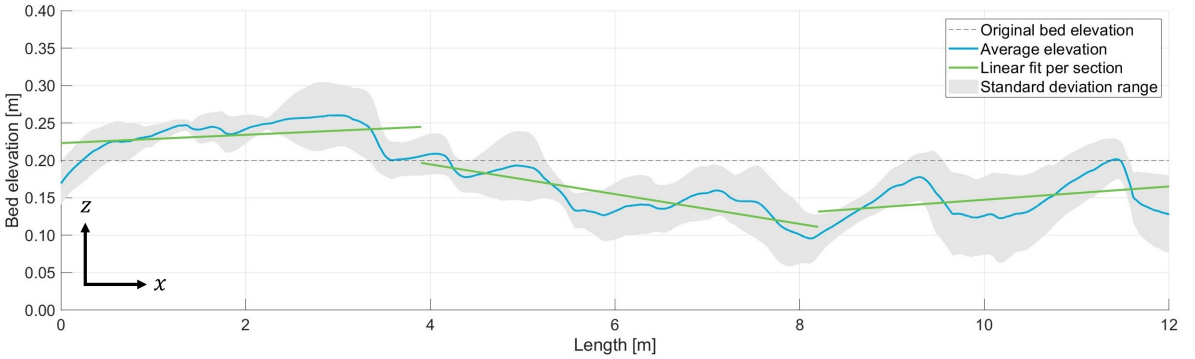

(b) Average bed elevation

Figure 4.6: Analysis of average bed elevation after the experiment featuring the stone abutment.

The green lines shown in figure 4.6b depict the linearly interpolated fits of the bed elevation upstream, at, and downstream of the structure. In an ideal setup, these lines should correspond to the long-term changes in bed elevation due to river narrowing, as shown in figure 4.2. Nonetheless, it can be observed that the bed elevation, on average, resembles the initial response to river narrowing more closely. This is a consequence of the continuous recirculation of transported sediment. In real-world conditions, the amount of material supplied from upstream is not equal to the amount eroded by river training works.

When plotting a similar graph for the Xstream structure experiment, as shown in figure 4.7b, the pattern is very similar: in the first section, the average bed elevation gradually increases, it then suddenly drops and decreases rapidly. In the downstream section of the obstruction, bedform developments continue and the average bed elevation increases again.

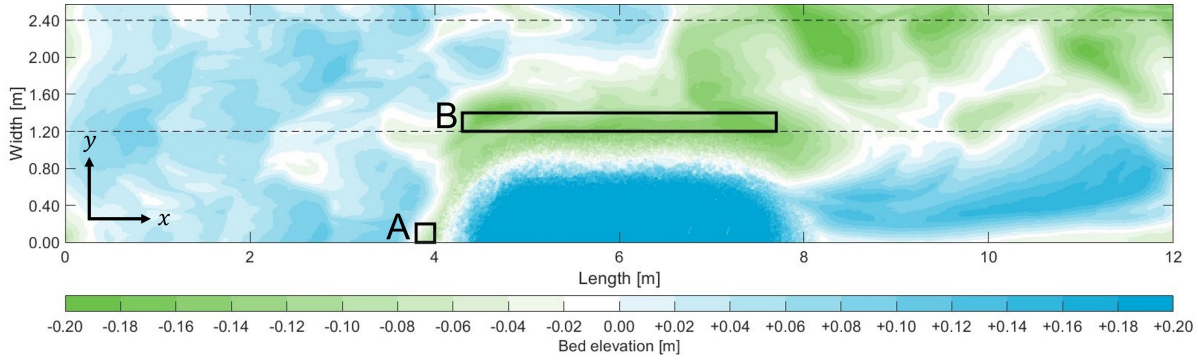

(a) Bed morphology with analysis indicators

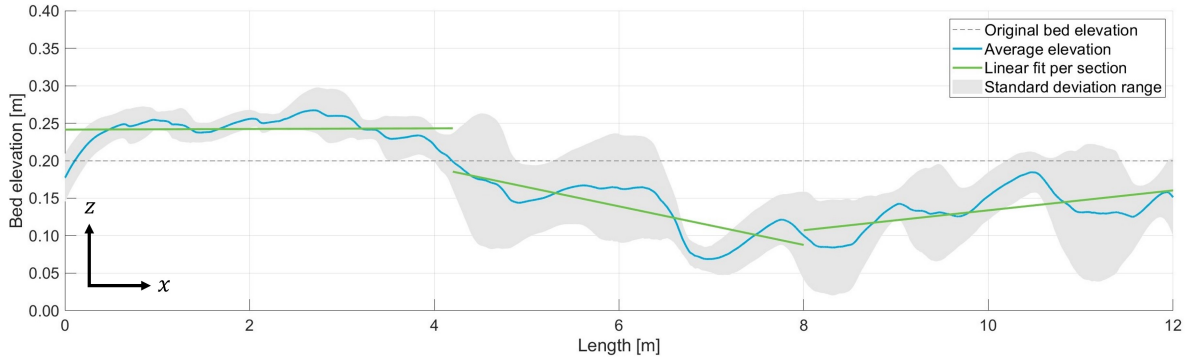

(b) Average bed elevation

Figure 4.7: Analysis of average bed elevation after the experiment featuring the Xstream abutment.

Regarding the dunes formed downstream, there is a clear distinction in length and depth between the two experiments. The dune length in the experiment with the stone structure is around 2 m. Dunes with a maximum length of 1.5 m were measured after the experiment with the Xstream structure. Interestingly, the sediment upstream of the two structures shows a similar pattern. Although, in absolute terms, the troughs of the dunes are deeper in the Xstream experiment, the greatest disparity between the crest and trough of the dune measures approximately 12 cm in both experiments. This suggests that the overall mean bed elevation downstream of the abutment is lower in the Xstream experiment than in the stone experiment.

The more porous structure of Xstream units absorbs and dissipates the kinetic energy of the flowing water more efficiently. This results in a lower average flow velocity in the main stream, enhancing the sediment settling process. As the sediment carrying capacity is smaller for lower flow velocities, the sediment particles have a greater tendency to settle and accumulate on the riverbed. The primary mode of sediment transportation is bed load, in which sediment is transported by rolling or saltation. At higher flow velocities sediment is increasingly transported in suspension. This is amplified by the lightweight granulates used in this physical model. At lower velocities, sediments tend to be deposited and build up, leading to high crests and deep troughs whereas the length of the dunes is limited.

As explained in section 4.1.3, peak velocities are often held responsible for the stability and erosion of bed material. At the horizontal constriction, these are found in the mixing layer whereas from the horizontal expansion the peak velocities are found in the main stream. This seems to correspond well with the general pattern of erosion in the two experiments.

Two particularly intriguing regions are at the head and along the length of the structure. In the former, the downward pressure gradient is the greatest, resulting in vertical flow. The vortex formed accelerates in streamwise direction at the toe of the structure. These areas are identified as A and B in figures 4.6a and 4.7a respectively. Summing up the number of cells within a specific range, the following histograms in figure 4.8 are obtained:

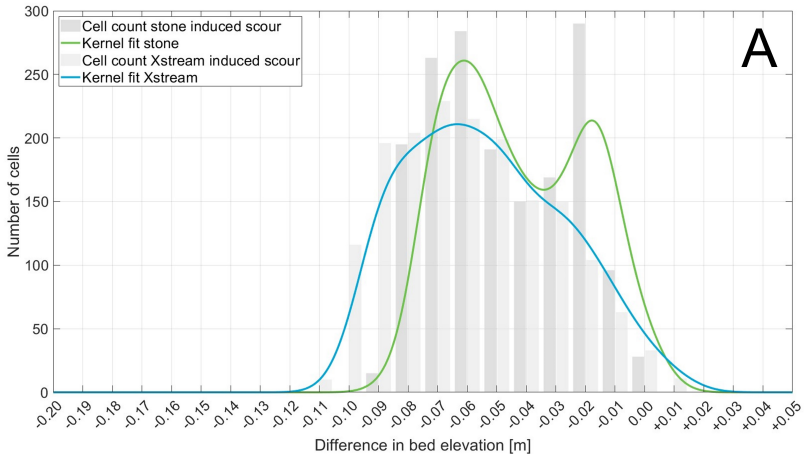

(a) Area A

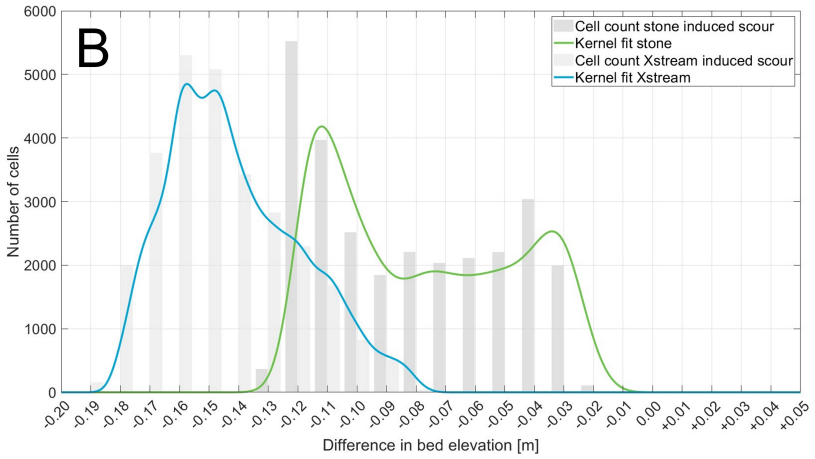

(b) Area B

Figure 4.8: Histograms of the number of cell values within a specific range. Areas A and B match the outlined areas in figures 4.6a and 4.7a. The dark grey bars represent the stone experiment and the light grey bars the Xstream experiment. The green and blue coloured lines are best-fitted kernel density estimations respectively.

Looking at the histogram of area A, it can be seen that the depth of the scour hole is slightly deeper in the Xstream experiment, with a wider distribution towards lower cell values. Also noticeable is the high peak in the number of cell values at -0.02 m after the stone experiment. Generally, however, the two scour holes correspond well.

From the histogram of area B it is clearly deducible that the scour depth along the length of the structure is greater in the Xstream experiment than in the stone experiment. With an average scour depth in the Xstream experiment twice as deep as the stone experiment, there is a significant difference between the two. This cannot be explained with the available data using the time-dependent scour equation.

The deepest scour observed in experiment XG2 is 19 cm whereas this is 13 cm in experiment SG2. As the scour depth is fluctuating around its equilibrium depth in live-bed conditions, these measured depths can be either 10% higher or lower than their equilibrium. Assuming that the deepest scour next to the Xstream structure is at this moment at its maximum depth, so 10% higher compared to its equilibrium, this would mean that the equilibrium scour depth is about 17 cm. For the other structure, if this observed value is 10% below its equilibrium depth, the equilibrium depth at the toe of the stone structure would be somewhere close to 14 cm. Still the difference in scour depth is significant.

Based on calculations for h_s with equation 4.1, the maximum scour depth in both SG1 and XG2 should be more or less equal with 23 cm. This is based on a run time of 4 hours.

Two other areas of interest are the ridges formed behind both structures and the erosion pits at the upstream end of the abutments but more towards the other side of the flume. Starting with the ridges, they are of the same height and have the same curvature. These ridges appear to be evolving, adding a new 'layer' with each migrating dune. Particularly visible in the Xstream experiment in figure 4.7a is the scour at the beginning of the constriction, but more into the flume, partially falling in area B. This erosion pit is somewhat detached from the local scour occurring due to the increased turbulence caused by the high roughness. As this scour progresses downstream, reaching the accelerating flow at this point, it will further develop into a dune trough.

4.3.4. Flow velocities

Around x = 4.8 m and y = 1.20 m the flow velocity was measured in three dimensions. The obtained data was used to plot figure 3.11, which displays the normal distribution of the average flow velocity in the x direction for both experiments. It is evident that the graph of the stone experiment has a steeper curve and a higher peak. This indicates that the standard deviation was lower for the results of this experiment, implying a lower degree of variation in the data set.

In comparison to the Xstream abutment experiment, the relative turbulence is lower at 12% compared to 14%. This is calculated based on the average flow velocity and the root mean squared error, as described in equation 2.1. It implies a greater variability and dispersion in the flow characteristics, indicating that the flow conditions are more unpredictable or unstable in the Xstream experiment. Stronger turbulence is the underlying cause of this observation.

Peak velocities, which are approached by $(1 + 3r)\overline{u_x}$, were roughly equal in both experiments. The decrease in average streamwise flow velocity was compensated for by the increase in relative turbulence in experiment XG2. It is important to emphasize that the flow velocity is only measured at one fixed point at about 30 cm from the leading edge and at a depth of 0.6 times the initial water depth.

Again, the streamwise velocities inside both structures, measured by the Vectrino Profiler, were considered too low to be valid.

4.3.5. Observations

In the real world, a bed protection layer ensures the stability of conventional hydraulic training structures. Pitched blocks or rocks are fixed and do not move or sink into the river bed, or at least minimally. In the model, however, this turned out to be possible to some extend, despite the attempt to prevent it by placing a filter fabric under the stone abutment. By sealing the bed material with the geometrically closed filter, it could not wash away and collision of the structure was prevented.

The absence of a filter fabric under the Xstream abutment in experiment XG2 provided valuable insights into the behaviour of the toe of the structure. As was observed, the toe of the structure lost its strength because of the interlocking ability of the Xstream model units has weakened as individual elements rolled or slid into the erosion pit. To the point where the structure was at least 4 elements high, the elements fell apart covering one slope of the scour hole.

The structure elevation scans around x = 5 m in figure 4.9 reveal that the toe of the Xstream structure collapsed about 15 cm further towards the flumes' wall compared to to stone structure. Both slopes feature a 30° angle which is slightly steeper than the 1:2.5 construction slope. However, notable is the difference in length between the scour hole slopes. The slope of the scour hole at the toe of the Xstream structure is almost twice as long as the slope of the scour hole at the base of the stone structure. Local turbulence levels close to the scour slope covered with erratic Xstream elements were expected to be higher. This contributed to the formation of a deeper scour hole which became a positive feedback loop, enhancing scour development.

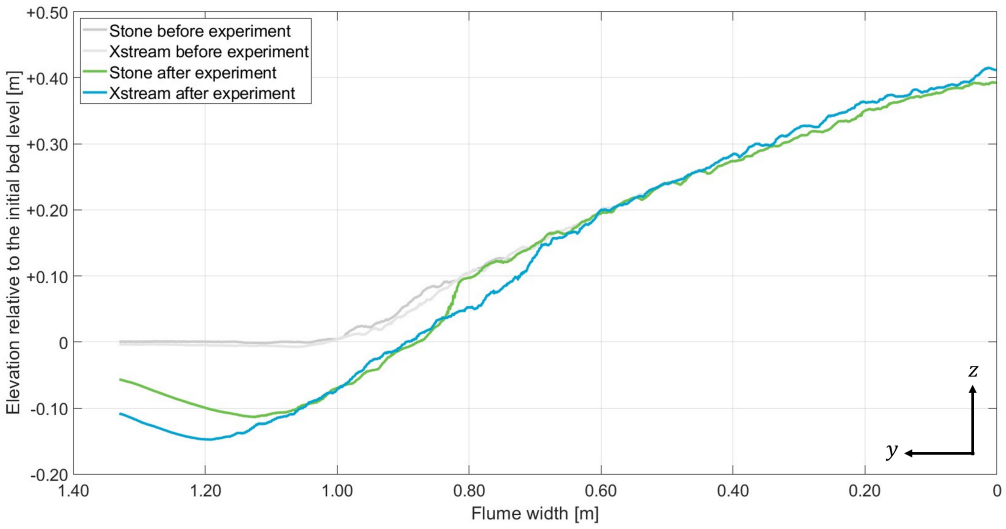

Figure 4.9: Cross sectional scans of the stone and Xstream structures before and after both runs averaged between x = 5 m and x = 5.4 m.

This phenomenon strongly resembles the falling apron principle, where a stack of granular material self-launches onto the slope of the scour hole when the revetment is undermined. The side of the scour hole will be protected by a layer of rock, retaining the bed material and preventing the formation of a slope that is too steep (Van der Hoeven, 2002). In this case, the granular material consisted of Xstream elements. Figure 4.10a to 4.10d schematically represent the mechanism behind a falling apron.

(a) Initial situation where the structure is directly built on the bed material.

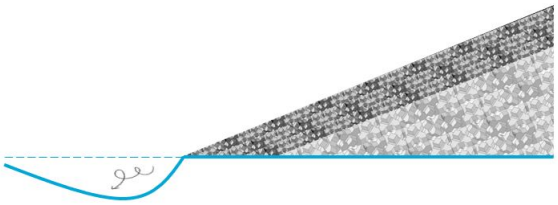

(b) A scour hole develops as the flow accelerates and a principal vortex originates.

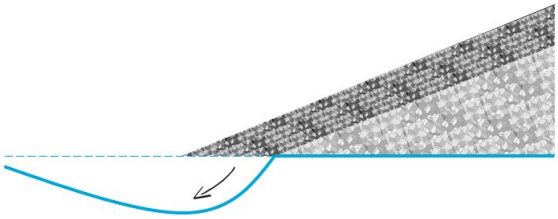

(c) The development of a scour hole continues as the flow velocity in the toe of the structure results in shear stresses that are above the critical value of the bed material.

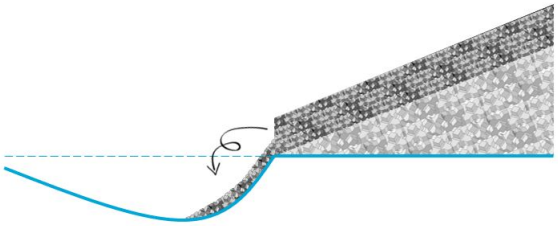

(d) Individual elements loose their interlocking capacity and tumble into the scour hole, covering its slope.

Figure 4.10: Mechanism of a falling apron.

4.4. Slope

4.4.1. Geometry

Instead of varying the porosity and roughness, the slope of the abutment was changed for this configuration. An Xstream unit structure with a steep 1:1 slope was constructed in the setup exactly as intended. The steep and gently sloped structures are the same in length, with the steep one positioned slightly further upstream in the flume.

4.4.2. Bed morphology

For this analysis, the resulting bed morphology after the steep Xstream experiment, as shown in figure 4.11, is compared with figure 4.7 from the previous section. Figure 4.11b presents the average bed elevation with the blue line and the standard deviation around it in grey. The green lines correspond to the linear fits for the bed elevation in the three sections.

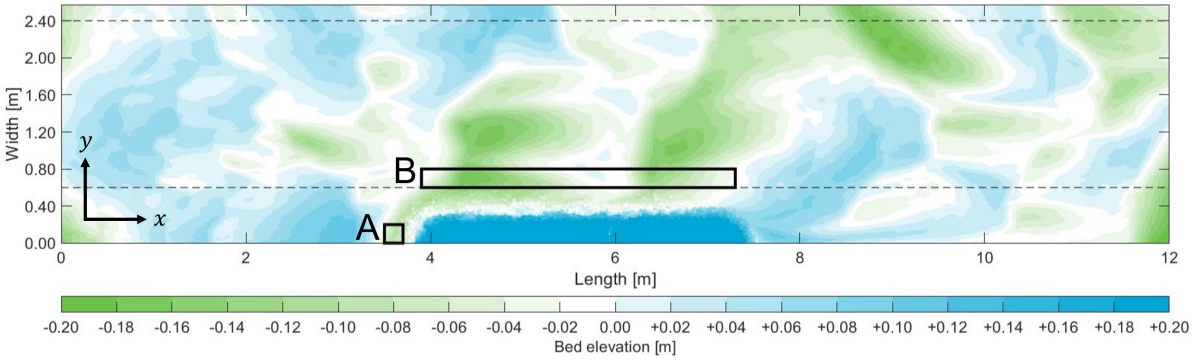

(a) Bed morphology with analysis indicators

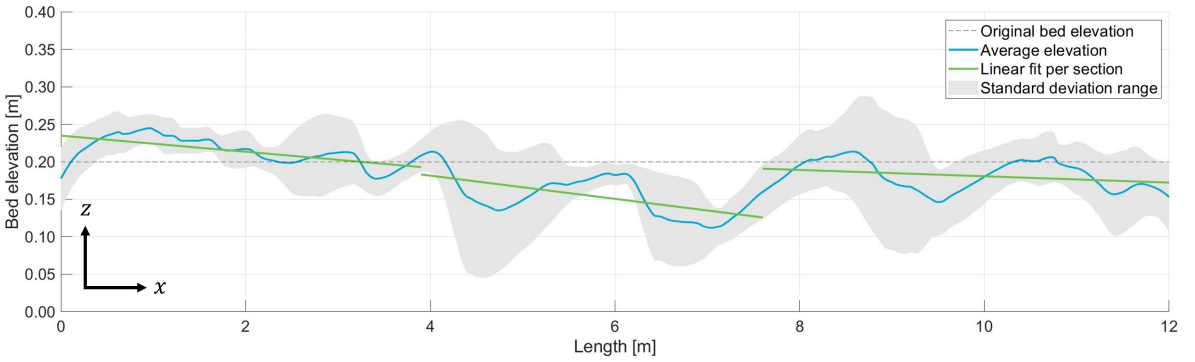

(b) Average bed elevation

Figure 4.11: Analysis of average bed elevation after the experiment featuring the steep Xstream abutment.

Unlike the gently sloping Xstream abutment, where the upstream sediment supply kept the bed level close to horizontal in the first section, in this experiment the bed level decreases on average in this section. This gradual decrease continues in the section where the obstruction is built. Aggregation of sediment is observed directly after the structure, but even in the most downstream section, the average bed elevation within the dashed lines decreases slightly.

Overall, the sediment pattern is less obvious in the steep Xstream experiment compared to the gentle slope structure. Areas affected by erosion or sedimentation are dispersed throughout the flume, resulting in less sediment being collected in the sediment catch and therefore less entering the recirculation. One of the most notable differences from the reference is the dune-like pattern at the base of the steep slope. Where the principal vortex resulted in severe scour along the entire length of the 1:2.5 slope structure, in the 1:1 slope structure experiment, the bed lowered only 2 cm at the shallowest point.

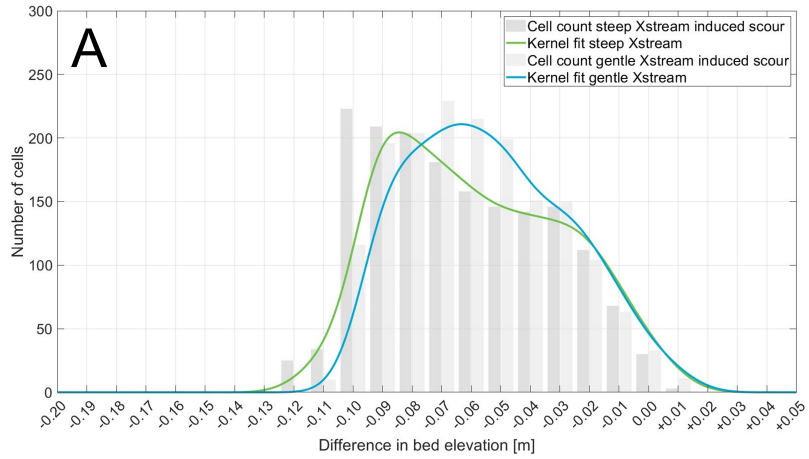

(a) Area A

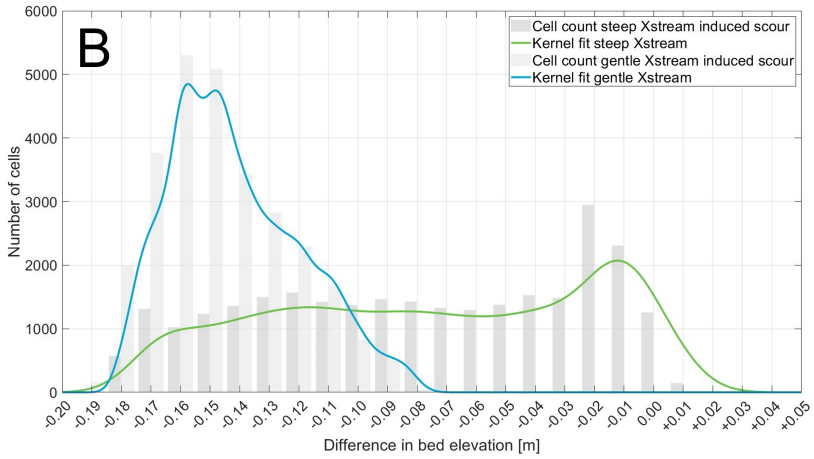

(b) Area B

Figure 4.12: Histograms of the number of cell values within a specific range. Areas A and B match the outlined areas in figures 4.7a and 4.11a. The dark grey bars represent the steep sloped Xstream abutment experiment and the light grey bars the gently sloped Xstream abutment experiment. The green and blue coloured lines are best-fitted kernel density estimations respectively.

For the examination of areas A and B, as indicated in figure 4.11a, the histograms in figure 4.12 are used. Note that the erosion pits in area A match each other quite well. Nevertheless, the steep Xstream abutment induced a slightly deeper excavation compared to the gentle Xstream abutment. This can be explained by the energy dissipation of the porous structure. The vertically driven flow loses slightly more energy as it runs over a longer length of the coarse 1:2.5 inclined structure. As a result, the shear stresses on the river bed are higher at the base of the 1:1 abutment, leading to more severe erosion at the head of the steeper obstruction.

Calculations of h_s with equation 4.1 again result in a maximum scour depth which is deeper than observed in the model. For experiment XS2, h_s should theoretically be around 21 cm.

There is a clear contrast between the two experiments when we consider the histogram of area B. It indicates that the scatter of the cell values is much wider in the experiment employing the steep Xstream abutment. The abutment with a 1:2.5 slope resulted in a relatively constant scour depth of 14 cm on average over the entire length of the structure. The Xstream structure with a 1:1 slope had an average depth that was half as deep, just like the stone experiment of the preceding section, but with much greater variation in the measured values. There is a difference of 20 cm between the highest and lowest measured point in area B of the steep Xstream experiment. Additionally, there is no clear

higher density of any particular value: all readings occur at approximately the same frequency in this area.

Along the leading edge of the steep Xstream experiment, a similar pattern to that of the gently sloped experiment is found in the resulting bed profile. Very locally, in a band about 20 cm wide around the head, the high roughness of the structure has led to an increase in turbulence, causing sediment to erode. A small ridge separates the local scour from scour due to contraction of the flow width. However, this effect only persists to about x = 6 m, rather than over the entire length of the structure as seen in figure 4.7a. Behind the steep Xstream abutment, a ridge has formed as well. Compared to the ridge behind the gently sloped Xstream structure, this ride is less developed in terms of height, length and shape. The length of the formed dunes corresponds to the areas where the flow velocity is likely to be highest. Close to the structure, in the mixing layer, the dunes are 2 m long, while on the opposite side of the flume the dunes are about 1.5 m in length. This shorter dune length corresponds to the dune length observed in the gently sloping Xstream experiment.

4.4.3. Flow velocities

The mean flow velocity, measured within the mixing layer near the upstream end of the two Xstream structures, is slightly different, with the steep abutment experiment having a lower value. Flow acceleration through the effect of horizontal contraction is less in the steep Xstream experiment since a smaller fraction of the cross-sectional flow area is obstructed by the structure.

The curved shape of both normal distributions in figure 3.17 closely match each other. This implies that there is no significant difference in the degree of variation as the standard deviation is approximately the same in both experiments. As a result, the calculated r-values of both configurations are only minimally different. A steeper slope of the abutment does not necessarily lead to a significantly increased level of turbulence.

Due to the average streamwise flow velocity being lower in experiment XS2, however, the peak velocities in this experiment were also lower. While peak velocities are often held responsible for stability and erosion, this may explain why scour is less severe near the steep Xstream abutment.

In the experiment with the 1:1 inclined Xstream structure, the flow velocity inside the structure was measured as well. Nevertheless, the velocities obtained were again too low to make any reliable statements about the permeability of the Xstream structures.

4.4.4. Observations

Since less material was used for the construction of the steep Xstream abutments, compared to the abutments featuring a gentle slope, a smaller number Xstream elements tumbled down into the erosion pit which has formed at the base of the structure. In addition, the interlocking capacity of individual Xstream elements appeared to hold stronger as the toe of the structure collapsed until the structure reached a height equal to only 3 elements.

This may be attributed to the use of a filter fabric. Similar to experiment SG1, the bed material under the structure is protected in experiment XS2, especially at the upstream end of this abutment. The falling apron effect may be reduced, resulting in an underestimation of the scour depth.

5

Discussion

This chapter elaborates on the validity of the most important assumptions and design parameters by discussing their effects on the obtained results.

5.1. Literature comparison

Based on literature, the findings of this study may be questioned and potentially disproved.

Mixing layer

The spill-through shape of the abutments tested in the experiments is a shape that is rarely described in literature. As such, the definition of the mixing layer shown in figure 4.4 is based on a combination of the horizontal contraction according to Ariëns (1993) and the horizontal expansion of the flow width as found by Zuurveld (1998). To gain a better understanding of how the mixing layer develops in the near-field of such a structure, it would be necessary to take flow velocity measurements at several locations in the flume. This would give insight into the average flow velocity dispersion in the downstream direction.

Dune dimensions

The model produced dune lengths between 1.5 and 2 m. Given the used length scale factor, n_L, this corresponds to 12 to 17 m in reality. Moreover, the height of the dunes, the vertical distance between the dune's trough and crest, is about 12 cm, which is more than 1 m in the real environment. Typically, dunes in Dutch rivers are 58 m in length and 30 to 85 cm in height, as reported by Van Rijn (1984b). Ten Brinke et al. (1999) reported comparable dune lengths, but variations in the vertical bed level of up to 1.15 m during high water conditions in the Waal river. Still, when examining the height:length ratio of the dunes, the model overestimates reality. This is in contrast to the results of De Ruijsscher (2020) and Vermeulen et al. (2014), who concluded that the morphological behaviour of the riverbed is properly reproduced using lightweight sediments. Although this study focuses mainly on locally developed erosion pits and aggregation patterns, it is good to know that the model overestimates bedforms, especially in the length direction.

Porous influence

Leu et al. (2008) concluded that with an increase in structure porosity, the flow velocity, turbulence intensity and Reynolds shear stress all decrease when water flows over a porous medium. The impact of increased roughness, or small scale irregularities in geometry, on the wall turbulence structure is predominantly confined to the near wall region. According to Bushnell and McGinley (1989), experiments and theory suggest that rough surfaces do not usually lead to a rise in net drag. This is also supported by the experimental findings of Shahsavari et al. (2017), who concluded that increased roughness of semi-cylindrical abutments reduces the severity of the scouring process.

These conclusions contradict the results of the present study, which indicate an increase in local scour as the porosity and roughness of the structure increase. The differentiation between microturbulence, a turbulent pattern that varies across small distance scales, and macro-turbulent flows, where coherent flow structures extend throughout the whole water column, appears to be crucial in this context. It seems that there is a positive feedback mechanism whereby the macro-turbulent flow develops further as water depth increases due to an increase in micro-turbulence caused by increased porosity and roughness. The complexity and non-linearity of turbulent flows pose great uncertainty in this understanding. Obtaining additional flow velocity measurements in the direct vicinity of the two structures could provide insight into the difference in turbulence levels induced by the two types of construction material.

Wall steepness

The measurements of present study are consistent with the findings of Van Alderwegen (2021), who numerically modelled hydraulic flows patterns around the flexible groyne. A steeper slope results in an increase in the Reynolds shear stresses. Although slightly, the bed shear stress in the x direction becomes higher. The shape of an hydraulic structure therefore has an impact on the scour depth as suggested earlier by the K_S value in equation 3.3 following Breusers and Raudkivi (1991).

5.2. Boundary conditions

Field data

The flexible groyne in the model is subjected to the scaled highest recorded water level until the summer of 2023, which was measured on the 7th of April 2023. However, the bed morphology measurements from the field survey date back to March 2023. Prior to this month, the extended flexible groyne had not experienced high water conditions with a discharge of 619 m^3/s. This has led to an exaggerated picture of the river morphology created by water and sediment flows in the physical model.

Field measurement data from October 2023 may unveil a morphological state that better aligns with the physical model of this study. However, these results have not yet been looked into.

Xstream model units

As noted in section Constrictions and concessions, the number of available 4 cm high Xstream model units was limited to about 7000 pieces. To maximize the length of the abutment, a combination of larger-sized model units was used for the construction of the core. To maintain consistency in the setups and to save expenses on the stone material, the core of experiment SG1 was also built using these large Xstream model units. The larger pore size inside the structures, compared to that in the cover layer, decreased the resistance to flowing water. This may have caused an overestimation of the streamwise velocity inside the structures and led to an underestimation of the velocity outside. The bigger pore size could also have influenced the development of turbulent flow structures. The velocity data obtained from the Vectrino Profiler was deemed unusable.

Length scale

The deployed length scale, n_L of 8.3, in these experiments is much smaller than the length scale used in the model tests described by De Ruijsscher (2020) and Vermeulen et al. (2014). This meant that for this study a river section of 100 m prototype could be simulated in the 12 m long flume. Interventions in the river system often affect the water level and morphology of the riverbed for many kilometres both upstream and downstream of the structure. Nevertheless, for the objective of present study, to explore the influence of applying Xstream elements in hydraulic structures on local erosion and sedimentation patterns, this constriction is not major obstacle. In fact, by testing on a relatively large scale, even the slightest distortions and distinctions have become evident

However, the ratio of structure width to flow width in the model was much greater than in reality. The mimicked flexible groyne head obstructed 3 times more cross sectional flow area as happens in reality. The abutments blocked even 10 times more of the cross sectional flow area as the LTWs in the river Waal only gradually narrow the flow width. Local scour effects extend about 3 times the diameter of the obstruction towards the axis of the river, whereas in the model the spacial width was limited by the flume's wall. Although the discharge into the flume was calculated based on the water depth and cross sectional flow area at the structures, the severe flow contraction caused the flow velocity at the toe of the structures to be exaggerated. This also exacerbated the turbulence adjacent to the structure. Combined, this led to the scour in the near-field region being overestimated.

To properly scale the desired flow conditions, certain adjustments were required to maintain the Froude number and Shields parameter within reasonable ranges of their ideally scaled values, due to the length scale. The limitations of the test facilities were compensated for by reducing the Reynolds number in particular. Turbulence in the model was still high enough to produce fully turbulent flow conditions. The hydraulic gradient at the structure may have been greater than in reality as the constriction of the flow may have caused a change in the pressure gradient. This could have led to over-predicted sediment displacement and subsequently, the morphological pattern.

Internal flow velocities

Based on Froude scaling, as explained in Appendix C, the flow velocities inside Xstream structures should have been about one third of the velocities measured in the field. For the flexible groyne in the model, this would mean an average streamwise velocity of around 0.02 m/s. A much lower velocity, however, was observed in all experiments.

In reality, the flow is turbulent through the flexible groyne. With pocket sizes in the order of 10 cm in between the randomly placed 33 cm high Xstream elements, the Reynolds number can be calculated using equation 2.6. The open spaces between the Xstream scale model units are a factor 10 smaller whereas the flow velocity should be about three times as small compared to real life conditions. Table 5.1 summarises the calculated values of the Reynolds number in both situations.

Table 5.1: Reynolds number inside the flexible groyne.

Symbol	Variable	Unit	Prototype	Model
$\overline{u_x}$	Mean streamwise flow velocity	m/s	0.05	0.02
d	Open spaces size	m	0.10	0.01
v	Kinematic viscosity	m^2/s	$1.33e^{-6}$	$1.08e^{-6}$
Re	Reynolds number	-	3800	180

With a Reynolds number of 3800, the flow through the flexible groyne in the river IJssel is on the boundary between the critical and the turbulent regime. In the model, the flow through the structure got laminar inside the structure. The Darcy-Weisbach equation relates head loss due to friction to the average velocity. This equation contains a dimensionless friction factor, f_D. In the diagram by Moody and Princeton (1944), the Darcy-Weisbach friction factor is plotted against the Reynolds number.

For laminar flows, the friction factor can be approached by $f_D = \frac{64}{Re}$. For high Reynolds numbers, the resistance to flow it is almost constantly proportional to the square of the mean flow velocity. The resulting friction factors in both prototype and model are listed in table 5.2.

Table 5.2: Darcy-Weisbach friction factor inside the flexible groyne.

Symbol	Variable	Unit	Prototype	Model
f_D	Darcy friction factor	-	0.03	0.36

Resistance to flow was about 10 times as high in the model compared to reality. This has resulted in more water being directed towards the main flow instead of flowing through the structure. The effect of contraction, accelerating the flow, initiating and enhancing erosion, is therefore strengthened in the model. This applies to all test setups of present study. Testing on an even smaller scale would exaggerate this discrepancy.

A small note to this approach is that the flow velocity in the flume was already not perfectly scaled according to Froude due to the limitations of the test facilities resulting from the small length scale factor.

Backwater curves

The flow of water over the weir at the end of the flume results in the establishment of a backwater curve. The influence of this backwater curve, due to the comparatively small length scale, may extend far towards the upstream end of the flume. Accordingly, the backwater curve could potentially have affected the water surface slope, which was calculated based on water level measurements in the stilling wells. The presence of a backwater curve may have affected the average flow rate in the flume and, in turn, the erosion and sedimentation process. Due to the moving bed, measuring the extent to which a backwater curve might have influenced the resulting bed morphology was challenging. Taking more measurements of the water level along the length of the flume would provide a more comprehensive understanding of the flow and upstream impact of any backwater curve.

Material properties

The densities of the stone and Xstream model units used exactly match the density of these actual materials. The lightweight sediment, however, is much lighter than sand. Its density is 1055 kg/m^3 compared to approximately 1650 kg/m^3 for river sand. Using lightweight material achieves dynamic similarity in physical scale models and their prototypes as it allows for realistic scaling of the Froude number and Shields parameter. According to the latter, initiation of motion scales well but the settling velocity does not. However, this is of negligible importance as bed load was the primary mode of sediment transport, with only a minimal amount of sediment in suspension.

5.3. Model inaccuracy

Of course, failures were made in the preparation of the experiments, in the collection of the data and in the analysis of the results.

Run time

The total time at which the pumps supplied the flume with the planned flow rate was not always tracked accurately. The aim was to run each experiment for at least four consecutive hours. Though, it was not always precisely achievable due to the necessity to manage multiple operations simultaneously. In the end, each setup was exposed to the scaled high water conditions for 4 to 4.5 hours. In one of the experiments, the maximum scour depth was roughly determined by hand approximately every half an hour. At a certain point in time, the erosion pit remained at a more or less constant depth and the scour stagnated. It is assumed that within the total run time, the depth of the erosion pits have reached their equilibrium depth.

Weight distribution

Figure 5.1 illustrates the subsidence of both Xstream and stone experiments with a 1:2.5 slope. This figure gives another perspective on why the scour is more severe in experiment XG2 compared to SG1 while the flow velocity and turbulence intensity are dissipated more due to the higher porosity and roughness of the structure. The crucial difference is the use of a geotextile under the structure. Unlike the stone structure, the Xstream structure lacks support, leading to an uneven distribution of the load over the lightweight sediment bed. The leading edge of the Xstream structure in particular sank into the polystyrene layer under its own weight because the scour hole created by the vortex has made the structure unstable. The material was pushed into the accelerating flow where it was subjected to shear stresses that are above its critical value and transported downstream. Also in experiment SG1 individual stones slid into the scour hole at the structure's toe. As they did, they pulled the geometrically closed filter fabric with them, trapping the material underneath and preventing it from moving. This can be seen in one of the photos in Appendix D.

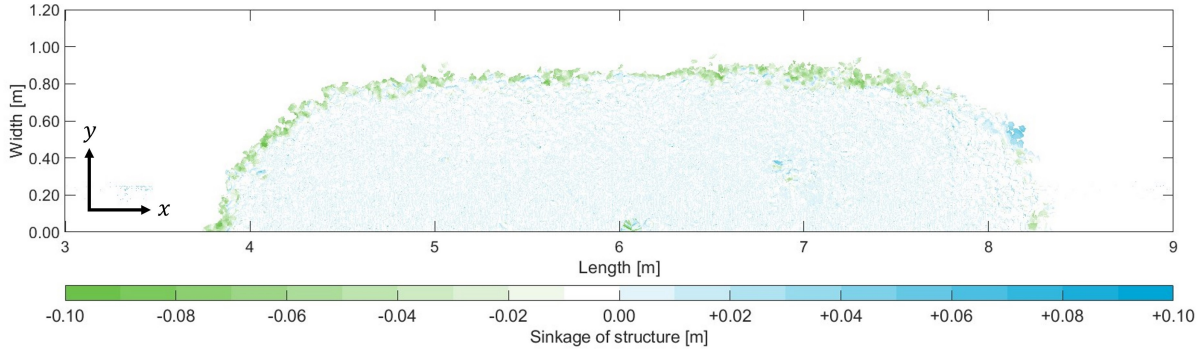

(a) Difference in stone structure elevation

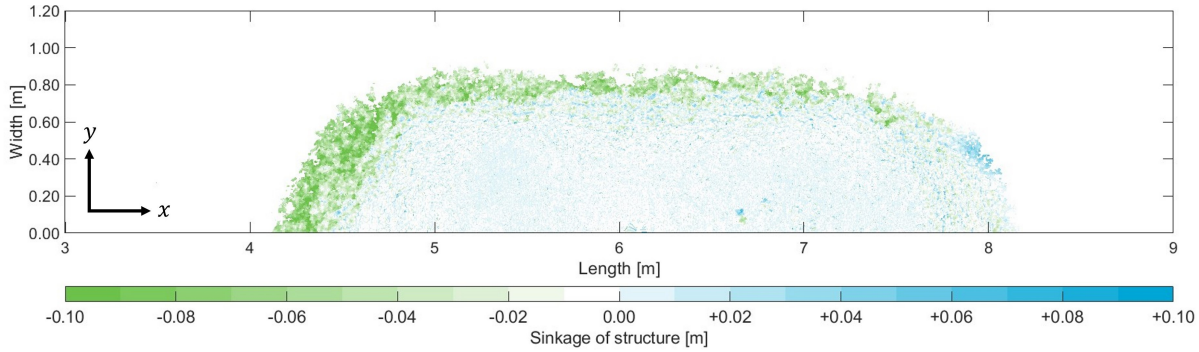

(b) Difference in Xstream structure elevation

Figure 5.1: Comparison between the amount of sinkage of both structures in experiments SG1 and XG2.

The falling apron mechanism is much more present at the Xstream structure compared to the stone structure, which is expected to happen in reality as well. In the design of hydraulic structures of Xstream, this characteristic should be taken into account.

Construction

All configurations were built manually. This has resulted in some setups deviating slightly from their design. For example, the slope of the 1:2.5 Xstream experiment was steeper than designed, as shown in figures 3.8 and 3.14. This factor may have contributed to an increased erosion rate in experiment XG2. Moreover, the length of the structures was also not exactly the same, which may have affected the downstream formed dune length. The construction of such structures in reality cannot be much more precise than it was attempted in the experiments of this study. Outside, the flowing water or the crane may compact the structure somewhat.

5.4. Interpretation of results

It is important to emphasise the way the data is read and how it is linked to the real world.

Resolution

The riverbed was scanned at a much higher resolution in the laboratory flume than the measurements taken on-site. The data obtained from the scans of the experimental models was interpolated onto a regular grid of 1 x 1 cm, which corresponds to an area of nearly 70 cm^2. The field data of the morphology around the extended flexible groyne head was plotted on a 50 x 50 cm grid. It is possible that figures 3.4 and 3.5 would be more consistent with each other if the resolutions were better matched. However, this level of precision is not required to provide a general picture of the performance of the model relative to reality.

Static perspective

The recirculation of discharged sediment caused live-bed scour conditions during the experiments. Yet, the scanned bed morphology after each experiment is only a static image of a dynamic and evolving system. Bed load transport with migrating dunes was identified as the main transport mode as $\overline{u} < 4u_c$. The fluctuation of scour depth corresponded to the dune migration through the scour hole (Ettmer et al., 2015). According to Arneson et al. (2012), the fully developed scour depth is at most 10% more and at least 10% less than the equilibrium scour depth. Visual observations indicated that the depth of the scour pit at the upstream end of the structure, formed by eddies created by frontal flow, indeed changed with the passage of bedforms.

Dunes migrating downstream increased in length as they passed the structure where the flow accelerated. Unfortunately, no measurements were taken of the rate of dune migration, which could have been done easily by measuring Δx per defined time step. Also for the position of the dunes, the bed scans only provided a momentary overview.

Systematic errors

In addition to the random errors previously described, there were also systematic errors that occurred throughout the experiments. These systematic errors can be categorised as environmental, observational, and instrumental. Environmental errors are those caused by external factors in the environment that introduce noise or distortion into the results. These errors are minimised in a regulated laboratory setting. Observational errors result from human mistakes in reading or analysing data. Instrumental errors are considered as part of the constant errors which arise from incorrect calibration of measuring equipment or their inaccuracy.

The discharge into the flume was regulated with an accuracy of 1 l/s, measured by an electromagnetic flow meter, by manually turning a wheel. The stilling well readings were super constant as the linear position sensors themselves pre-processed the data with an accuracy up to tenths of millimetres. The ADV with the side-looking probe also generated filtered data based on their values for correlation and the signal-to-noise ratio, which both must be above certain thresholds. The camera-laser combination measured the bed elevation from a physically defined starting position where x = 0, y = 0 and z = 0. Assuming the calibrations, performed by the lab technician, went well, the accuracy of the instruments was considered sufficient for the purposes of this study.

6

Conclusion and recommendations

6.1. Conclusion

To conclude the findings of present study, answers will be given to the research questions as formulated in the Introduction chapter of this thesis.

What flow patterns influence the morphodynamics around Xstream river training works?

Rivers are constantly changing natural dynamic systems. The morphology of the river bed is largely determined by flow characteristics and sediment properties. Interventions in river systems alter these water and sediment flow patterns. Among others, the primary reasons for building river training works are to maintain navigability during low water levels and provide flood protection by facilitating water discharge during high water levels. There is a wide variety in design of these structures, with present study having focused particularly on groynes and abutments. The construction of lateral river constrictions enhances two types of scour: contraction scour and local scour. Contraction scour occurs when the water accelerates due to narrowing of the flow width, leading to an increase in shear stresses on the bed and the initiation of sediment transport. Local scour results from the frontal encounter of flowing water with an obstruction, creating a vertical downward gradient and a vortex that intensifies with depth, resulting in complex sediment relocating flow patterns. The porosity of a structure determines the extent to which it can efficiently absorb and dissipate the kinetic energy of flowing water, thereby reducing the flow velocity and turbulence levels, which mitigates scour formation. Additionally, the geometry of the structure also has a minor impact on the scour pattern in the hydraulic structure's near-field. Homogeneous structures of Xstream are believed to behave like an open filter construction, where the bed material can freely move through the structure if the parallel critical gradient is above a certain threshold.

How well does the used physical scale model perform in mimicking reality?

A physical scale model of the flexible groyne head with a length scale factor (n_L) of 8.3 was subjected to high water simulations based on flow characteristics in the river IJssel. To achieve dynamic similarity with the real-world conditions, lightweight sediments were used to imitate river sand. The model results were compared to field measurements of the bed morphology and flow velocity. In terms of length and width of the resulting scour hole, the model did not correspond to the field observations due to scale effects. Whilst the effect of local scour is confined, it extends much further in the actual river. Furthermore, the maximum depth of erosion was overestimated by about 40%. This could be due to the 3 times stronger contraction in the model, not only because of the larger ratio of structure width to flow width, but also because the magnitude of flow acceleration induced by contraction is likely to be less significant in the real situation given the presence of existing groynes upstream and downstream of the flexible groyne. The location of the deepest erosion aligned reasonably well with the field data. By conducting the experiments on a relatively large scale, even the smallest morphological patterns were revealed and the interaction between the structural behaviour and the river bed became apparent.

Flow through the structure was, in contrast to the real world, laminar in the model. This resulted in a friction factor that was 10 times as high, leading to the flow experiencing much more resistance than it would in the field. Overall, the physical scale model seems to approximate reality to some extent, especially in the vicinity of the hydraulic training works. Nevertheless, several factors contribute to the disparities observed.

To what extent plays a higher porosity and wall roughness part in local sediment displacement?

Two abutments, identical in shape, were built in a physical scale model to monitor the effects of increased porosity and roughness on the morphodynamics of the river bed. The studied materials were in size scaled down quarry stone, based on traditionally applied rocks in hydraulic structures, and Xbloc model units of equal density to concrete. The 15% porosity disparity between bodies of stone and Xstream was determined through the quantification of water required to saturate a known volume of construction material. Moreover, water level readings indicated a build-up twice as heavy in front of the stone structure, suggesting a lower permeability of the structure. The results of the velocimeter showed that the streamwise flow velocities in the main channel were consistently lower but more variable during the experiment featuring the Xstream abutment. As a result, a 17% higher relative turbulence level was calculated, revealing the impact of Xstream. River bed scans illustrate that the scour depth was significantly greater along the length of the Xstream abutment. Despite the live-bed conditions potentially causing scour depths to fluctuate by up to 10% from their equilibrium, a significant difference of about 20% remained. The absence of a supporting fabric in the Xstream experiment most likely led to uneven load distribution while in the experiment with the stone structure, this fabric prevented the low-density bed material to erode. This observation was described as the falling apron mechanism, where the slope of the scour hole at the base of the Xstream structure was covered with individual elements that had lost their interlocking capacity as the stability of the structure was undermined. It is plausible that the increased roughness and length of the eroded slope intensified complex turbulence levels, enhancing scour in a positive feedback loop. When considering only the flow velocity, the primary driver of sediment transport which was exaggerated by the increased resistance of water to flow through the structure, it can be deduced that the porous structure absorbs more motional forces, thereby reducing erosion in the near-field. However, discrepancies in the physical scale model contradict this suggestion.

How does the slope of an embankment affect erosion and sedimentation?

A steeply 45° inclined abutment made from Xstream elements was tested in the identical physical scale model employed previously. The porosity and roughness were similar to those measured in the experiment featuring the 1:2.5 sloped Xstream abutment, as it was built from the same material. Flow velocity measurements found that the average streamwise velocity was 7% lower in the experiment with the steep Xstream abutment, with only a slight increase in the mean deviation from this average. The observed lower flow acceleration can be attributed to the reduced effect of contraction, as the cross-sectional flow area decreased proportionally less at the 1:1 sloped abutment. Both structures induced relatively equivalent scour depths at the upstream ends. Only a slightly deeper erosion pit, by approximately 1 cm, was measured in front of the steep Xstream abutment. This observed difference was considered too insignificant to be conclusive. A wave-like sediment pattern emerged in the longitudinal direction directly at the base of the steep Xstream structure. Along the length of this structure, the erosion was not as severe and consistent as at the gently sloped Xstream abutment. The effect of the principal vortex causing these irregularities appeared to extend less far downstream compared to what was found earlier. Again, the less exaggerated effect of contraction seems to underlie this. An alternative possibility could be that a supporting filter fabric was placed underneath the steep Xstream structure, which distributed the weight load more evenly over the bed. Furthermore, the interlocking capacity of randomly placed Xstream elements was noted to be higher, with a reduced number of individual Xstream elements covering the scour hole slope.

6.2. Recommendations

A few of the recommendations for future research are given in this section. This list, however, is infinite, because the application of Xstream elements in the Dutch river system entails a lot of innovation and lacks fundamental knowledge and experience on water and sediment flow patterns.

Length scale factor

In the physical scale model employed for this research, the setups were designed with a length scale factor n_L = 8.3. This forced to make a lot of concessions and assumptions about the real world conditions. In addition, the effects of all changes to the river's course stretch far upstream and downstream of the intervention. Therefore, increasing the length scale factor allows for the mimicking of a larger river section in which the effect of contraction is not as present.

The applied length scale factor in present study is workable when the local flow characteristics are known. In this case, for example, the average flow velocity across the whole river was scaled down but locally, very close to the hydraulic structures, these velocities could be different in reality. Therefore, to realistically mimic a river section, the aim of the study should specify what information is required from the field.

Increasing the length scale factor decreases the size of the open spaces in between Xstream elements. This would lead to even smaller Reynolds numbers for flow through the structure and more resistance to water, forcing it to flow through the main channel. Both raising and lowering the length scale factor comes with uncertainties. Making concessions and assumptions are unavoidable in physical scale modelling. Therefore, the most realistic image is obtained by designing and implementing a real life pilot study, although expensive. In this case, even the most local effects of Xstream to the riverbed morphology can be observed.

Material density

Based on this study, no solid conclusions can be drawn about the stability of the structures because of the density difference between the bed and construction material. Geometrically, the polystyrene granules are expected to act differently compared to normal river sand. As a result, the heavy stones and Xstream elements put a relatively higher pressure on the bed leading to more severe instability of the structure. To limit this effect, a mesh fabric supported the structure by evenly distributing the load onto the bed, preventing it from subsiding due to its own weight. If the main objective would be to study the stability of steep Xstream structures, the model units should be scaled down in density accordingly.

Mitigating the density difference by using less dense construction material would probably give a more realistic behaviour of the structure's stability. This is due to the fact that lighter weighing material can be supported by a less stable foundation. The suggested positive feedback loop of scour formation is suppressed. Still, the D_{50} of the lightweight granules is bigger in the model compared to reality.

Velocity measurements

Taking velocity measurements on multiple positions in the flume would have resulted in better understanding of the flow patterns governing sediment relocation. By reading the flow velocity in one point only, insight has been gained on the changes in time due to, for example, migrating dunes passing by. However, especially for the purpose of this study, it would have been interesting to measure the decreased velocity and the increased turbulence close to the structure walls.

Hypothetically, this reveals stronger turbulence levels in the scour hole at the base of the Xstream structure as erratic shaped elements cover one side of the scour hole, increasing roughness. Velocity measurements using an ADCP, measuring the velocity profile throughout the water column from the water surface, would be preferred as there is no physical device interacting with the flow patterns, thereby disturbing the bed.

Live bed scans

The bed scans made of the experimental setup of this study only represent one moment in time whereas the morphology was constantly developing. Being able to scan the bed elevation through the water column during the experiments would yield valuable insight into the dynamic processes of erosion and sedimentation. By measuring the bed forms live, dune decay and migration rates could be determined. Additionally, fluctuations in scour depth due to the live bed conditions could be monitored.

In theory, the line laser scanner combination as used in this study is able to scan the bed through water. The measurements should then be corrected for the refraction of light at the air-water interface. However, obtaining good elevation measurements appeared to be impossible due to the turbidity of the water in combination with the water depth and the reflection of day and artificial light at the water surface. Under ideal circumstances, the water is crystal clear and the experiments are carried out in a dark laboratory. This increases the ability to scan through deeper water columns. However, it remains uncertain whether it would be enough to reach through the water depth as used in present study.

References

Ariëns, E. (1993). *Relatie tussen ontgrondingen en steenstabiliteit van de toplaag* (Doctoral dissertation). TU Delft. Delft. https://repository.tudelft.nl/islandora/object/uuid%3A4632b183-6052-4a5e-861f-84563444f8a5

Arneson, L., Zevenbergen, L., Lagasse, P., & Clopper, P. (2012). *Evaluating Scour around Bridges* (Fifth). Federal Highway Administration, U.S. Department of Transportation.

Barbhuiya, A. K., & Dey, S. (2004). Local scour at abutments: A review. *Sadhana - Academy Proceedings in Engineering Sciences*, *29*(5), 449–476. https://doi.org/10.1007/BF02703255/METRICS

Bilgili, E. (2018). Hydraulica - Evaluatie afvoerbepaling van de IJssel te Olst.

Blazejewski, R., Pilarczyk, K., & Przedwojski, B. (1995). *River Training Techniques: Fundamentals, Design and Applications*. A.A. Balkema.

Blom, A. (2016). Bed degradation in the Rhine River (G. Balint, B. Antala, C. Carty, J.-M. A. Mabieme, I. B. Amar, & A. Kaplanova, Eds.). *TU Delft DeltaLinks*, *7*(1), 343–354. https://doi.org/10.2/JQUERY.MIN.JS

Blom, A. (2021). Lecture slides River Dynamics 1 (CIE4345) TU Delft.

Breusers, H., & Raudkivi, A. (1991). *Scouring* (First). Balkema. https://www.abebooks.com/first-edition/Scouring-Breusers-H-Raudkivi-Balkema-Rotterdam/30055900943/bd

Buschman, F., & Kosters, A. (2021). *Pilot flexibele kribben in de Ussel* (tech. rep.). Deltares.

Bushnell, D. M., & McGinley, C. B. (1989). Turbulence control in wall flows. *Fluid Mechanics*, *21*, 1–20. www.annualreviews.org

Busnelli, M., Schuurman, F., Sieben, A., Wal, M. v. d., & Hector, H. (2011). Morphodynamic responds of groyne fields to the lowering of crest level of the groynes in the Waal River, The Netherlands. *River, Coastal and Estuarine Morphodynamics*, 1450–1463. https://dspace.library.uu.nl/handle/1874/280100

Czapiga, M. J., Blom, A., & Viparelli, E. (2022). Efficacy of Longitudinal Training Walls to Mitigate Riverbed Erosion. *Water Resources Research*, *58*(12). https://doi.org/10.1029/2022WR033072

De Graauw, A. F., Van der Meulen, T., & Van der Does de Bye, M. R. (1984). Granular Filters: Design Criteria. *Journal of Waterway, Port, Coastal, and Ocean Engineering*, *110*(1), 80–96. https://doi.org/10.1061/(ASCE)0733-950X(1984)110:1(80)

De Jong, W., Van de Waart, M., & Driessen, T. (2012). *Planstudie IJsseldelta-Zuid Deelproduct 9: Hydraulica en Veiligheid* (tech. rep.).

De Ruijsscher, T. V., Vermeulen, B., & Hoitink, A. J. (2020). Diversion of Flow and Sediment Toward a Side Channel Separated From a River by a Longitudinal Training Dam. *Water Resources Research*, *56*(6). https://doi.org/10.1029/2019WR026750

De Ruijsscher, T. V. (2020). *Aligned with the flow: Morphodynamics in a river trained by longitudinal dams* (Doctoral dissertation). Wageningen University. https://doi.org/10.18174/503236

De Vriend, H. (2010). *Morfologische effecten kribverlaging - Deskundigenoordeel project kribverlaging* (tech. rep.). TU Delft.

De Vries, M. (1975). *Waterloopkundig onderzoek*. https://repository.tudelft.nl/islandora/object/uuid%3A965c4e6f-ed4e-429a-bd0d-b8e4f1cfc864

Duró, G., & Gradussen, B. (2022). *Morfologische Analyse Rijntakken* (tech. rep.). Rijkswaterstaat Oost-Nederland.

Eerden, H. (2022). *WaalSamen, Pilot Langsdammen: Samenvatting rapportages integrale evaluatie pilot* (tech. rep.). Rijkswaterstaat. 's-Gravenhage.

Engelund, F., & Hansen, E. (1967). A monograph on sediment transport in alluvial streams. *Technical University of Denmark 0stervoldgade 10, Copenhagen K.* https://repository.tudelft.nl/islandora/object/uuid%3A81101b08-04b5-4082-9121-861949c336c9

Ettema, R., & Muste, M. (2004). Scale Effects in Flume Experiments on Flow around a Spur Dike in Flatbed Channel. *Journal of Hydraulic Engineering*, *130*(7), 635–646. https://doi.org/10.1061/(ASCE)0733-9429(2004)130:7(635)

Ettema, R., Nakato, T., & Muste, M. (2003). *An Overview of Scour Types and Scour-Estimation Difficulties Faced at Bridge Abutments* (tech. rep.). https://www.researchgate.net/publication/228611557_An_Overview_of_Scour_Types_and_Scour-Estimation_Difficulties_Faced_at_Bridge_Abutments

Ettmer, B., Mueller, F., & Link, O. (2015). Live-Bed Scour at Bridge Piers in a Lightweight Polystyrene Bed. *Journal of Hydraulic Engineering*, *141*(9).

Fakhimjoo, M., Ardeshir, A., Behzadian, K., & Karami, H. (2023). Experimental investigation and flow analysis of clear-water scour around pier and abutment in proximity. *Water Science and Engineering*, *16*(1), 94–105.

Frings, R. M. (2015). Sand and Gravel on the Move: Human Impacts on Bed-Material Load Along the Lower Rhine River. *Geomorphic Approaches to Integrated Floodplain Management of Lowland Fluvial Systems in North America and Europe*, 9–26. https://doi.org/10.1007/978-1-4939-2380-9{_}2/FIGURES/6

Frostick, L., McLelland, S., & Mercer, T. (2011). *Users Guide to Physical Modelling and Experimentation Experience of the HYDRALAB Network*. CRC Press.

Gorrick, S., & Rodríguez, J. F. (2014). Scaling of sediment dynamics in a laboratory model of a sand-bed stream. *Journal of Hydro-environment Research*, *8*(2), 77–87. https://doi.org/10.1016/J.JHER.2013.12.001

Graf, W. H., & Altinakar, M. S. (2016). Local scour. In N. Sharma (Ed.), *River system analysis and management* (pp. 145–166). Springer Singapore. https://doi.org/10.1007/978-981-10-1472-7{_}8/FIGURES/12

Groenewege, R., & Buschman, F. (2023). Flexibele krib fase 2: Tussentijdse resultaten.

Havinga, H. (2020). Towards Sustainable River Management of the Dutch Rhine River. *Water*, *12*(6), 1845. https://doi.org/10.3390/W12061827

Hooijer, A., Barneveld, H., Bos, M., Hoffmans, G., Schropp, M., & Struijk, R. (2007). Leidraad Rivieren. *L16- isbn 9789036914086*. https://repository.tudelft.nl/islandora/object/uuid%3Ac14b8a5d-322d-4e2e-8780-cd03a9973cdb

Hughes, S. A. (1993). *Physical Models and Laboratory Techniques in Coastal Engineering* (Vol. 7). WORLD SCIENTIFIC. https://doi.org/10.1142/2154

Jammers, S. (2017). *Sediment transport over sills of longitudinal training dams* (Doctoral dissertation). TU Delft. https://repository.tudelft.nl/islandora/object/uuid%3A4570fe94-c2f2-4d4c-96a0-fb53d7e7dc3f

Jongschaap, R. (2022). *Het effect van Xstream-blokken op de stroming bij extreme afvoer* (Doctoral dissertation). De Haagse Hogeschool.

Kirby, A., Roca, M., Kitchen, A., Escarameia, M., & Chesterton, O. (2015). *Manual on scour at bridges and other hydraulic structures, second edition* (second). CIRIA. https://www.ciria.org/CIRIA/Resources/Free_publications/manual_on_scour.aspx

Kleinhans, M. G., Van Der Vegt, M., Terwisscha Van Scheltinga, R., Baar, A. W., & Markies, H. (2012). Turning the tide: experimental creation of tidal channel networks and ebb deltas. *Netherlands Journal of Geosciences*, *91*(3), 311–323. https://doi.org/10.1017/S0016774600000469

Kocyigit, O., Lin, B., & Falconer, R. A. (2005). Modelling sediment transport using a lightweight bed material. *Proceedings of the Institution of Civil Engineers: Maritime Engineering*, *158*(1), 3–14. https://doi.org/10.1680/MAEN.2005.158.1.3

Le, T. B., Crosato, A., & Montes Arboleda, A. (2020). Revisiting Waal River Training by Historical Reconstruction. *Journal of Hydraulic Engineering*, *146*(5). https://doi.org/10.1061/(ASCE)HY.1943-7900.0001688

Le, T. B., Crosato, A., Mosselman, E., & Uijttewaal, W. S. (2018). On the stability of river bifurcations created by longitudinal training walls. Numerical investigation. *Advances in Water Resources*, *113*, 112–125. https://doi.org/10.1016/J.ADVWATRES.2018.01.012

Lely, C. (1890). Afd. XI - Rivieren en Rivierwerken. In N. Henket, C. Schols, & J. Telders (Eds.), *Waterbouwkunde*. De Gebroeders Van Cleef. https://books.google.nl/books?id=5FHevwEACAAJ&printsec=frontcover&hl=nl#v=onepage&q&f=false

Leu, J. M., Chan, H. C., & Chu, M. S. (2008). Comparison of turbulent flow over solid and porous structures mounted on the bottom of a rectangular channel. *Flow Measurement and Instrumentation*, *19*(6), 331–337. https://doi.org/10.1016/J.FLOWMEASINST.2008.05.001

Liefveld, W., Emond, D., & Van der Valk, M. (2011). *Kribverlaging Waal fase 3 en Langsdammen Wamel en Ophemert* (tech. rep.). Rijkswaterstaat Oost-Nederland.

Moody, L., & Princeton, N. (1944). Friction Factors for Pipe Flow. *Transactions of the ASME*, *66*(8), 671–684.

Mosselman, E., Buijse, T., Van der Deijl, E., De Jong, J., Chavarrias, V., Ottevanger, W., Asselman, N., De Grave, P., Van der Mark, C., Van der Wijk, R., Collas, F., Van der Vat, M., Sloff, C., Verbrugge, L., & Van den Born, R. (2021). *Eindevaluatie pilot Langsdammen in de Waal: hoofdrapport* (tech. rep.). Deltares.

Mosselman, E. (2020). Studies on River Training. *Water*, *12*(11), 3108. https://doi.org/10.3390/W12113100

Muste, M., Lyn, D. A., Admiraal, D. M., Ettema, R., Nikora, V., & García, M. H. (2017). *Experimental Hydraulics: Methods, Instrumentation, Data Processing and Management*. CRC Press/Balkema. https://www.routledge.com/Experimental-Hydraulics-Methods-Instrumentation-Data-Processing-and/Muste-Lyn-Admiraal-Ettema-Nikora-Garcia/p/book/9780367573355

Ong, M., Lim, S., Yu, G., & Tan, S. (2004). Abutment Scour Using Lightweight Bed Material. *2nd International Conference on Scour and Erosion (ICSE-2)*.

Reeze, B., Van Winden, A., Postma, J., Pot, R., Hop, J., & Liefveld, W. (2017). *Watersysteemrapportage Rijntakken 1990-2015. Ontwikkelingen waterkwaliteit en ecologie* (tech. rep.). Bart Reeze Water & Ecologie. Harderwijk.

Rijkswaterstaat. (2012). *Rivierkundige Informatiemap Rijn, Waal en IJssel* (tech. rep.). Rijkswaterstaat Oost-Nederland.

Schiereck, J. (2019). *Introduction to bed, bank and shore protection* (H. Verhagen & B. Hofland, Eds.; 2nd). Delft Acedemic Press / VSSD.

Shahsavari, H., Heidarpour, M., & Mohammadalizadeh, M. (2017). Simultaneous Effect of Collar and Roughness on Reducing and Controlling the Local Scour around Bridge Abutment. *Acta Universitatis Agriculturae et Silviculturae Mendelianae Brunensis*, *65*(2), 491–499.

Sieben, J. (2007). *Ontgrondingskuilen in de Waal* (tech. rep.). RIZA werkdocument 2005.082x.

Sloff, C., Van der Sligte, R., & Ottevanger, W. (2014). *Morfologische Pakketsom Waal, Morfologische effecten Ruimte-voor-de-Riviermaatregelen* (tech. rep.). Deltares.

Ten Brinke, W. (1997). *De bodemsamenstelling van de Waal en IJssel in de jaren 1966, 1976, 1984 en 1995* (tech. rep.). Ministerie van Verkeer en Waterstaat, Rijkswaterstaat, RIZA, Rijksinstituut voor Integraal Zoetwaterbeheer en Afvalwaterbehandeling.

Ten Brinke, W., Wilbers, A., & Wesseling, C. (1999). Dune growth, decay and migration rates during a large-magnitude flood at a sand and mixed sand-gravel bed in the Dutch Rhine river system. *Spec. Publs int. Ass. Sediment.*, *28*, 15–32.

Van Alderwegen, E. (2021). *Modelling open channel flow for the features of a flexible groyne: Effects of permeability and head steepness of groynes on local flow characteristics* (Doctoral dissertation). TU Delft Civil Engineering and Geosciences. Delft. https://repository.tudelft.nl/islandora/object/uuid%3Afe7a1bbb-1599-4ce6-b044-8f6b6fb34c5b

Van Broekhoven, R. (2007). *Het effect van kribverlaging op de avoercapaciteit van de Waal ten tijde van hoogwater* (Doctoral dissertation). TU Delft. Papendrecht.

Van de Mortel, J. H. B. (2005). "Samen werken aan de Midden Waal": Alternatieven voor rivierverruiming tussen Nijmegen en Tiel.

Van der Hoeven, M. (2002). *Behaviour of a falling apron* (Doctoral dissertation). Delft University of Technology. Delft.

Van Rijn, L. C. (1984a). Sediment Transport, Part I: Bed Load Transport. *Journal of Hydraulic Engineering*, *110*(10), 1431–1456. https://doi.org/10.1061/(ASCE)0733-9429(1984)110:10(1431)

Van Rijn, L. C. (1984b). Sediment Transport, Part III: Bed forms and Alluvial Roughness. *Journal of Hydraulic Engineering*, *110*(12), 1733–1754. https://doi.org/10.1061/(ASCE)0733-9429(1984)110:12(1733)

Van Weerdenburg, R. (2018). *Measured change in bed elevation and surface texture near longitudinal training dams in the Waal River* (Doctoral dissertation). Delft University of Technology. Delft.

Verheij, H., Heijer, F. d., Schijndel, S. v., Sloff, C., Wal, M. v. d., & Voorthuizen, J. v. (1997). *Effectiviteit van kribben* (tech. rep.). Waterloopkundig Laboratorium. Deltares (WL). https://repository.tudelft.nl/islandora/object/uuid%3Af43b7c81-8e0f-4452-a956-049039d259d0

Vermeulen, B., Boersema, M., Hoitink, A., Sieben, J., Sloff, C., & van der Wal, M. (2014). River scale model of a training dam using lightweight granulates. *Journal of Hydro-environment Research*, *8*(2), 88–94. https://doi.org/10.1016/J.JHER.2013.05.004

Visser, M., & Klopstra, D. (2002). *Onderzoek nauwkeurigheid debietrandvoorwaarden Noordelijk Deltabekken* (tech. rep.). HKV Lijn in Water.

Yalla Arbós, C., Blom, A., Van Vuren, S., & Schielen, R. (2019). *Bed level change in the upper Rhine Delta since 1926 and rough extrapolation to 2050* (tech. rep.). Delft University of Technology. Delft.

Zuurveld, J. (1998). *Hoofdstroming contra menglaag: De invloed van een menglaag op het begin van bewegen van bodemmateriaal* (Doctoral dissertation). TU Delft. Delft. https://repository.tudelft.nl/islandora/object/uuid%3Ad4ba530a-eebe-456e-8d61-2a3300380f45

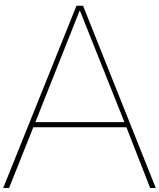

Technical drawing

Tilt your head 90° and turn the page.

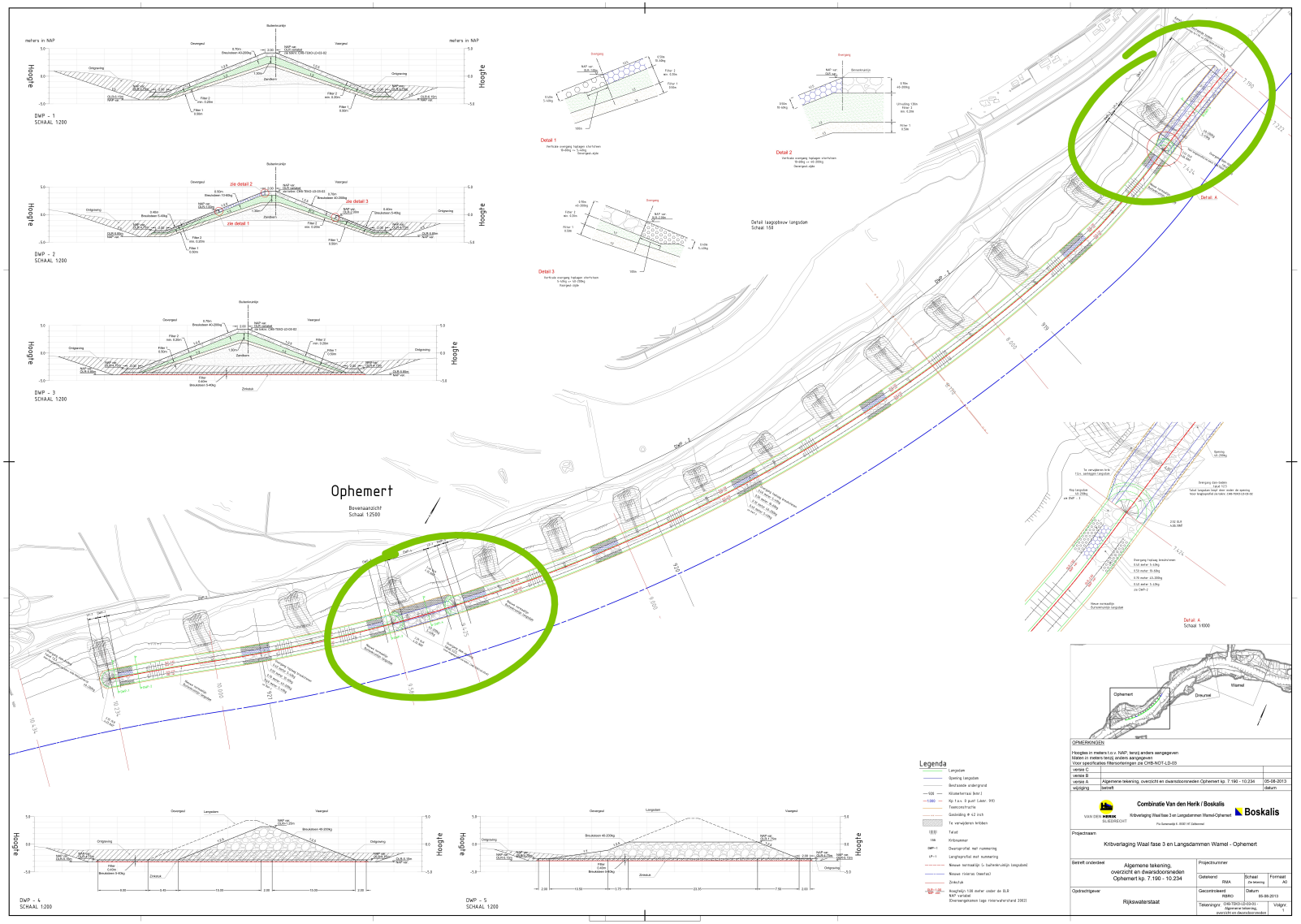

Figure A.1: Technical drawing of the LTW at Ophemert

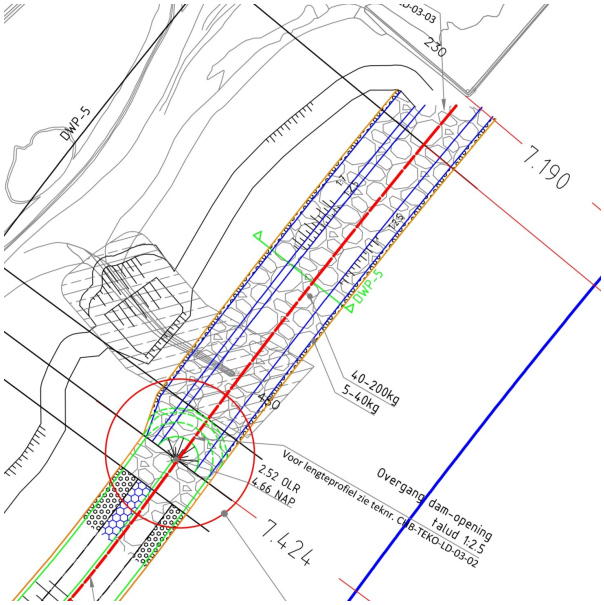

(a) Detail of the technical drawing of the LTW inlet

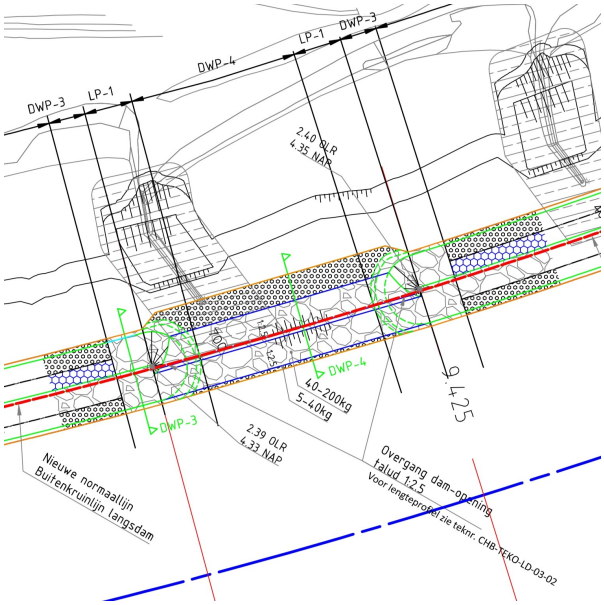

(b) Detail of the technical drawing of the LTW sill

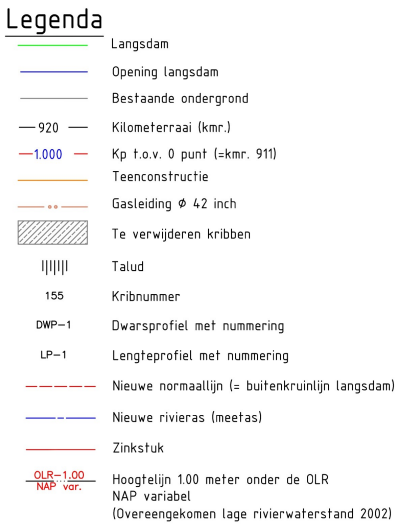

B

Research process

From an educational point of view, it is important to understand the whole thesis process. This Appendix summarises the steps taken over the past 12 months by listing the former sets of research questions.

My graduation trajectory started in September 2022 by contacting multiple (mainly construction) companies with the question if they have an interesting thesis topic that is related to concepts like: integrated river management, building with nature, Room for the River, river and coastal dynamics and remote sensing. I wanted to graduate within a company to experience to some extend what it means to work for an engineering company. Luckily, the BAM invited me and very naturally the idea arose to do physical scale model experiments into the potential of longitudinal training walls made of Xstream. As their pilot with a flexible groyne in the river IJssel showed promising results and Rijkswaterstaat's keen interest in building more LTWs in the future, it was interesting to investigate whether Xstream elements could be used for the construction of LTWs. I kicked my thesis off with the following research questions:

1. What is the effect of turbulence, induced by high roughness, on sediment movement around the dam?
2. How much is the stability of an Xstream LTW affected at high water?
3. To what extend does an LTW of Xstream separate water and sediment flows between the main and the side channel?
4. Can Xstream LTWs potentially be a compatible alternative to traditional dams with a layered structure?

In the meantime, I had made arrangements with professors at the Wageningen University to contribute with their facilities and expertise to my research. The project would be financed half by the BAM and half by Rijkswaterstaat. Limitations in the number, size and density of the Xblock model units available from BAM meant that concessions had to be made with the model and uncertainties had to be dealt with. To increase the length scale, I considered producing a large number of small Xstream models. I also had the idea of creating weight-scaled Xstream scale models that would be compatible with the polystyrene present in the WUR laboratory. I refined and simplified my research questions to explore the feasible options that were available to me:

1. What physical processes influence morphodynamics around and inside Xstream LTWs?
2. To what extent plays wall roughness part in relocating sediment?
3. How does the geometry of the LTW effect erosion and sedimentation?

For the last iteration of these research questions, I completely let go of the LTW idea and included a verification issue. This has resulted in the set of research questions answered in the final report. Valuable insights into the interaction between the base of an Xstream structure and the riverbed are the main findings of this study.

C

Model designs

This Appendix elaborates on each of the model setups built for this study. A brief description of each experiment is followed by a top-view and cross-sectional sketch of the flume. Hereafter, in accordance with the path of iterating the parameter values, a table of the intended parameter values per experiment is shown.

C.1. Froude scaling

Scaling of real world hydraulic conditions to the physical scale model of this study is done in accordance with Froude similarity. The principle of Froude scaling is based on the the idea that geometrically similar model and prototype systems, when constructed to certain scale ratios and subjected to the same Froude number, will exhibit similar dynamic behaviour. The ratio of velocities between the model and prototype should be the same as the ratio of the square roots of their characteristic lengths:

$$\frac{u_{model}}{u_{prototype}} = \frac{\sqrt{L_{model}}}{\sqrt{L_{prototype}}} \quad [C.1]$$

When keeping the Froude number similar in the model compared to reality, the other force ratio, the Reynolds number, will not be identical and may therefore result in significant scale effects. The most important scaling ratios for this study are listed below in table C.1.

Table C.1: Froude scaling conversion factors.

Physical parameter	Unit	Multiplication factor
Length	m	n^1
Area	m^2	n^2
Density	kg/m^3	n^0
Mass	kg/m^3	n^3
Time	s	$n^{0.5}$
Speed	m/s	$n^{0.5}$
Acceleration	m/s^2	n^0

C.2. Parameter iterations

The constraints listed in section 2.5.2 result in the need to iterate through model parameter values. To obtain a reliable and accurate scaling of real world conditions, the main objective is to keep both Shields and Froude number similar to reality. Figure C.2 presents the iteration path of all relevant parameters. The coloured numbers in between square brackets refer to the equations described in the Methodology chapter.

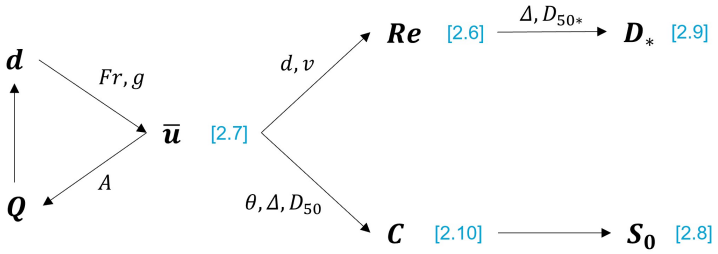

Figure C.1: Path of iterating parameters.

As a starting point for the iteration process, the perfectly scaled water depth following the geometric scaling factor of n_L = 8.3 is taken. This results in a water depth that is too deep for the height of the flume. Next, whereas the maximum discharge of the pumps is 180 L/s and the width of the flume is given, the water depth should be reduced further in order to keep the flow velocity high enough for scaling of the Froude number. With appropriate values for d, Q and $\overline{u}$ iteratively found, the other parameter values could be deducted.

The model setups cause a significant loss in cross-sectional area, A. To account for this loss, where it is assumed that absolutely no water is flowing through the structure, new values for Q were found. The values of all other parameters were not changed. This was done to ensure that scaling of the real world conditions was appropriate at the lengthwise position of the structure in the flume.

C.3. Model accuracy

Bed elevation data of the river IJssel is available at river kilometer 992. With a resolution of 50 x 50 cm, the bed was read using an autonomous sailing vessel equipped with sonar technology. This was done before the construction of the flexible groyne in November 2022 and five months after construction, in March 2023. The measured bed elevation difference will be used to verify the accuracy of the physical scale model. In addition, observations of coloured tracers flowing through the flexible groyne were translated into streamwise velocities.

The head of the flexible groyne will be built to scale in a laboratory setup. The base of the groyne reaches 1.3 m into the flume covering the right half of the flume, looking in the downstream direction. In the x direction, along the length of the flume, the structure will be build upstream of the middle as the most interesting scour and sedimentation zones for this study will form behind it. The slope of the groyne will be at a 45° angle. Figure C.2 presents a sketch of the top view of the model setup with the black arrow indicating the flow direction and figure C.3 shows a cross-sectional drawing of the flume. The legend items below apply for all hereafter clarified experiments.

The width of the river IJssel at the location of the flexible groyne is about 185 m. The beacon line of the groynes reaches 30 m into the river. The structure width to flow width ratio is therefore $\frac{1}{6}$ in reality. However, with the flexible groyne head reaching 1.3 m into the flume, this ratio is close to $\frac{1}{2}$. The effect of contraction will therefore be three times as severe as in reality. Moreover, the model does not take the influence of upstream and downstream groynes, waves and curvature of the river into account.

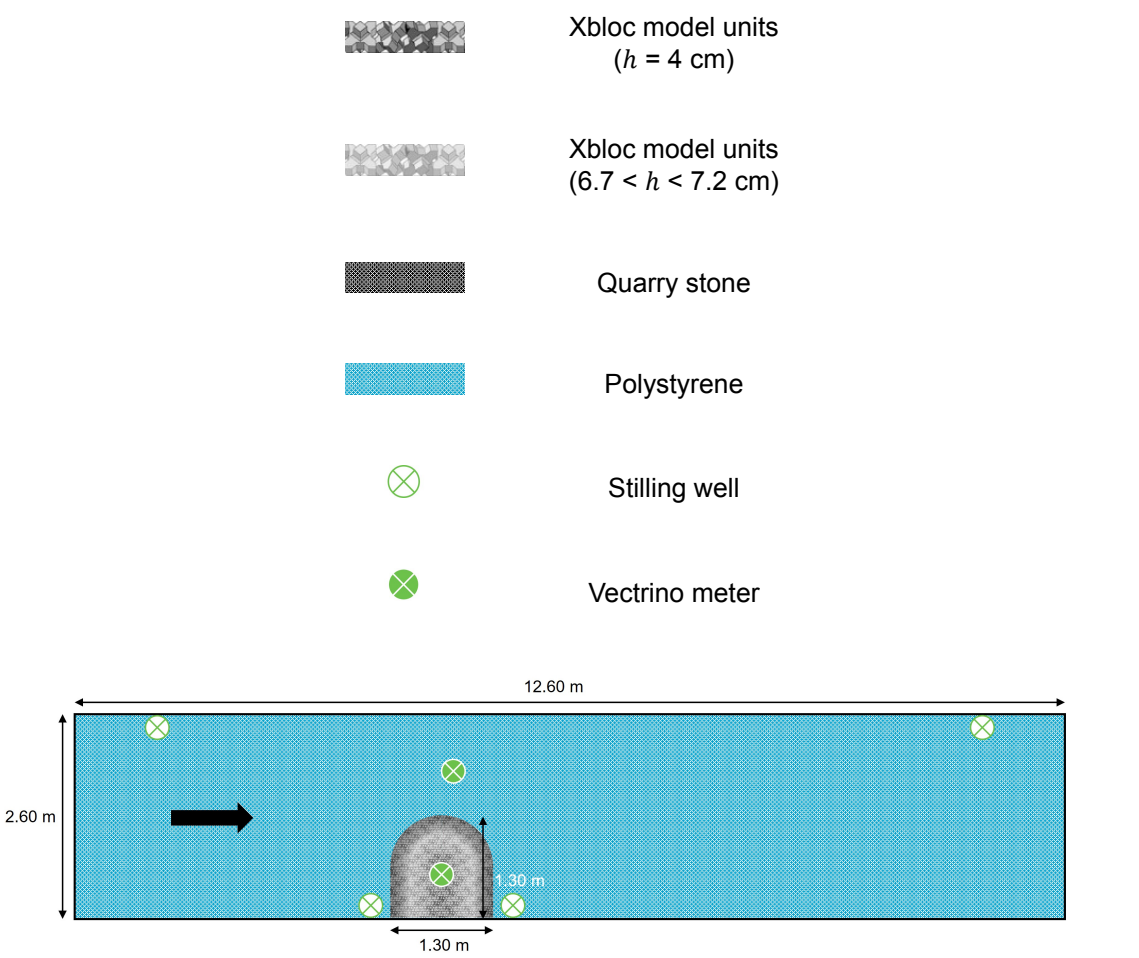

Figure C.2: Top view drawing of flexible groyne experiment.

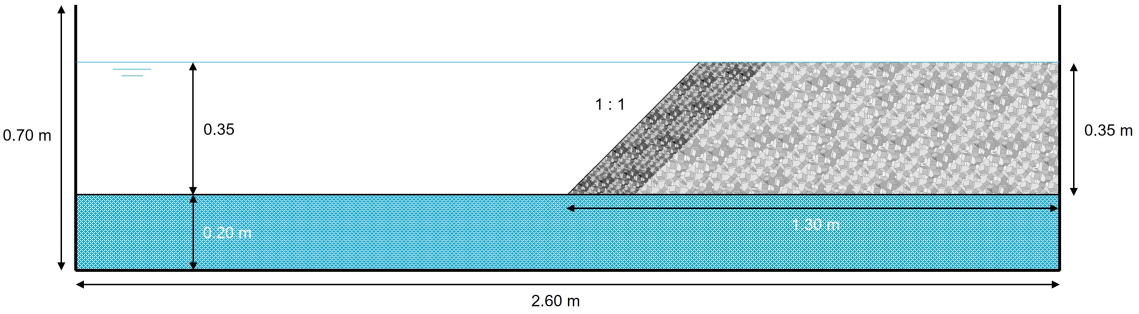

Figure C.3: Cross sectional drawing of flexible groyne experiment.

The hydraulic conditions in the river IJssel that were measured during fieldwork in April 2023 will be used as the starting point for scaling of this experiment. On this day, the highest water levels since the completed construction of the flexible groyne in November 2022 were measured. The depth-averaged flow velocity around the groyne head was roughly 0.8 m/s at a discharge of 619 m^3/s, with a water depth of approximately 6 m (Bilgili, 2018; Buschman & Kosters, 2021).

Scaling down these conditions according to the path of iterations as described in section C.2 results in the set of target parameter values presented in table C.2. It is important to emphasize that the hydraulic conditions in the IJssel differ from those in the Waal.

Table C.2: Envisioned parameter values Xstream groyne at high water conditions in the river IJssel.

Symbol	Variable	Unit	Prototype	Model	Ratio
d	Water depth	m	6.00	0.35	17.14
Q	Discharge	m^3/s	619	0.101	6130
C	Chézy coefficient	$m^{1/2}/s$	33	33	1
$\overline{u}$	Average flow velocity	m/s	0.80	0.19	4.21
Re	Reynolds number	-	3600000	60500	60
Fr	Froude number	-	0.10	0.10	1
S_0	Water surface slope	m/m	$1e^{-4}$	$9e^{-5}$	1
D_*	Particle number	-	25	16	1.54
θ	Shields parameter	-	0.30	0.30	1

To observe the morphological changes in the riverbed induced by a groyne entirely built with Xstream elements during an extreme discharge situation, the hydraulic conditions that occur once every 2000 years were simulated. In such an event, the water level reaches 10 m and the river IJssel discharges 2600 m^3/s of water. The flow velocity around the head of the groyne is approximately 1.5 m/s in this situation (Bilgili, 2018; De Jong et al., 2012). Table C.3 gives the target parameter values for this situation.

Table C.3: Envisioned parameter values Xstream groyne at extreme high water conditions in the river IJssel.

Symbol	Variable	Unit	Prototype	Model	Ratio
d	Water depth	m	10.00	0.35	28.57
Q	Discharge	m^3/s	2400	0.131	18320
C	Chézy coefficient	$m^{1/2}/s$	47	33	1.42
$\overline{u}$	Average flow velocity	m/s	1.50	0.25	6
Re	Reynolds number	-	11500000	81000	142
Fr	Froude number	-	0.15	0.15	1
S_0	Water surface slope	m/m	$1e^{-4}$	$1e^{-4}$	1
D_*	Particle number	-	25	16	1.54
θ	Shields parameter	-	0.51	0.51	1

C.4. Porosity and roughness

A comparison will be made between the riverbed's morphology and flow characteristics with a stone and an Xstream abutment. Following the scope of the present study, the abutments have a spill-through shape, built against the wall of the flume. Specifically for these two experiments, the abutments will have a slope of 1:2.5, which is based on the design of the LTW as shown in Appendix A. This ratio means that for every 1 metre of rise in the z direction, 2.5 metres towards the centre of the LTW in the y direction are needed.

Figure C.4 depicts a plan view of the stone abutment. On the exact same place in the flume, the Xstream abutment will be made as illustrated in figure C.6. From the cross-sectional drawings of both stone and Xstream structures, shown in figures C.5 and C.7 respectively, it can be seen that both cores are made from the larger Xstream model units. Only the external cover of both structures is composed of two different materials. A mesh fabric that follows the contours of the abutments will be put underneath the stone structure to allow for more stability of the structure. The Xstream abutment experiment does not include this fabric because the whole idea of Xstream is to build without a filter layer. This experiment was repeated once. The first time there were complications affecting the bed morphology when draining the flume.

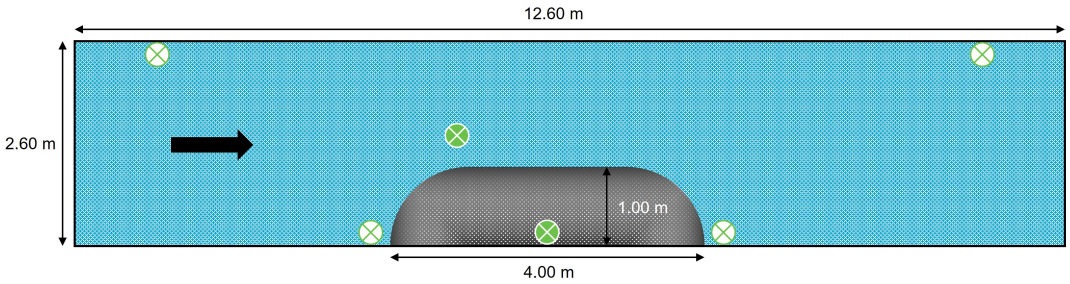

Figure C.4: Top view drawing of the flume with the 1:2.5 stone abutment.

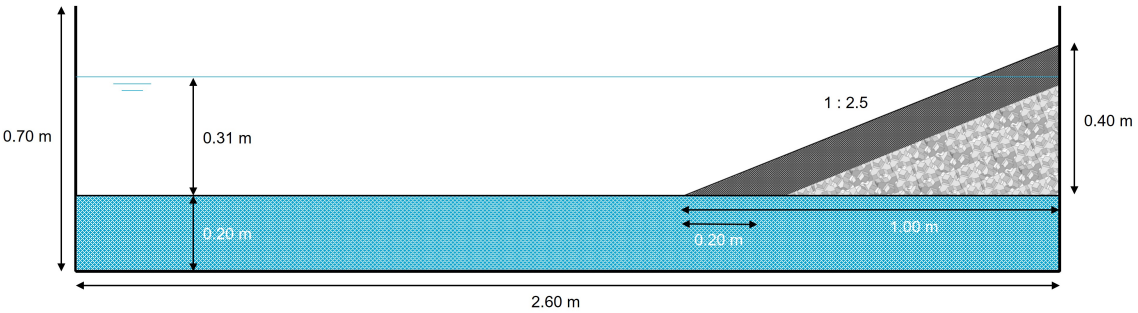

Figure C.5: Cross sectional drawing of the flume with the 1:2.5 stone abutment.

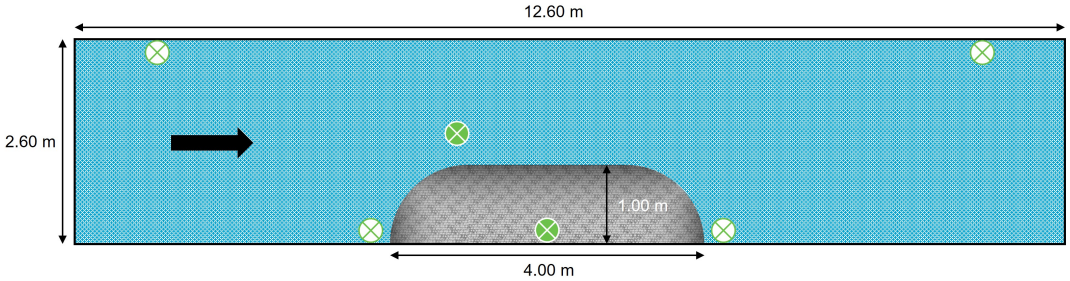

Figure C.6: Top view drawing of the flume with the 1:2.5 Xstream abutment.

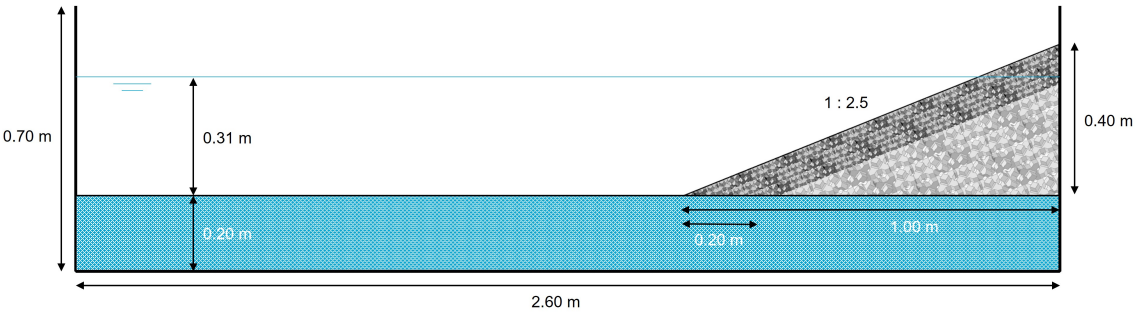

Figure C.7: Cross sectional drawing of the flume with the 1:2.5 Xstream abutment.

As mentioned before, the high water conditions in the river Waal are aimed to be mimicked in these experiments. Scaling down these hydraulic properties gives the set of parameter values listed in C.4, valid for both the stone and Xstream experiment. During the experiments, these values are aimed for but might be fluctuating slightly.

Table C.4: Envisioned parameter values 1 on 2.5 stone and Xstream abutment.

Symbol	Variable	Unit	Prototype	Model	Ratio
d	Water depth	m	8.00	0.31	25.81
Q	Discharge	m^3/s	4600	0.145	32000
C	Chézy coefficient	$m^{1/2}/s$	45	38	1.19
$\overline{u}$	Average flow velocity	m/s	1.00	0.20	5
Re	Reynolds number	-	6000000	66000	91
Fr	Froude number	-	0.11	0.11	1
S_0	Water surface slope	m/m	$6e^{-5}$	$8e^{-5}$	1
D_*	Particle number	-	25	16	1.54
θ	Shields parameter	-	0.25	0.25	1

Going back to the example of the LTW in the river Waal, the abutments in the model contract the flow lines 10 times as much as happens in the real world. In the design of the LTW, it is built in line with the bank of the inside bend and therefore does not actively narrow the river.

C.5. Slope

The local morphology and flow characteristics resulting from an Xstream abutment with a 1:1 slope are compared to the Xstream abutment with a 1:2.5 slope from the previous experiments. By only adjusting the abutment's slope, the effect of a steeper slope will be examined. This experiment was exclusively conducted with Xstream model units as quarry stone has an angle of response which is smaller than 45°. The experiment was run twice, once with and once without geotextile underneath. A top view on the flume with the 1:1 Xstream abutment is given in figure C.8 and its cross-sectional drawing in C.9.

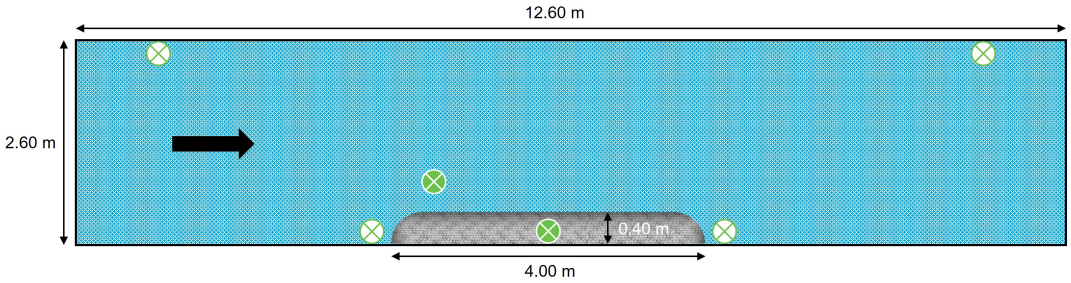

Figure C.8: Top view drawing of the flume with the 1:1 Xstream abutment.

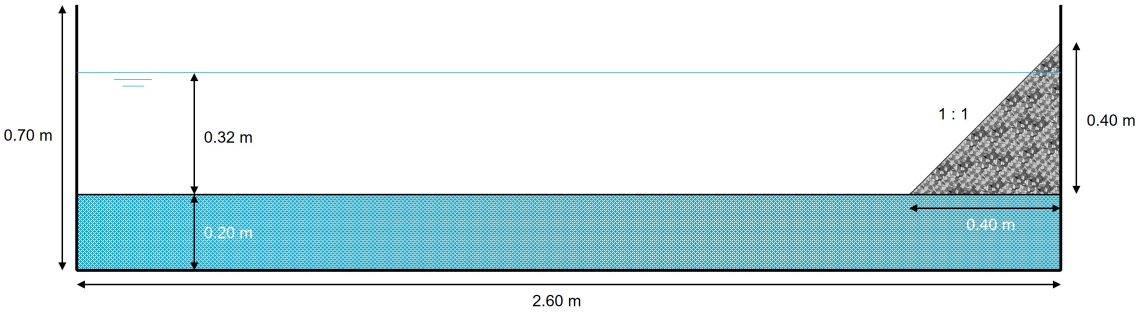

Figure C.9: Cross sectional drawing of the flume with the 1:1 Xstream abutment.

Again, the hydraulic conditions are kept the same. Only the discharge is adjusted to account for the increased cross sectional flow area at the position of the structures along the length of the flume.

Table C.5: Envisioned parameter values 1 on 1 Xstream abutment.

Symbol	Variable	Unit	Prototype	Model	Ratio
d	Water depth	m	8.00	0.32	25.00
Q	Discharge	m^3/s	4600	0.168	27000
C	Chézy coefficient	$m^{1/2}/s$	45	38	1.19
$\overline{u}$	Average flow velocity	m/s	1.00	0.20	5
Re	Reynolds number	-	6000000	66000	91
Fr	Froude number	-	0.11	0.11	1
S_0	Water surface slope	m/m	$6e^{-5}$	$8e^{-5}$	1
D_*	Particle number	-	25	16	1.54
θ	Shields parameter	-	0.25	0.25	1

D

Photos

Kraijenhoff van de Leur Laboratory for Water and Sediment Dynamics at the Wageningen University and Research

Stilling wells with linear position sensors

Flow laminator at the inlet of the flume

Filters to prevent suspended sediment ending up in the large reservoir

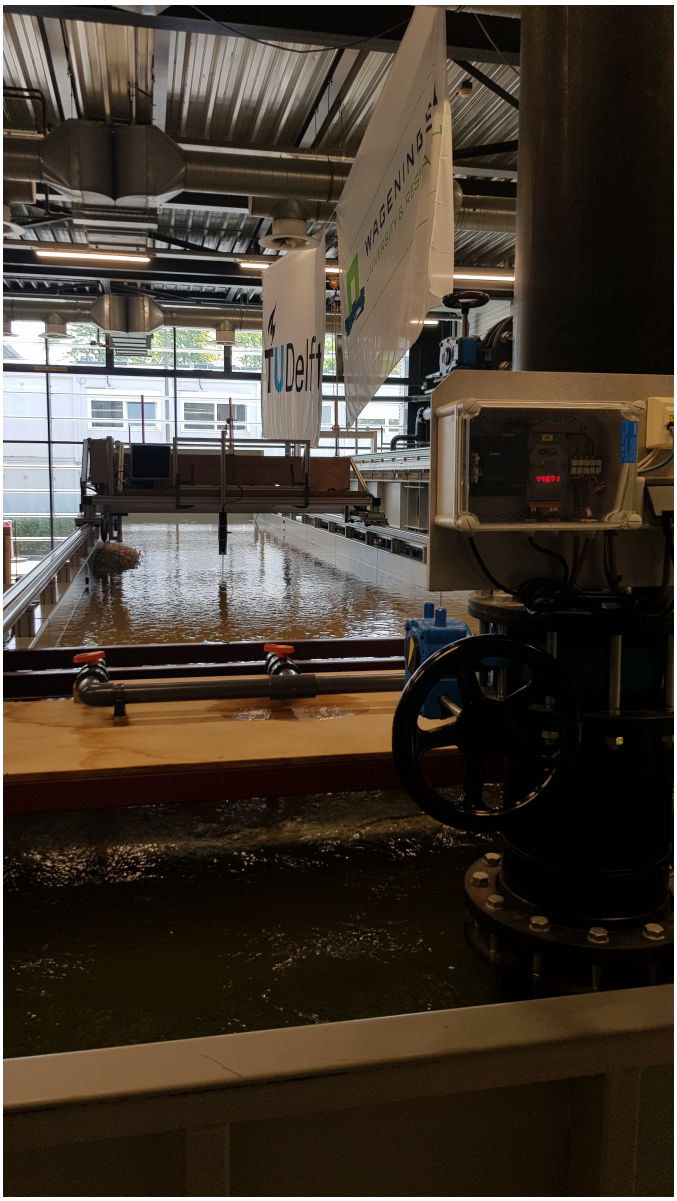

Valve regulating the discharge into the flume measured by an electromagnetic flow meter

Line-laser scanner combination measuring bed elevation

Installation of the velocimeters, the left one has side-looking probes and the one inside the structure is the Vectrino Proifler

Determination of the porosity inside a stone body

Determination of the porosity inside an Xstream body

Setup for experiment SG1

Scour at the upstream end of the stone structure in experiment SG1 where the geometrically closed filter protects the bed material from erosion

Drawn lines to assist in building the structures

Construction of experiment XG1

Resulting bed morphology after experiment XG2

Collapsed structure after experiment XG2

Setup for experiment XS2

Resulting bed morphology after experiment XS1

Setup for experiments FG1 and FG2

Scour formation around the flexible groyne head after experiment FG1

Breaking down the setup of experiment SG1

Removing all polystyrene from the flume and cleaning

E

Additional results

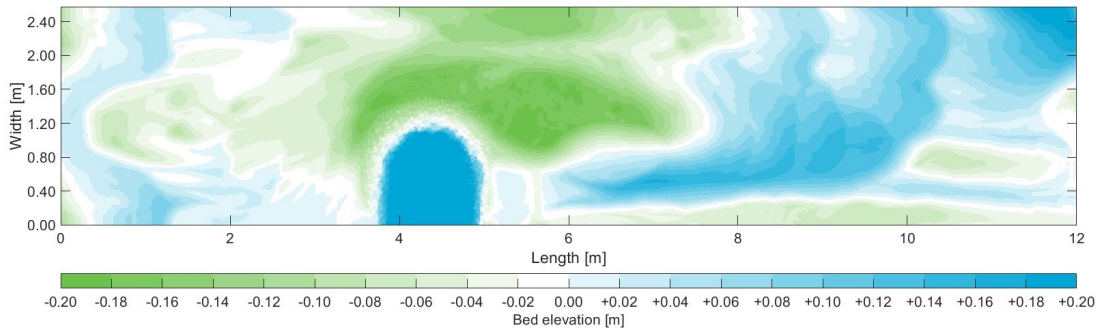

Figure E.1: Resulting bed morphology experiment FG2.

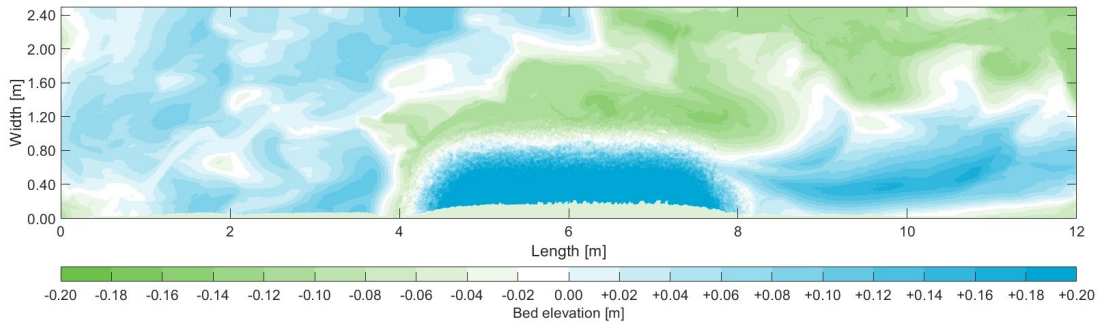

Figure E.2: Resulting bed morphology experiment XG1.

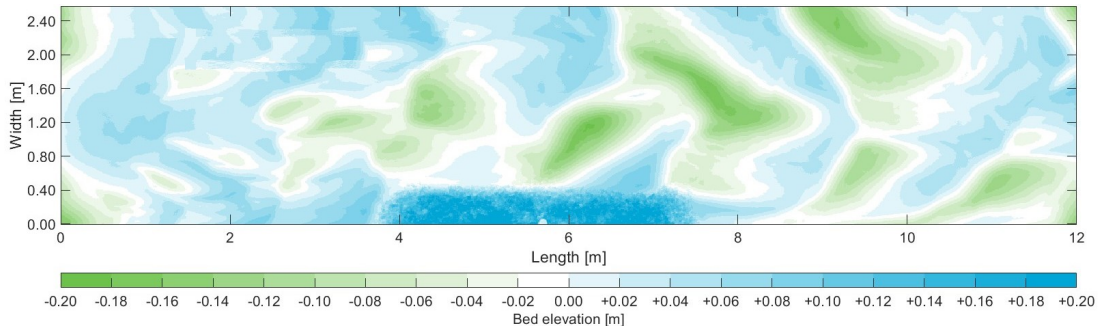

Figure E.3: Resulting bed morphology experiment XS1.

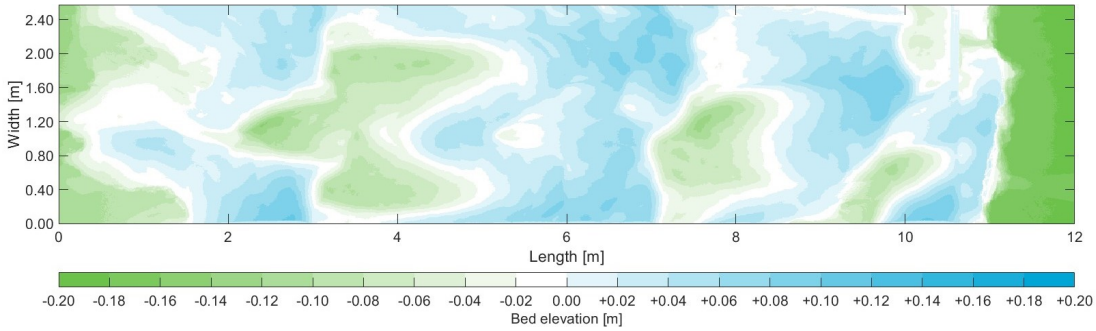

Figure E.4: Resulting bed morphology experiment T1.

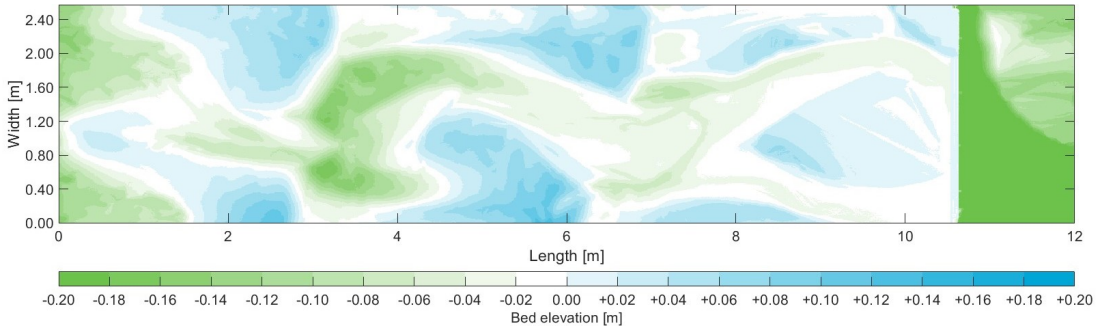

Figure E.5: Resulting bed morphology experiment T2.

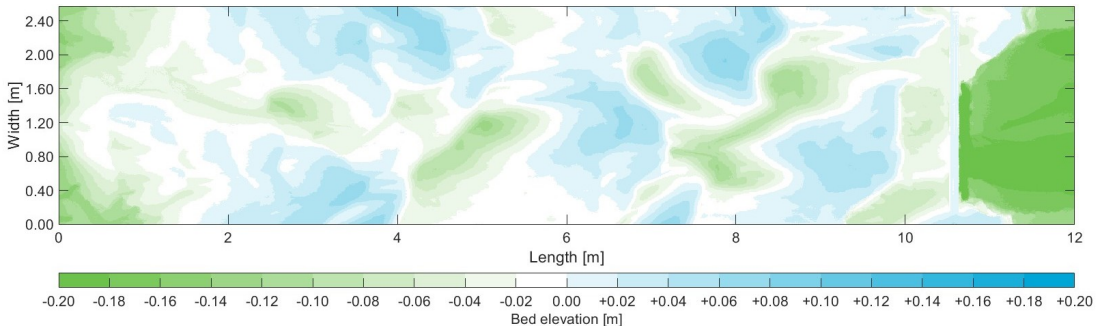

Figure E.6: Resulting bed morphology experiment T3.

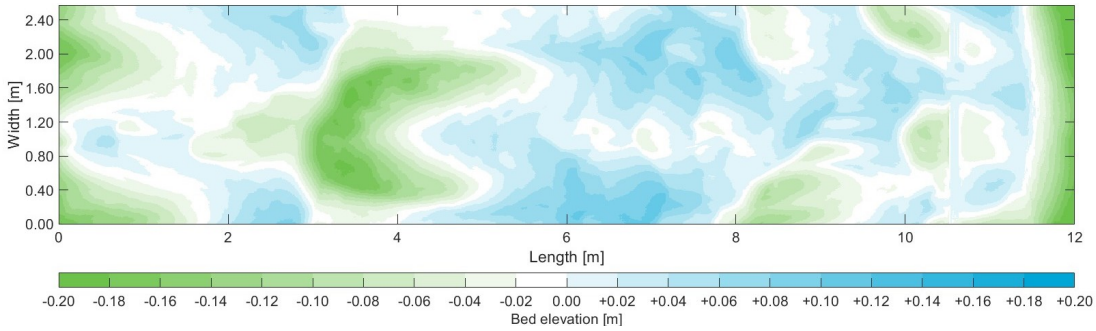

Figure E.7: Resulting bed morphology experiment T4.

F

Field data

This appendix contains the field measurement data as presented by Groenewege and Buschman (2023) from Deltares.

Foto door IGL op 7 april 2023

Datum	Afvoer Olst (m^3/s)	Tijdsduur (s)	Opmerkingen
1 februari 2023	440	90	Afgelegde weg is 3-4 m
7 april 2023	619	<15	Aan oppervlakte < 10 s
17 mei 2023	488	66	Minder verkleuring

- Gekleurd water gaat door de flexibele krib heen, niet door traditionele kribben
- Bij de hoogste afvoer is de duur ongeveer 4-5 keer korter.

Figure F.1: Picture of the flexible groyne on the 7th of April 2023 and the results of the dye tests. The reference situation for this study was the 619 m^3/s discharge.

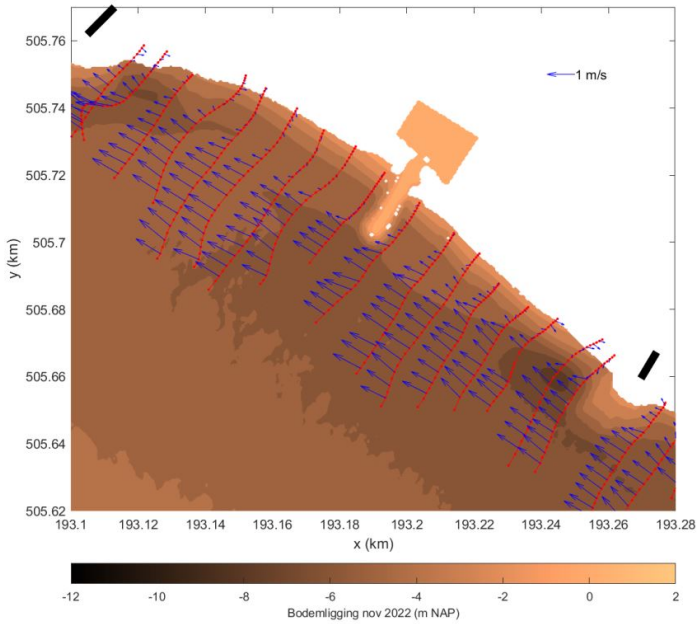

Detail rond de flexibele krib
- Circulaties in kribvakken
- Geen stroming door de krib zichtbaar
- vergelijkbaar stromingsbeeld als bij traditionele kribben

Ook op vijf punten stil gelegen...

Figure F.2: Measured flow velocity over cross-river transects using an ADCP.

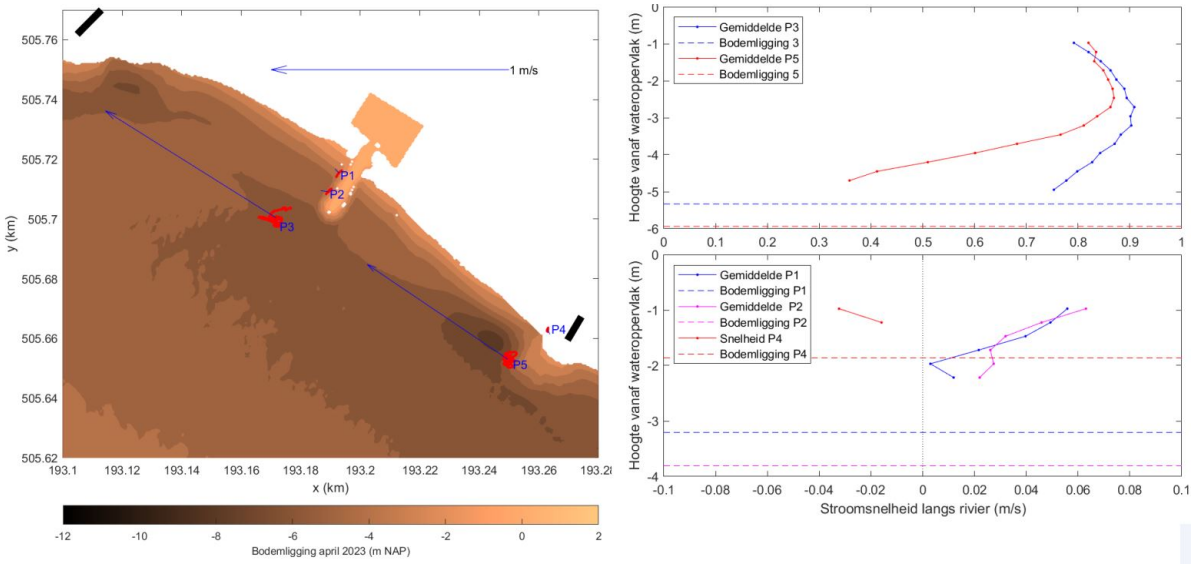

Figure F.3: Computed flow velocity profiles at 5 points near the flexible and a traditional groyne. Location P2 was used to compare the flow velocity through the groyne in the physical model with reality.